INSTITUTO DE FÍSICA
Universidade Federal Fluminense

Theoretical and experimental approaches using $\Delta^{14}C$ for estimating system diagnostic times in the central Amazon rainforest

Ingrid Silva Chanca

Niterói – RJ
2022

Ingrid Silva Chanca

Theoretical and experimental approaches using $\triangle^{14}$C for estimating system diagnostic times in the central Amazon rainforest

Tese apresentada ao programa de pós-graduação do curso de Física da Universidade Federal Fluminense como requisito parcial para a obtenção do Grau de Doutora em Física.

Universidade Federal Fluminense – UFF

Instituto de Física

Programa de Pós-Graduação

Supervisor: Prof. Dr. Kita Macario

Dr. Carlos Sierra

Niterói - RJ

2022

Ficha catalográfica automática - SDC/BIF
Gerada com informações fornecidas pelo autor

C454t Chanca, Ingrid Silva
Theoretical and experimental approaches using ?14C for estimating system diagnostic times in the central Amazon rainforest / Ingrid Silva Chanca ; Kita Chaves Damasio Macario, orientadora ; Carlos A. Sierra, coorientador. Niterói, 2022.
135 p. : il.

Tese (doutorado)-Universidade Federal Fluminense, Niterói, 2022.

DOI: http://dx.doi.org/10.22409/PPGF.2022.d.14218757720

1. Isótopo de carbono. 2. Isótopo radioativo. 3. Ciclo do carbono. 4. Amazônia. 5. Produção intelectual. I. Macario, Kita Chaves Damasio, orientadora. II. Sierra, Carlos A., coorientador. III. Universidade Federal Fluminense. Instituto de Física. IV. Título.

CDD -

Bibliotecário responsável: Debora do Nascimento - CRB7/6368

Ingrid Silva Chanca

Theoretical and experimental approaches using $\triangle^{14}$C for estimating system diagnostic times in the central Amazon rainforest

Tese apresentada ao programa de pós-graduação do curso de Física da Universidade Federal Fluminense como requisito parcial para a obtenção do Grau de Doutora em Física.

Niterói - RJ, ... de.....de 2022:

Prof Dr Kita Macario
Orientadora - IF/UFF

Dr Carlos Sierra
Co-orientador - MPI-BGC

Dr Carlos Alberto Nobre Quesada
INPA

Prof Dr Corina Solís Rosales
UNAM

Prof Dr Ingeborg Levin
Heidelberg University

Prof Dr Lucas Maurício Sigaud
IF/UFF

"Both pure and applied science have gradually pushed further and further the requirements for accuracy and precision. However, applied science, particularly in the mass production of interchangeable parts, is even more exacting than pure science in certain matters of accuracy and precision."

Walter A. Shewhart

"It always seems impossible until it's done."

Nelson Mandela

Acknowledgements

First, I would like to thank my family. To my mom, for her endless support throughout all these years, including the ones of the PhD. Even from far away, you were always present. To my sister, thanks for being there listening to my struggles and making me laugh in every call or encounter. To my brother, Júlio César, thanks for holding up when everything was so heavy.

Thanks to this PhD project, I had the opportunity to work with incredible scientists. I appreciate all the encouragement I found with the radiocarbon colleagues from all stages in research. I will bring the same enthusiasm with me wherever I go.

I would like to thank Carlos Sierra for the infinite patience, support and great debates about Science. Thanks for the opportunity in discovering the Brazilian Amazon together.

I would like to thank Ingeborg Levin for teaching me so much about radiocarbon and encouraging me to think problems from other perspectives. Thanks for being so kind and supportive in one of my hardest moments during the past years.

I would like to thank Sue Trumbore for all the support all those years and for the enjoyable conversations even in my spontaneous visits.

Thanks to Axel Steinhof for the kindness and patience to discuss several aspects of the AMS, radiocarbon measurements and any questions I would have from time to time.

To Kita, my deepest thanks for supporting my career as a mentor, my personal life as a friend, and my dreams as an inspiration.

I thank to all my friends for being who they are. Some friends are entangled as family members. Thanks Gik for being the *persona fofa* you are and for bringing Maikai to illuminate us. From the PhD time, I thank my friends at UFF, especially Marcelo, Renata, Mariana, Fabiana, Bruna Brandão, Eduardo, Maikel, Luiz, Nelson, Cauê, Bruno Basílio. At the MPI-BGC, special thanks go to John Kula, Steffi, David Herrera, Mina, Markus Mueller, Holger, Veronika, Santiago, Andres, Carsten. In Germany, to the amazing friends Eliane, Tito, Carol, Tiago, Dani and Victor Hiroshi.

At MPI-BGC I found a wonderful work environment that I will always remember. Thanks Karl Kübler and Martin Göbel for your support when I was building the purification line. You were not only technically helpful but also made the process very fun! Thanks also to Kerstin Lohse and Anita Maercker for helping me so much with all kind of doubts especially concerning the bureaucracies.

At INPA I had always a great time with kind people and great scientific discussions. Thanks to Roberta, Bruno, Fernanda, Sabrina, Beto, Seu Adi, Layon, Antonio, Yago, Val, Nagibe, Alessandro, Cybelli, Flávia and all the team of ATTO and LBA. You are amazing!

Last but not least, I thank my *amore* David. Thanks for your support and for all your love.

P.S.: This thesis would not be made possible without the work and support of several people. It always hard to thank everyone, but be sure I am grateful to everyone.

ABSTRACT

The Amazon rainforest is a very relevant ecosystem in terms of its biodiversity and its contribution to the global carbon balance. Despite a large number of studies in the Amazon estimating biomass and fluxes from west to east, in different seasons and ecosystems, there is still a lack of information regarding the time scales of carbon cycling. To fill this gap, I coupled two powerful tools: radiocarbon (^{14}C) measurements and the theory of compartmental dynamical systems. On the one hand, the ^{14}C can be used as a tracer of the carbon cycle to determine how fast carbon moves between different reservoirs such as plants, soils, rivers or oceans. On the other hand, the theory of compartmental dynamical systems is useful to describe the transport of matter and it facilitates the estimation of ecosystem metrics such as ages and transit times.

Most studies using ^{14}C to estimate time metrics emphasize the mean value (as $\Delta^{14}C$) of an unknown probability distribution. Here a novel algorithm to compute $\Delta^{14}C$ distributions from knowledge of the age distribution of carbon in linear compartmental systems at steady-state was introduced. The results demonstrated that the shape of the distributions might differ according to the speed of cycling of ecosystem compartments and their connectivity within the system, and might contain multiple peaks and long tails. The theoretical distributions of radiocarbon are also sensitive to the variations of $\Delta^{14}C$ in the atmosphere over time, as influenced by the counteracting anthropogenic effects of fossil-fuel emissions (^{14}C-free) and nuclear weapons testing (excess ^{14}C).

Since 2015, the Amazon Tall Tower Observatory (ATTO) is in operation in the central Amazon, ca. 150 km north from the city of Manaus. The scientific infra-structure of the ATTO project provides an excellent opportunity to better study the topic of time scales of the carbon cycling in the Amazon forest. $\Delta^{14}C$ of different compartments sampled in ATTO site showed variabilities corresponding to the speed of carbon cycling in the compartments. The $\Delta^{14}C$ of the ecosystem respiration ($\Delta^{14}C_{ER}$) was estimated based on mixing models applied to the $\Delta^{14}C$-CO_2 of ambient air collected below and above the canopy. From the $\Delta^{14}C_{ER}$ it was estimated a mean transit time of 7 to 9 years. To perform analyses of $\Delta^{14}C$ in atmospheric CO_2, I built a dedicated purification line at LAC-UFF. Such equipment contributed to the expansion of type of samples that can be prepared independently at LAC-UFF.

RESUMO

A floresta Amazônica é um ecossistema muito relevante em termos de biodiversidade e quanto ao seu papel no balanço total de carbono. Apesar do grande número de estudos na Amazônia estimando biomassa e fluxos de oeste a leste, em diferentes estações do ano e em diferentes ecossistemas, ainda há pouca informação sobre as escalas de tempo envolvidas. Para preencher essa lacuna, eu combinei duas ferramentas poderosas: medidas de radiocarbono (^{14}C) e a teoria de sistemas dinâmicos compartimentais. Por um lado, ^{14}C pode ser usado como um traçador do ciclo do carbono para determinar a velocidade com a qual o carbono se move em diferentes compartimentos, como plantas, solos, rios ou oceanos. Por outro lado, a teoria de sistemas dinâmicos compartimentais é útil na descrição do transporte de matéria, além de facilitar a estimativa de métricas em ecossistemas, como idades e tempos de trânsito do carbono.

A maioria dos estudos usando ^{14}C para estimativa de métricas temporais tem foco nos valores médios (na forma de Δ^{14}C) de uma distribuição de probabilidade desconhecida. Nesse trabalho foi desenvolvido um algoritmo inédito para computar distribuições de Δ^{14}C a partir de distribuições conhecidas de idade de carbono em sistemas compartimentais lineares em equilíbrio dinâmico. Os resultados obtidos demonstraram que o formato e dispersão das distribuições de radiocarbono pode mudar de acordo com a taxa com a qual o carbono é transferido entre os compartimentos e com a maneira com a qual esses compartimentos são interligados. Em certos casos, as distribuições podem apresentar diversos picos e caudas longas. As distribuições de radiocarbono obtidas teoricamente também se apresentaram sensíveis a variações de Δ^{14}C na atmosfera ao longo do tempo. Essas variações são influenciadas principalmente por efeitos antropogênicos como as emissões relacionadas a queima de combustível fóssil (sem ^{14}C) e os testes de armas nucleares (^{14}C em excesso).

Desde 2015, o Observatório da Torre Alta da Amazônia (ATTO) está em operação na Amazônia central, a cerca de 150 km ao norte da cidade de Manaus. A infraestrutura científica do projeto ATTO oferece uma excelente oportunidade para melhor entendimento do tópico das escalas de tempo do carbono sendo reciclado na floresta Amazônica. Δ^{14}C em diferentes compartimentos amostrados no sítio ATTO mostraram variabilidades que correspondem a velocidade com a qual o carbono é reciclado nos compartimentos. Já o Δ^{14}C da respiração total do ecossistema ($\Delta^{14}C_{RE}$)

foi estimado com base em modelos de mistura aplicados Δ^{14}C-CO_2 do ar ambiente coletado abaixo e acima do dossel. A partir do $\Delta^{14}C_{RE}$ foi-se estimado um tempo médio de trânsito do carbono entre 7 e 9 anos. Para realizar análises de Δ^{14}C em CO_2 atmosférico, eu construí uma linha de purificação no LAC-UFF. Tal equipamento contribuiu para a implementação de mais um tipo de material que pode ser preparado de forma independente no LAC-UFF.

palavras-chave: radiocarbono, modelos compartimentais, ciclo do carbono, ATTO, tempo de trânsito

Contents

ACKNOWLEDGEMENTS **vii**

ABSTRACT **ix**

RESUMO **x**

LIST OF ABBREVIATIONS **xix**

1 INTRODUCTION **1**
1.1 Objectives and research questions 8

2 RADIOCARBON: CHRONOMETER AND TRACER **11**
2.1 Radiocarbon dynamics 12
2.1.1 Production 12
Natural variations 13
Anthropogenic effects 14
2.1.2 Assimilation 15
Fractionation effect 16
2.1.3 Decay 17
2.2 Chronometer: Radiocarbon dating 19
2.3 Tracer: Radiocarbon in ecology 22
2.4 Accelerator Mass Spectrometry 24
2.5 Gas and Air Samples Purification System - GASPS 27
2.5.1 List of materials and technical scheme 30

3 PROBABILITY DISTRIBUTIONS OF RADIOCARBON **35**
3.1 Compartmental systems 37
3.2 Time metrics in ecology 39
3.2.1 Age distributions 39

3.2.2 Transit Time distributions . . . 40
3.3 Estimating radiocarbon distributions from compartmental models . . 40
3.3.1 Homogenization of input data . . . 41
Atmospheric radiocarbon datasets . . . 41
3.3.2 Discretization . . . 43
3.3.3 Aggregation . . . 44
3.3.4 Set of parameters . . . 47
3.4 Application in ecological compartmental models . . . 48
3.4.1 Harvard Forest soil model . . . 48
3.4.2 Porce Model . . . 58
3.4.3 Emanuel Model . . . 61
3.5 Discussion . . . 65
3.5.1 How do distributions of radiocarbon change over time as a consequence of changes in atmospheric radiocarbon? . . . 66
3.5.2 How do empirical data compare to these conceptual radiocarbon distributions? . . . 67
3.5.3 What insights can these distributions provide for experimental and sampling design for improving model-data comparisons by capturing the entire variability of $\Delta^{14}C$ values? . . . 68
3.6 Conclusions . . . 69
3.7 Availability Statements . . . 70

4 Measuring carbon isotopes in the central Amazon **71**
4.1 Theoretical background . . . 72
4.1.1 The Keeling plot method . . . 74
4.1.2 Miller-Tans mixing model . . . 75
4.2 Study area . . . 76
4.3 Collection of samples . . . 78
4.4 Preparation of samples for ^{14}C-AMS . . . 81
4.5 Carbon isotopes in terrestrial compartments . . . 83
4.6 Carbon isotopes in atmospheric CO_2 . . . 84
4.7 Comparison between $\Delta^{14}C$ in the canopy air and fast pools . . . 88
4.8 Discussion . . . 90
4.8.1 Can we observe differences in the cycling rates between *campinarana* and *terra-firme* using $\Delta^{14}C$ measurements alone? . . . 90

4.8.2 How do $\Delta^{14}C$ values give us insights into the cycling rates of different compartments? 92
4.8.3 How long does carbon take to be respired by a *terra-firme* ecosystem in central Amazon? 95
4.9 Conclusions 98

5 General Conclusion **101**
5.1 Future research 104

A Supplementary material of chapter 3 **107**

Bibliography **119**

List of Figures

1.1 Calculation of mean age of ecosystem respired CO_2 as an average of the respired CO_2 from different ecosystem compartments in Amazon. 4

2.1 Processes between production of ^{14}C and formation of $^{14}CO_2$. 16
2.2 Distribution of C in reservoirs within the Earth System. 22
2.3 Distribution of ^{14}C in reservoirs within Earth System. 23
2.4 MICADAS technical scheme. 26
2.5 SSAMS technical scheme. 26
2.6 Pictorial representation of a graphitisation tube (GT) with the reagents for graphitisation. 27
2.7 Technical scheme of cooling trap at EGL. 30
2.8 Picture of glass cooling trap. 31
2.9 Technical drawing of GASPS line. 32

3.1 Scheme of assembling of atmospheric radiocarbon contents obtained from empirical curves. 43
3.2 Scheme of main algorithm steps for computation of probability distributions of radiocarbon in open systems. 45
3.3 Third step of the algorithm: aggregation. 46
3.4 Scheme of compartmental model for Harvard Forest soil fractions. . . 50
3.5 Pool age distributions (a) and system radiocarbon distributions for the years 1965 (b), 2027 (c) and 2100 (d) for the HFS model. 53
3.6 Transit time distribution (a) and total outflux radiocarbon distribution (b) for HFS model. 54
3.7 Comparison between theoretical distributions of radiocarbon for HFS model and distribution of observation radiocarbon values from soil samples from Harvard Forest. 57
3.8 Scheme of compartmental model for the tropical forest in the Porce region (Colombia). 58

3.9 Pool age distributions (a) and system radiocarbon distributions for the years 1965 (b), 2027 (c) and 2100 (d) for Porce model. 60
3.10 Transit time distribution (a) and total outflux radiocarbon distribution (b) for Porce model. 61
3.11 Scheme of compartmental model for the global carbon cycle conceptualized by Emanuel et al. (1981). 62
3.12 Pool age distributions (a) and system radiocarbon distributions for the years 1965 (b), 2027 (c) and 2100 (d) for Emanuel model. 64
3.13 Transit time distribution (a) and total outflux radiocarbon distribution (b) for Emanuel model. 65

4.1 Vegetation in *campinarana* and *terra-firme*. 77
4.2 Study area. 78
4.3 3-L ICOS Flask 80
4.4 Portable air sampler. 81
4.5 Boxplots of the radiocarbon contents in samples collected in 2018 from four different compartments in two different ecosystems in the ATTO site. 84
4.6 Picarro vs Flasks CO_2 concentrations at 24 m agl. 86
4.7 Keeling plot of $\Delta^{14}CO_2$ from air samples. 87
4.8 Miller-Tans model of $\Delta^{14}CO_2$ from air samples. 87
4.9 Linear regression of carbon isotopic ratios with height above ground level. 88
4.10 $\Delta^{14}C$ of samples from different compartments and $\Delta^{14}CO_2$ of atmospheric air in *terra-firme*. 89
4.11 CO_2 versus leaf radiocarbon values in a vertical profile. 89

A.1 Evolution of the expected $\Delta^{14}C$ values of outflux and whole system for the HFS model between the years 1900 and 2100. 108
A.2 Change over time (AD 1996 - 2010) of the expected $\Delta^{14}C$ values and of the mean $\Delta^{14}C$ values of observations from samples of total soil CO_2 efflux in the Harvard Forest (HFS model). 109
A.3 $\Delta^{14}C$ distributions of the HFS model for each of the seven pools, outflux, and whole system in 1965 CE. 110
A.4 $\Delta^{14}C$ distributions of the HFS model for each of the seven pools, outflux, and whole system in 2027 CE. 111

A.5 $\Delta^{14}C$ distributions of the HFS model for each of the seven pools, outflux, and whole system in 2100 CE. 112
A.6 $\Delta^{14}C$ distributions of the Porce model for each of the seven pools, outflux, and whole system in 1965 CE. 113
A.7 $\Delta^{14}C$ distributions of the Porce model for each of the seven pools, outflux, and whole system in 2027 CE. 114
A.8 $\Delta^{14}C$ distributions of the Porce model for each of the seven pools, outflux, and whole system in 2100 CE. 115
A.9 $\Delta^{14}C$ distributions of the Emanuel model for each of the seven pools, outflux, and whole system in 1965 CE. 116
A.10 $\Delta^{14}C$ distributions of the Emanuel model for each of the seven pools, outflux, and whole system in 2027 CE. 117
A.11 $\Delta^{14}C$ distributions of the Emanuel model for each of the seven pools, outflux, and whole system in 2100 CE. 118

List of Tables

3.1 $\Delta^{14}C$ ranges with masses of carbon above 100 gC m^{-2} according to our estimations; $\Delta^{14}C$ expected values according to weighted mean of mass distribution of radiocarbon; and observed $\Delta^{14}C$ mean values of soil CO_2 efflux. 56

4.1 Summary of $\Delta^{14}C$ results for different compartments in two ecosystems in the ATTO region. 83

List of Abbreviations

AGE	**A**utomated **G**raphitisation **E**quipment
agl	**a**bove **g**round **l**evel
AMS	**A**ccelerator **M**ass **S**pectrometry
ATTO	**A**mazon **T**all **T**ower **O**bservatory
BP	**B**efore **P**resent
CE	**C**ommon **E**ra
CEZA	**C**urt-**E**ngelhorn **Z**entrum **A**rchäometrie
CT	**C**ombustion **T**ube
DBH	**D**iameter at **B**reast **H**eight
EA	**E**lemental **A**nalyzer
EGL	**E**xtraction and **G**raphitisation **L**ine
ER	**E**cosystem **R**espiration
ESM	**E**arth **S**ystem **M**odel
GASPS	**G**as and **A**ir **S**amples **P**urification **S**ystem
GCR	**G**alactic **C**osmic **R**ays
GT	**G**raphitisation **T**ube
HFS	**H**arvard **F**orest **S**oil (model)
IAEA	**I**nternational **A**tomic **E**nergy **A**gency
ICOS	**I**ntegrated **C**arbon **O**bservation **S**ystem
ICOS-CRL	**ICOS** – **C**entral **R**adiocarbon **L**aboratory
ICOS ERIC	**ICOS E**uropean **R**esearch **I**nfrastructure **C**onsortium
IPCC	**I**ntergovernmental **P**anel on **C**limate **C**hange
IRMS	**I**sotope **R**atio **M**ass **S**pectrometry
LAC-UFF	Radiocarbon Laboratory at **U**niversidade **F**ederal **F**luminense
LBA-ECO	**L**arge Scale **B**iosphere – **A**tmosphere **E**xperiment
MAI	**M**ean **A**nnual **I**ncrement
MFC	**M**ass **F**low **C**ontroller
MICADAS	**MI**ni **CA**rbon **DA**ting **S**ystem

MPI-BGC	**M**ax **P**lanck **I**nstitute for **B**io**G**eo**C**hemistry
MS	**M**ass **S**pectrometer
NBS	**N**ational **B**ureau of **S**tandards
NE	**N**orth**e**ast
NEC	**N**ational **E**lectrostatics **C**orporation
NH	**N**orthern **H**emisphere
NIST	**N**ational **I**nstitute of **S**tandards and **T**echnology
ODE	**O**rdinary **D**ifferential **E**quation
OxII	**O**xalic **A**cid **II**
PDB	**P**ee **D**ee **B**elemnite
PTBT	**P**artial **T**est **B**an **T**reaty
RCP	**R**epresentative **C**oncentration **P**athway
RDS-Uatumã	*Reserva de Desenvolvimento Sustentável – Uatumã*
SEP	**S**olar **E**nergetic **P**articles
SH	**S**outhern **H**emisphere
SNICS	**S**ource of **N**egative **I**ons by **C**esium **S**puttering
SRM	**S**tandard **R**eference **M**aterial
SSAMS	**S**ingle **S**tage **A**ccelerator **M**ass **S**pectrometer
trop	**Trop**osphere
UFF	**U**niversidade **F**ederal **F**luminense
VPDB	**V**ienna **P**ee **D**ee **B**elemnite
WSE	**W**hite-**s**and **E**cosystems

Dedicated to my brother Carlinho and my father Jair.
(In Memoriam).

Chapter 1

Introduction

Since the discovery of the natural greenhouse effect over 100 years ago, debate on the anthropogenic influence on the climate has been on the table. It was suggested by Ahrrenius at the end of 19^{th} century that burning of fossil fuels could increase Earth's temperature through an enhanced greenhouse effect. It took about a century to better understand the mechanisms underlying climate and find a general agreement on the role of humankind on global climate change. During this journey, a miryad of studies from a variety of fields have been published and discussed in scientific meetings. In Physics, *"groundbreaking contributions to our understanding of complex physical systems"* have awarded three climate scientists on the Nobel Prize in Physics 2021. One of the Laureates, Klaus Hasselmann, demonstrated that Earth System Models (ESMs) are a reliable approach to predict the evolution of climate under anthropogenic and natural radiative forcing. The greater consensus among the scientific community in the past 30 years has also helped to move the political and media debate into taking actions to mitigate global warming. The Intergovernmental Panel on Climate Change (IPCC) aids this initiative through reporting reliable data and up-to-date scientific findings revised by a body of hundreds of scientists from diverse fields. The reports of the IPCC also communicate the sources of uncertainties in ESMs.

There are several greenhouse gases in the atmosphere, namely carbon dioxide (CO_2), methane (CH_4), water vapour, nitrous oxide (N_2O), sulphur hexafluoride (SF_6), among others. Among the carbon (C) greenhouse gases, CO_2 is the most prominent as its emissions has been the main driver of global warming since the Industrial Revolution. Despite CH_4 has a higher heat-trapping capacity, it is far less abundant in the atmosphere. Natural mechanisms can reduce the CO_2 concentrations in the atmosphere by storing it in C reservoirs. Terrestrial ecosystems play

a major role in climate change mitigation by sequestering about 25 % of anthropogenic CO_2 through photosynthesis, where plants convert inorganic CO_2 from the atmosphere into organic C used for their metabolism and growth (Luo et al., 2017; Lu et al., 2018; Friedlingstein et al., 2019). However, the net C sink in terrestrial ecosystems is subjected to human-induced imbalances in the C cycle (Keeling and Graven, 2021). Moreover, the ability of ESMs to accurately project future climate is limited by uncertainties in the major fluxes between biosphere and atmosphere, ultimately affecting the predictions on the role of terrestrial ecosystems to work as a sink or source of C in future climatic scenarios.

Undisturbed tropical forests, in particular, might have strong C uptake rates (Stephens et al., 2007). Additionally, it has been estimated that tropical forests store around 46 % of the C in terrestrial ecosystems worldwide (Soepadmo, 1993), even though they account only for ca. 13 % of the ice-free land on the Earth's surface (Saugier et al., 2001). Especially tropical rainforests are relevant for regulating the heat and moisture being transported in the tropics, holding substantial biodiversity and storing C in a variety of ecosystems (Fu et al., 2018). The largest rainforest in the world is the Amazon rainforest, located in the Amazon Basin which is drained by the Amazon river, the largest river in the world in volume discharge, and its tributaries. This biome spans eight countries in South America, including Brazil, Bolivia, Peru, Ecuador, Colombia, Venezuela, Guyana, and Suriname, in addition to French Guiana (an overseas territory of France). The Amazon rainforest also contains a variety of ecosystem types such as *terra-firme*, *várzea*, *igapó*, *campina*, savanna, and *campinarana* (Villa Zegarra, 2017). All these ecosystems play particular roles in the C cycle within the Amazon rainforest, and in terms of extension, *terra-firme* is the dominant ecosystem.

Taking into account the importance of the Amazon rainforest for climate, including potential global warming mitigation, it is crucial to (i) better understand the carbon cycle in this biome and (ii) estimate quantities that might help to characterise its land C sequestration.

Soepadmo (1993) enumerated basic ecological data, whose accurate and up-to-date quantification are fundamental requirements for establishing whether tropical rainforests are net sources or sinks of C:

1. actual extent, structural and floristic variation and the developmental stages of the forest;

2. capacity of the different forest types of store/release organic matter/carbon;

3. rate of primary production; and

4. rate of deforestation.

The second point on Soepadmo (1993) recommendations can be tackled by the estimation of the mean transit time of C in the ecosystem (Lu et al., 2018), one of the objectives addressed in this doctoral thesis.

Despite the high complexity of Amazon forests, several studies have been performed in the whole Amazon Basin, helping to tackle with the requirements pointed by Soepadmo (1993). Previous studies in Amazon forests have shown a tremendous degree of spatial and temporal variability. It has been shown that not only the above- and belowground biomass, but also the mean residence time of woody biomass can largely vary from eastern to western Amazon (Malhi et al., 2009). Studies measuring net biomass changes and net CO_2 flux exchange have shown large variability from wet to dry years, and as well as a consequence of forest disturbances such as winds. Nevertheless, these previous studies have seldom focussed on the ecosystem scale, directing attention instead to specific components such as roots (e.g. Telles et al. (2003) and Trumbore et al. (2006)), wood (e.g. Vieira et al. (2005)), and soils (e.g. Trumbore et al. (1995) and De Camargo et al. (1999)).

Another relevant aspect concerning the carbon cycle of this biome is the time scales of carbon cycling and storage, which has been less explored in previous research. Nevertheless, some important studies have been able to determine the time that carbon stays in an ecosystem and in different pools. For instance, Trumbore and De Camargo (2009) have shown that carbon can stay for less than a year in leaves and labile compartments, while it can stay for decades and centuries in wood and soil organic matter. They estimated the mean age of the ecosystem respired CO_2 and built a simple scheme synthesizing data from different studies (Figure 1.1), where the fluxes are based on Chambers et al. (2004); mean age of decomposing wood based on Vieira et al. (2005) and wood decomposition rates of Chambers et al. (2001a); age of C derived from dead root decomposition from Trumbore et al. (2006); mean age of litter respired CO_2 from Brando et al. (2008) and, by the time of publication (2009), unpublished data from Trumbore and De Camargo (2009).

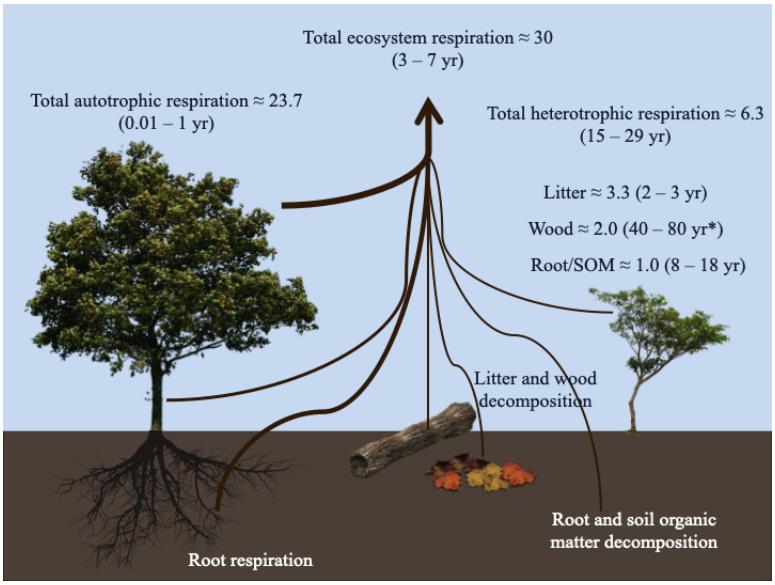

FIGURE 1.1: Calculation of mean age of ecosystem respired CO_2 as an average of the respired CO_2 from different ecosystem compartments in Amazon. Fluxes are given in Mg C ha^{-1} yr^{-1} (1 Mg C ha^{-1} yr^{-1} = 0.264 μmol m^{-2} s^{-1}). Figure adapted from Figure 3 in Trumbore and De Camargo (2009).

Hence if one wants to get a better insight into the biogeochemical processes that govern the carbon cycle and intend to have any degree of predicability regarding the response of those ecosystems to climate change, it becomes fundamental to determine accurately the time metrics involved in carbon cycling. Given that Amazon forests are highly heterogeneous in terms of biomass and fluxes, it is less clear than in other forests how variable are they in terms of their time scales of carbon cycling.

The carbon cycle, a quite dynamical process, can be described by linear ordinary differential equations (ODEs); however, it is more realistically modelled through nonlinear ODEs. In the latter case, the results cannot be easily obtained analytically, though, numerically. Moreover, a better description of ecological models is based on non-autonomous (i.e. time-dependent) ODEs (Metzler et al., 2018). Indeed, when studying terrestrial carbon dynamics responding to climate changes, we can find examples of terrestrial carbon models with time-dependent functions instead of constant model parameters (Rasmussen et al., 2016). Nevertheless, most of the uncertainties with respect to the predicability of ESMs related to C storage and the capacity of ecological systems to function as a sink or source of C are associated with the uncertainty in estimating C outputs and cycling rates or the processes that control them (Sierra et al., 2017), even in the autonomous case. In this sense,

calculating metrics, most of them related to the time that the C spends in a compartmental system, thus, called *system diagnostic times*, can be decisive in determining the performance of a model (Randerson et al., 2002).

The main system diagnostic times that can contribute to our understanding of the C cycle are *age* and *transit time*. In the literature, there are some slightly different definitions for those quantities. Sometimes this lack of a consensual definition can generate problems for the estimations of these time scales and their interpretations (Sierra et al., 2017). Here, I will use *age* as the time elapsed since a C species entered the system until the time of observation in a specific compartment, whereas *transit time* is defined here as the time between the C species entered the system until it leaves. Equivalently, the transit time can be defined as the age of the C species when it leaves the system boundaries (Sierra et al., 2017). For tropical forests, we can thus think about age as the time that has passed since the C entered the ecosystem through photosynthesis and our measurement inside a compartment, and the transit time as the time since the C entered the system through photosynthesis until it is observed in the efflux (e.g. as respired CO_2).

Besides the importance of knowing the C transit times to understand and integrate the rate of different ecosystem processes (Trumbore, 2006), the transit time distribution can also be used as an important diagnostic metric for vegetation models (Ceballos-Núñez et al., 2018). However, to correctly quantify ages and transit times in dynamical ecosystems, it is crucial to correctly design the corresponding dynamical model, since these quantities are not directly measured in the field, but theoretically calculated in a mathematical framework. There have been recent advances in the theoretical framework for the quantification of time scales using the theory of compartmental dynamical systems (Rasmussen et al., 2016; Luo et al., 2017; Metzler et al., 2018).

The C transit time depends on information on the C age structure of all the different compartments and their contribution to total respired CO_2, which are challenging quantities to measure in the field (Lu et al., 2018). Radiocarbon (^{14}C) analysis is a powerful tool to approximate the age structure of ecosystem compartments and respired CO_2 (Trumbore and De Camargo, 2009; Sierra et al., 2017; Lu et al., 2018), and therefore can provide the required data for the estimation of ecosystem-level transit times.

Radiocarbon is a radioactive isotope of C with a half-life of 5,700 $\pm$ 30 years

(Kutschera, 2013). It can be produced either naturally from the interaction of cosmic rays with the upper atmosphere of Earth - known therefore as cosmogenic - or artificially, e.g. in nuclear power plants or through nuclear weapon tests.

Radiocarbon in closed systems is being explored since the 1950s, when W. Libby developed the radiocarbon dating method (Libby, 1952; Libby, 1960). For such applications the cosmogenic origin of ^{14}C is considered. In closed systems, due to the absence of a flux within the environment, there is no mixing of C of different ages and therefore radioactive decay can be used to date artifacts. However, in open systems C of different ages mixes and therefore there is a mix of matter with different ^{14}C signatures. In addition, in contexts where the C sample is modern, we should take into account the human-made ^{14}C contribution, especially from the nuclear bomb tests, being called bomb ^{14}C. In this case it is possible to obtain information on the exchange of C occurring in time scales of years to decades, which is not possible with cosmogenic ^{14}C.

The so-called bomb spike is represented by an empirical curve built with data of the ^{14}C content in the atmospheric CO_2, which includes measurements during the nuclear weapons tests occurring in the atmosphere (1955 - 1963) (Hua et al., 2013; Hua et al., 2021). As thermonuclear bombs release a large amount of energetic neutrons, the same reaction responsible for the production of ^{14}C in the upper atmosphere, i.e. the nuclear reaction of a thermal neutron with a ^{14}N atom, takes place. Therefore, the curve shows the excess of ^{14}C released into the atmosphere, achieving its maximum – almost the double of the natural level (Nydal, 1968; Levin et al., 1985) – around 1963 CE, when the Partial Test Ban Treaty was signed.

An important remark is that diagnostic times such as ages in multiple-pool systems are not simply the conventional radiocarbon age, which relies on some assumptions such as the system being closed and represented by one single homogeneous pool of well mixed C. These assumptions are clearly not met in the case of terrestrial ecosystems. Thus ^{14}C content in terrestrial ecosystem's compartments is reported not as radiocarbon age but as $\Delta^{14}C$. $\Delta^{14}C$ includes the $^{14}C/C$ of the sample normalised to $\delta^{13}C$ (stable C isotope ratio of sample with respect to reference material) by oxalic acid standard (OxII). Additionally, $\Delta^{14}C$ is corrected for radioactive decay since 1950 using the updated ^{14}C decay constant $\lambda = \frac{1}{8{,}267}\ yr^{-1}$ (Stuiver and Polach, 1977).

Although it is possible to use the $\Delta^{14}C$ values to constrain models, there is still a gap in how exactly such quantity distributes inside the compartments, mainly due

to the lack of theory and methods to compute radiocarbon distributions for open systems. This is addressed as one of the objectives of this thesis.

To model systems that are cycling material over time due to dynamical processes, we can take advantage of the theory of dynamical compartmental systems. Basically, one should parametrize a system as a set of compartments, where each compartment consists of some material amount kinetically homogeneous (Jacquez and Simon, 1993; Metzler and Sierra, 2018). For the compartmental system it is possible to define contents (e.g. C) and fluxes from and to other compartments as well as beyond the system boundaries. The influxes and outfluxes can be dependent on or independent of time and the dynamics of the configuration is described by ODEs. Additionally, and for the sake of simplicity, one can write the set of equations using a matrix representation. Therefore, the mathematical representation of a time-dependent compartmental system reduces to:

$$\frac{d\vec{x}(t)}{dt} = \vec{u}(t) + \mathbf{B}(t)\vec{x}(t) \tag{1.1}$$

where $\vec{x}$(t) is the vector of contents, $\vec{u}$(t) is the vector of inputs, and $\mathbf{B}(t)$ is a compartmental matrix, whose off-diagonal entries b_{ij} are the fractional transfer coefficients.

We can solve such equations analytically (for autonomous systems) or numerically (non-autonomous systems) and obtain diagnostic times, as ages and transit times, which have the form of phase-type distributions.

When the material considered in the compartment are ^{14}C atoms, the equation (1.1) includes an additional term to account for radioactive decay and becomes (Sierra et al., 2014):

$$\frac{d^{14}\vec{C}(t)}{dt} = \vec{I}_{^{14}C}(t) + \mathbf{B}(t)^{14}\vec{C}(t) - \lambda\ ^{14}\vec{C}(t) \tag{1.2}$$

where $^{14}\vec{C}$(t) is a vector that represents the amount of ^{14}C in the compartments, $\mathbf{B}(t)$ is again the compartmental matrix, $\vec{I}_{^{14}C}$(t) represents the vector of ^{14}C inputs, and λ is the ^{14}C decay constant.

Thus, the inputs are intrinsically time-dependent, since the input of ^{14}C in a living system is labelled by the bomb spike, and the isotopic signals vary among the years. It is also important to notice that the equation (1.2) contains an additional term, referring to the radioactive decay. This term represents a small contribution to the ^{14}C content changing over time for modern samples, as it is equal to

0.00012096 yr^{-1}. However, it is a relevant term in the estimation of time distributions from radiocarbon values, as the C mass changing in the compartment becomes isotope-dependent, because only ^{14}C undergoes radioactive decay. In principle, one cannot account for this dependency with the current theory.

1.1 Objectives and research questions

The **main objective** of this thesis was to *advance the theory of open compartmental systems by developing methods to use radiocarbon for the quantification of system diagnostic times*. In particular, I focused on developing a numerical algorithm to relate the concept of age distribution in a compartmental system with the corresponding distribution of radiocarbon. I tested these ideas with comprehensive measurements of radiocarbon in an Amazon rainforest, a test case that represents one of the most complex open compartmental systems on Earth.

This thesis is composed of **three specific objectives**, which are:

Objective 1. Develop an approach to use radiocarbon determinations for understanding C cycling in open compartmental systems.

Objective 2. Collect samples of compartments and ambient air for radiocarbon measurements on a highly complex ecosystem such as an Amazon rainforest.

Objective 3. Use radiocarbon measurements to estimate the mean transit time of C in the Amazon rainforest.

Objective 1 is covered in chapter 3, which addresses the following research questions:

(i) How do distributions of radiocarbon in terrestrial compartments change over time as a consequence of changes in atmospheric radiocarbon?

(ii) How do empirical data compare to these conceptual radiocarbon distributions?

(iii) What insights can these distributions provide for experimental and sampling design for improving model-data comparisons by capturing the entire variability of $\Delta^{14}C$ values?

Objective 2 requires not only a clear sampling strategy, but also a dedicated set up for the analysis of the samples, especially air samples, for ^{14}C-AMS. Such set up did not exist in the Radiocarbon Laboratory of the Universidade Federal Fluminense (LAC-UFF). It was developed as part of this thesis to complement LAC-UFF with a new line of research and it is described in the section 2.5.

Chapter 4 covers the results related to objectives 2 and 3 through the following research questions:

(i) Can we observe differences in the cycling rates between *campinarana* and *terra-firme* using Δ^{14}C measurements alone?

(ii) How Δ^{14}C values give us insights into the cycling rates of different compartments?

(iii) How long does carbon take to be respired by a *terra-firme* ecosystem in central Amazon?

Chapter 5, the final chapter of this thesis, summarises the main findings of the studies I performed in the past four years as a PhD student. It also provides an outlook for ideal strategies that would complement this thesis and are encouraged to be performed in (near) future research.

Chapter 2

Radiocarbon: Chronometer and tracer

Radiocarbon (^{14}C) is a long-lived radioactive isotope of C (half-life $t_{1/2}$ = 5,700 $\pm$ 30 yr, Kutschera (2013)). Radiocarbon is mostly know for its use as a dating tool, especially prominent in fields such as archaeology and palaeoclimate. In these contexts it can be used to build chronologies from 300 $\sim$ 55,000 years ago.

Radiocarbon is also prominent in environmental sciences for tracing the C dynamics of ecosystems. Recent changes in atmospheric radiocarbon driven by aboveground nuclear weapons tests allow tracking excess ^{14}C in C reservoirs on timescales shorter than what can be determined using radioactive decay.

Different applications of ^{14}C are linked to different data reporting and interpretations of the radiocarbon measurements. In this chapter the main processes related to ^{14}C production, its assimilation in C reservoirs and its spontaneous decay are presented. Further, the distinction and underlying assumptions on the use of ^{14}C as a chronological tool and as a biological tracer are discussed. These differences lead to distinct manners to report radiocarbon data, which are also described in this chapter.

Radiocarbon contents can be determined based on its emitted radiation (activity) or the number of ^{14}C atoms in a sample (concentration). Here, the focus is on the radiocarbon concentrations determined by accelerator mass spectrometers (AMS).

In South America, only one complete facility for ^{14}C-AMS is at disposal. A radiocarbon preparation laboratory and a single stage AMS compose the facility called LAC-UFF (Radiocarbon Laboratory at Universidade Federal Fluminense), located in Brazil (Macario et al., 2013). Since 2009, LAC-UFF collaborates with scientists of a variety of fields spanning from archaeology to environmental studies. As the range of collaborating fields expands, so do the experimental methods applied at LAC-UFF. In the scope of this thesis, it was necessary to extract CO_2 from air samples for radiocarbon measurements. To enable the preparation of air samples for ^{14}C-AMS

at LAC-UFF, a dedicated extraction and purification line was built. The details on the construction, required adaptations and installation of this line are also discussed in this chapter.

2.1 Radiocarbon dynamics

Carbon (C) is a nonmetal element of atomic number six, belonging to the Group 14 (IVa) of the periodic table. Carbon represents only ca. 0.025 % of the Earth's crust in its three natural isotopes: ^{12}C, ^{13}C and ^{14}C. These three isotopes of C differ according to their mass number, abundance in nature and nuclear stability. Carbon-12 (^{12}C) is a stable isotope, with mass number 12 and it represents ca. 98.9 % of the C on Earth. Carbon-13 (^{13}C) is a heavier stable isotope of C, representing 1.1 % of the C in nature (Rosman and Taylor, 1998). Carbon-14 or radiocarbon (^{14}C) is the only natural radioactive isotope of C, with eight neutrons in its nucleus, and corresponds to just ca. 10^{-10} % of the total amount of C on Earth. Radiocarbon emits beta particles (β^{-1}) to achieve stability and has a half-life of ca. 5,700 years.

2.1.1 Production

Radiocarbon can be produced through different nuclear reactions, always involving the absorption of a neutron by an atom of carbon, oxygen or nitrogen (Davis Jr, 1977). The natural production of ^{14}C on Earth occurs mostly in the stratosphere and it is dominated by the following nuclear reaction[1]:

$$^{14}N(n,p)^{14}C \tag{2.1}$$

where ^{14}N is a stable nitrogen atom with mass 14, n is a neutron and p is a proton.

In the nuclear reaction of equation (2.1) the neutrons are on thermal energy level, as they come as secondary particles slowed down by inelastic and elastic collisions of primary cosmic rays from outside the Solar System with the Earth's upper atmosphere. Therefore, the ^{14}C produced in this way is a cosmogenic element. Most of the cosmogenic ^{14}C is produced in the stratosphere and a small proportion is produced on the Earth's surface, being called cosmogenic *in situ* radiocarbon.

[1] An alternative notation is $^{14}N + n \rightarrow {}^{14}C + p$

Another channel for production of ^{14}C was recently discovered by Enoto et al. (2017). It is related to atmospheric photo-nuclear reactions triggered by lightnings. However, this route is still not well understood and it seems to produce rather negligible amounts of ^{14}C. Thus, it will not be further discussed in this thesis.

Other routes can produce ^{14}C through the reaction of neutrons with carbon-13, oxygen-16 or -17 and nitrogen-15. They can occur especially in nuclear power plants from the interaction of thermal or non-thermal neutrons with the atoms in the fuel or structural material of the reactors. In the global reservoir of carbon their contribution is rather negligible. However, nuclear weapon tests in the atmosphere may produce considerable amounts of radiocarbon. In this case, the presence of thermal neutrons in the atmosphere as a by-product of the hydrogen bombs produces radiocarbon after the interaction with ^{14}N, following the same nuclear reaction as equation (2.1).

The natural cosmogenic production of ^{14}C in the atmosphere occurs constantly at a rate of ca. 1.64 atoms cm^{-2} s^{-1} in the modern epoch (Kovaltsov et al., 2012).

Natural variations

The cosmic rays that will culminate in the production of radiocarbon are mostly from outside the Solar System (galactic cosmic rays, GCR). Solar Energetic Particles (SEP) have less energy than GCR to end up producing secondary neutrons in the range of energies necessary for the reaction 2.1 to take place. However, SEP events might influence the natural production of ^{14}C in the upper atmosphere. In events of solar flares or interplanetary coronal mass ejection, when high concentrations of SEP may be emitted, additional ^{14}C might be created. Indeed, it is estimated that in the last 50 yrs, SEPs have contributed to ca. 0.25 % of the global cosmogenic ^{14}C production (Kovaltsov et al., 2012).

The Sun's magnetic field is subjected to several periodic variations, e.g. in the Schwabe cycle (11-year amplitude change), Hale cycle (22-year polarity reversal of the magnetic field), Gleissberg cycle (80-year swaying of magnetic pole) and a few other variations in longer time scales. The variations in the solar magnetic activity modulate the energy spectrum of GCR penetrating Earth's atmosphere, influencing ultimately the production of cosmogenic radiocarbon (Masuda et al., 2009).

The magnetic field of Earth might also vary in intensity over time. Since cosmic rays are mostly composed by protons, the geomagnetic field intensification might

shield the charged particles and promote a decline on the production of ^{14}C that varies with latitude.

The rate of production of ^{14}C by GCR is, thus, ultimately dependent on solar magnetic activity and geomagnetic field. These parameters can be quantified through the Sun's modulation potential (ϕ) and the Earth's dipole moment (M) (Köhler et al., 2022).

The natural variations influencing the ^{14}C production lead to the alterations of the radiocarbon concentrations in the atmosphere in the past 55,000 years (Reimer et al., 2020; Hogg et al., 2020). The rapid increase of ^{14}C concentrations in the atmosphere within one year observed on the radiocarbon records from tree-rings might be associated to solar proton events in the past. These events have been known as Miyake events (Miyake et al., 2012; Miyake et al., 2013; Miyake et al., 2014; Miyake et al., 2017) and are related to a field of study using radiocarbon as a proxy for the solar activity variation in the past.

Anthropogenic effects

The observed variations in atmospheric ^{14}C concentrations are also connected to anthropogenic actions. Two main counteracting effects induced by humans influenced the atmospheric ^{14}C concentrations in the recent history: the burning of fossil fuels and the nuclear weapons tests.

From the second half of the 18^{th} century through the 19^{th} century, Europe experienced an increase in the development of society promoted by the Industrial Revolution. The emergence of machines fueled by coke (obtained from the heating of coal) allowed less expensive and larger production of goods. However, as coal is a fossil material, it contains effectively no ^{14}C. Therefore, the CO_2 product of the burning of fossil fuels increases the concentrations of $^{12}CO_2$ and $^{13}CO_2$ in the atmosphere, diluting the radiocarbon isotopologue. This effect is known as *Suess effect* (Suess, 1955).

In the late 1950s and early 1960s a counteracting effect on the radiocarbon concentrations in the atmosphere was supported by nuclear weapons tests. The thermal neutrons emitted by nuclear bombs reacted with the abundant ^{14}N in the stratosphere and produced ^{14}C (hereafter bomb ^{14}C) through the same reaction producing natural ^{14}C (equation 2.1).

Between 1955 and 1959, human-made ^{14}C was produced 15 times faster than by the natural mechanism (Broecker and Walton, 1959). Vries (1958) suggested an

increase of 4.3 % in the atmospheric $^{14}CO_2$ in the Northern Hemisphere (NH) for the period between 1953 and 1957 based on flesh of mussels. Münnich and Vogel (1958) also observed an increase on the atmospheric $^{14}CO_2$ in central Europe at a rate of 3.2 % yr^{-1} between 1954 and 1957. Indeed, nuclear weapons tests promoted a global rise of $^{14}CO_2$ concentrations until the Partial Test Ban Treaty (PTBT) took place in October 1963.

The PTBT limited the nuclear weapon tests to underground, which halted the production of bomb ^{14}C impelled by the nuclear weapon tests performed aboveground. After the PTBT, there was a decline on the radiocarbon concentrations in the atmosphere, as a consequence of the uptake of excess $^{14}CO_2$ by the biosphere and hydrosphere. The sharp rise and further decline of radiocarbon concentrations in the atmosphere is described as the 'bomb spike' or 'bomb peak'. The peak occurs in the NH in 1964 CE, when the radiocarbon concentrations are about 100 % higher than the natural level. In the Southern Hemisphere (SH), the peak occurs in 1965 CE and it is slightly lower. The lower SH ^{14}C peak is believed to be a consequence of a higher uptake by the extended area of the oceans in the SH. Additionally, the ^{14}C from the tests mostly performed in the NH takes about a year to get mixed worldwide.

The uniqueness and versatility of the isotopic signal from the bomb peak nurtured a myriad of applications ranging from archaeology and forensics to environmental sciences (Kutschera, 2022).

2.1.2 Assimilation

After its cosmogenic or anthropogenic production in the upper atmosphere, radiocarbon gets quickly associated with oxygen, becoming radiocarbon monoxide (^{14}CO). The ^{14}CO is further oxidised through the hydroxyl radical (OH^-) turning into $^{14}CO_2$ in a few months (Trumbore et al., 2016). The $^{14}CO_2$ is mixed in the global troposphere in roughly a year, and it is constantly exchanged among the biosphere and oceans through the carbon cycle (Figure 2.1).

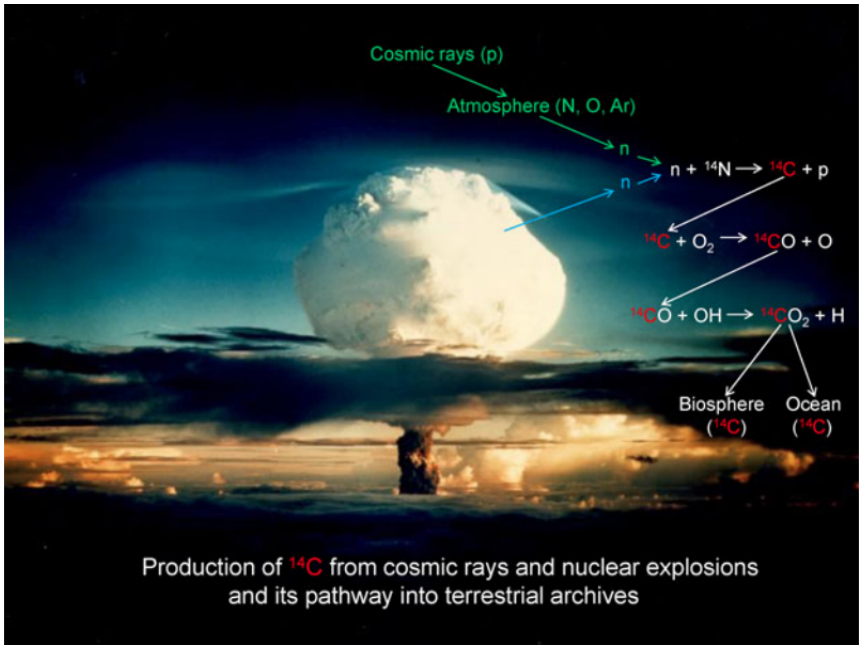

FIGURE 2.1: Main reactions related to the production of ^{14}C and formation of $^{14}CO_2$ in the atmosphere until its assimilation into the biosphere and oceans through the C cycle. Figure from Wild et al. (2019).

All the C isotopologues of CO_2 enter the carbon cycle through the photosynthesis, where they are absorbed from the atmosphere and converted into organic C. Some CO_2 is also diffused in the ocean through the air-water interface. While C isotopes travel through C reservoirs, they can suffer fractionation effects. This effect is responsible for alterations in the abundances of the isotopes when compared to the input (i.e. the atmosphere).

Fractionation effect

The chemical properties of ^{12}C, ^{13}C and ^{14}C are the same, as they have the same number of electrons. However, the differences in the number of neutrons in the nucleus, which corresponds to the differences in their atomic weights, determine the partition of C isotopes under chemical or physical processes. This discrimination for a heavier or lighter isotope in a natural system is the *fractionation effect* (Craig, 1953).

Ultimately, this implies that the relative abundances of C isotopes vary among C reservoirs. For instance, photosynthesis, especially in C_3 plants, tends to select ^{12}C over ^{13}C or ^{14}C, as the chemical bonds at lower energies with ^{12}C promote a faster

reaction and diffusion when compared to the heavier isotopes (Vogel, 1980). Fractionation effects are not restricted to natural processes. Isotopic fractionation might also occur in laboratories, during the chemical or physical treatments of samples; for example, due to an incomplete reduction of CO_2 to C_{gr} in the graphitisation reaction (e.g. Macario et al., 2015; Macario et al., 2016; Rinyu et al., 2013).

The stable C isotope ratio ($^{13}C/^{12}C$) on a sample when compared to a standard material, gives us the isotopic fractionation affecting the sample. The fractionation effect, however, generates relatively small differences in the isotope ratios of sample and standard. Therefore, the differences are referred in parts per thousand (‰), also called parts per mille. The δ-notation captures all these aspects:

$$\delta^{13}C = \left(\frac{\frac{^{13}C}{^{12}C}|_{\text{sample}}}{\frac{^{13}C}{^{12}C}|_{\text{standard}}} - 1 \right) \times 1000\ [‰] \tag{2.2}$$

The mass-dependent fractionation effect between ^{13}C and ^{12}C has about the same magnitude of the one between ^{14}C and ^{13}C, as the difference in both cases is of one neutron mass. Therefore, in a first approximation, the mass-dependent fractionation for ^{14}C to ^{12}C is nearly $2 \times \delta^{13}C$ (Craig, 1954). However, it is known that the fractionation ratio can deviate from this value of 2.0. Some experiments reporting the deviations of this value and an interesting discussion on the impacts of the deviation on radiocarbon dating is provided by Fahrni et al. (2017).

2.1.3 Decay

The radioactive decay is a physical phenomenon that is independent of environmental factors, such as temperature or physical state of the substance formed by the radioactive element. It is characterised by the spontaneous emission of radiation (α, β or γ) by an unstable nucleus.

Because radioactive decay is a stochastic process, we have to take into account ensembles of radioactive atoms when referring to decay properties, such as half-life. Half-life ($t_{1/2}$) is defined as the time that half of a given amount of radioactive nuclei take to decay.

Radioactive nuclei decay with at a constant rate λ, which is characteristic of each radionuclide. Additionally, considering a large number of disintegration events, the relation of number of nuclides decaying in a time interval Δt, can be approximate to a continuum and written as follows:

$$dN = -\lambda N dt \tag{2.3}$$

where N is a certain amount of radionuclides and λ is the decay constant.

Integrating 2.3 over time, we obtain:

$$N(t) = N_0 e^{-\lambda t} \tag{2.4}$$

where N_0 is the initial amount of radionuclides. The decay constant is inversely proportional to the half-life: $\lambda = \frac{ln(2)}{t_{1/2}}$.

N(t) can be simply substituted by activity or concentration of radionuclides. Activity is the number of disintegrations per time unit; the most common reporting units for activity are Becquerel (Bq) and Currie (Ci). One Bq represents one disintegration per second. One Ci = 3.7×10^{10} Bq.

The decay law in terms of activity (A) is

$$A(t) = A_0 e^{-\lambda t} \tag{2.5}$$

and in terms of concentration (C), i.e. the number of atoms of a radionuclide

$$C(t) = C_0 e^{-\lambda t} \tag{2.6}$$

Radiocarbon decays into ^{14}N through beta-minus decay:

$$^{14}C \rightarrow {}^{14}N + \beta^- + \overline{\nu}_e \tag{2.7}$$

where β^- is essentially an electron emitted by ^{14}C nucleus after the conversion of one neutron into a proton and $\overline{\nu}_e$ is an anti-neutrino. For ^{14}C, β^- has an energy around 156 keV (10^3 eletron-Volts).

Several experimental values for the radiocarbon half-life were reported since the detection of natural ^{14}C. Arnold and Libby (1949) estimated a half-life (called *Libby's half-life*) of 5,568 $\pm$ 30 yrs based on a weighted average (weights were the inverse square root of the errors) of the three most reliable estimations of the time. An updated value of 5,730 $\pm$ 40 yrs was reported by Godwin (1962). Kutschera (2013) performed a revised weighted average of ^{14}C half-life, taking also into account estimations performed after 1962. He obtained a half-life of 5,700 $\pm$ 30 yrs, which is also the one reported at the National Nuclear Data Center website.

2.2 Chronometer: Radiocarbon dating

The discovery of the natural radioactive decay of uranium by Antoine Henri Becquerel in 1896 has contributed to the understanding of fundamental mechanisms in theoretical Physics and instigated a multitude of applications, including the absolute dating of several materials. Shortly after, in 1898, the team of physicists formed by Marie Sklowodska Curie and Pierre Curie observed radiation being emitted by other elements and named this phenomenon radioactivity. In 1905, Ernest Rutherford suggested that the spontaneous decay of unstable nuclei could be used as a tool for calculating the age of minerals. In 1907, Bertram Boltwood follows the suggestion of Rutherford and publishes the ages of minerals based on the radioactivity of uranium (Boltwood, 1907). By the 1930s, the radiometric dating based on diverse long-lived radioactive elements was a sophisticated and accurate method of inferring the age of igneous rocks. In the 1940s, after the detection of cosmogenic radiocarbon, Willard F. Libby and colleagues led up to the radiocarbon dating method.

About 70 years ago Libby, Anderson and Arnold landmarked multidisciplinary science and established radiocarbon dating with two historical papers titled "Age determination by radiocarbon content" (Libby et al., 1949; Arnold and Libby, 1949). Libby was awarded in 1960 with the Nobel Prize in Chemistry (Libby, 1960) *"for his method to use carbon-14 for age determination in archaeology, geology, geophysics, and other branches of science"*. Although developments in diverse subareas of radiocarbon studies, such as measurements (Mäntynen et al., 1987; Fahrni et al., 2013; Synal et al., 2007; Freeman et al., 2015; Galli et al., 2013), pretreatments protocols (Brown et al., 1988; Bonneau et al., 2011; Bragança et al., 2021; Oliveira et al., 2021; Talamo et al., 2021), chronological modelling (Bayliss and Bronk Ramsey, 2004; Ramsey, 2009), theory assumptions and conventions (Stuiver and Polach, 1977; Millard, 2014), and applications (Alkass et al., 2010; Hajdas, 2009; Wild et al., 2019; Kutschera, 2022), there is still a gap in our understanding of how we indeed can interpret the radiocarbon content as an actual age. The mismatch becomes less intuitive in the open system's framework.

Minze Stuiver and Henry Polach have proposed in 1977 a standard manner to report radiocarbon ages (Stuiver and Polach, 1977). From that work three main assumptions are taken into account and two standard calculations are suggested when reporting ^{14}C data:

(i) the radiocarbon half-life as the Libby's half-life (5,568 years);

(ii) the atmosphere in the past as constant regarding its ^{14}C content;

(iii) the isotopic signal from the sample as equal to that from the coeval atmosphere, i.e. they were in isotopic equilibrium when the tissue was alive;

(iv) the standard activity as that from the NBS oxalic acid (SRM 4990B)[2], measured directly or indirectly;

(v) normalisation due to isotopic fractionation based on $\delta^{13}C$ = -25 ‰ (relative to the $^{13}C/^{12}C$ ratio of PDB[3]).

Thus the term *conventional radiocarbon age* incorporates these five assumptions. As a consequence of the standardisation with respect to the atmosphere of 1950 CE, the conventional radiocarbon ages are reported as years before 1950. Indeed, 1950 is assumed as present, then the conventional radiocarbon age is reported as *years before present* (yr BP).

Nevertheless, the conventional radiocarbon age is meaningful in closed systems, i.e. systems that do not exchange carbon with the surroundings. Therefore, it is related to the date after an organism's death or isolation.

In a closed system, the only process altering the ratios $^{14}C/C$ is the radioactive decay of radiocarbon. Therefore, to calculate radiocarbon ages we invert either equation (2.5) or equation (2.6), as they are equivalent.

$$t = -\frac{1}{\lambda} ln \left(\frac{A}{A_0} \right) \tag{2.8}$$

where $\frac{1}{\lambda} = \frac{t_{1/2}}{ln(2)}$, which is the mean lifetime. Using Libby's half-life, the mean lifetime is 8,033 yrs.

However, two points need attention here: (i) it is very hard to measure absolute values of C ratios; (ii) radiocarbon decays through a simple decay law, not in series, therefore A_0 is not easily obtained.

[2]NBS stands for National Bureau of Standards, the company which manufactured the SRM (Standard Reference Material) 4990B, an oxalic acid di-hydrate. This company had its name changed in 1988 to National Institute of Standards and Technology (NIST). NIST produced and still sells the new oxalic acid standard SRM 4990C. SRM 4990C is usually referred as OxII.

[3]Pee Dee Belemnite (PDB) was a standard based on calcium carbonate found in the Cretaceous Pee Dee formation in South Carolina, USA. When it was completely used up, it was substituted by the VPDB (Vienna-PDB), a limestone reference material provided by the International Atomic Energy Agency (IAEA) in Vienna.

The literature on radiocarbon notation, including the discussion paper presented by Stuiver and Polach (1977), describes the quantities to report ^{14}C data in terms of activities A. The technique to measure radiocarbon using mass spectrometers coupled to particle accelerators became more popular after the 1980s. Therefore, earlier papers focussed on the notation convenient for radiometric methods to determine radiocarbon contents. Here, I present the main definitions and terminologies based on the activities. However, keeping in mind the activity A = $\lambda \times$ number of radionuclides, one can easily translate the notation to C ratios.

Following the standard report of data presented in Stuiver and Polach (1977), item (v) agree the laboratories should report data that is normalised to -25 ‰, the postulate mean value of terrestrial wood. Back then, this value should be relative to PDB (standard in equation 2.2), however, as it is not available anymore, δ^{13}C is reported with respect to VPDB standard:

$$\delta^{13}C = \left(\frac{\frac{^{13}C}{^{12}C}|_{\text{sample}} - \frac{^{13}C}{^{12}C}|_{\text{VPDB}}}{\frac{^{13}C}{^{12}C}|_{\text{VPDB}}} \right) \times 1000 \; [‰] \tag{2.9}$$

Applying the normalisation to the standard activity of OxII (the current used, as OxI was also used up):

$$A_{ON} = 0.7459 A_{\text{OxII}} \left(\frac{1 - \frac{25}{1000}}{1 + \frac{\delta^{13}C_{\text{OxII}}}{1000}} \right)^2 \tag{2.10}$$

And applying the normalisation to the sample activity:

$$A_{SN} = A_{\text{S}} \left(\frac{0.975}{1 + \frac{\delta^{13}C_{\text{S}}}{1000}} \right)^2 \approx A_{\text{S}} \left[1 - \frac{2(25 + \delta^{13}C_{\text{S}})}{1000} \right] \tag{2.11}$$

where A_S is the activity of sample and $\delta^{13}C_S$ the stable C ratio in the sample. With that, one can define the Fraction Modern F^{14}C as

$$F^{14}C = \frac{A_{\text{SN}}}{A_{\text{ON}}} \tag{2.12}$$

Thus, we can write the **conventional radiocarbon age** as

$$T_{^{14}C} = -8033 \; ln \left(\frac{A_{\text{SN}}}{A_{\text{ON}}} \right) = -8033 \; ln \; F^{14}C \tag{2.13}$$

2.3 Tracer: Radiocarbon in ecology

The carbon cycle promotes a distribution of C in different reservoirs within the Earth System (Figure 2.2). It reflects the movement of C in different parts of the Earth System driven by biogeochemical processes. This distribution is distinct according to the C isotope, which is related to the fractionation effects each isotope suffers in the large number of biological, chemical and physical processes.

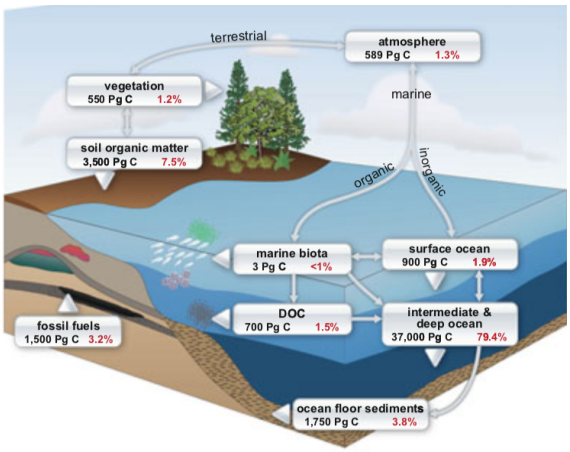

FIGURE 2.2: Distribution of carbon in reservoirs within the Earth System. Black numbers represent the midpoints of the ranges for C stocks (in Pg C) reported in IPCC (2014a) (except for the soil organic matter pool, whose numbers come from Schuur et al. (2015)). Red numbers are the fraction of total C represented by each pool. Figure originally in Schuur et al. (2016).

The dynamics of the C cycle among the pools was in quasi-equilibrium in preindustrial times (pre-1850 by convention), as inputs and outputs in the C reservoirs were roughly balanced out. However, in the Anthropocene (post Industrial Revolution) (Steffen et al., 2011) the effect of fossil fuel burning and other human activities (e.g. deforestation and land use) provokes an imbalance in the global C cycle, as the biosphere cannot keep up with the excess C in the atmosphere.

The formation of $^{14}CO_2$ allows radiocarbon to enter the biosphere through photosynthesis. The radiocarbon incorporated through the C cycle travels among the different C reservoirs. However, as discussed previously, the radiocarbon content in the atmosphere is influenced by anthropogenic activities. The bomb ^{14}C is particularly useful to comprehend the processes cycling C in terrestrial ecosystems in timescales of years to decades.

The distribution of radiocarbon in different C-pools gives us insights into C residence times and mixing rates within the reservoirs (Figure 2.3). Additionally, information on the sources of the C can be obtained from the radiocarbon measurements.

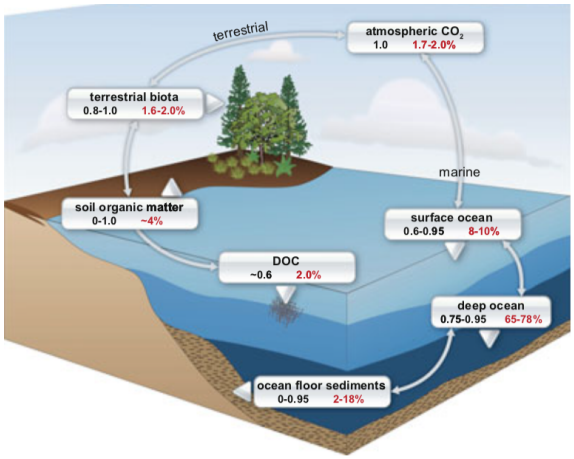

FIGURE 2.3: Distribution of radiocarbon in reservoirs within the Earth System. Black numbers represent the ranges of $^{14}C/C$ relative to atmospheric ^{14}C content in preindustrial times (defined as 1.0, based on wood from 1890). Red numbers (percent of total ^{14}C atoms in the Earth System) correspond to a combination of the total C pool size and the radiocarbon age of the pool. Figure originally in Schuur et al. (2016).

In open systems, the incorporation and release of carbon occurs continuously. So that, even the concept of age can be differently interpreted. While in closed systems the conventional radiocarbon age marks the moment when the system stopped its exchange of carbon with the surroundings, in open systems the *carbon age* represents the time elapsed since the carbon entry until an observation time. Additionally, it is useful to conceptualise a new quantity or time metric called *transit time*. The transit time, as the name suggests, is the time carbon needs to transit a system, i.e. the time passed between the carbon entry and its release.

There are several time metrics in ecological studies. The lack of a consensus in their definitions might be problematic, particularly when one aims to compare estimations (Sierra et al., 2017). The most common nomenclatures and definitions of time metrics of C in ecosystems are (Trumbore et al., 2016):

Turnover time The C stock (total reservoir size) divided by one of the fluxes (either input or output flux of C);

Residence time Across different studies this quantity can have different definitions; sometimes it is define similarly as the mean transit time;

Carbon age Time elapsed since the carbon entry until an observation time;

Transit time Age of the C in the outflux; equivalently, the time passed between the carbon entry and its release.

Radiocarbon can be used not only to understand the C exchange between reservoirs but also to estimate time metrics. The following chapters cover how radiocarbon can be used to better understand the dynamics of pools with different C cycling rates and to estimate time metrics in complex systems, such as the Amazon rainforest.

2.4 Accelerator Mass Spectrometry

Mass spectrometers (MS) were developed in the early 20^{th} century for studies on the fundamental atomic properties. In the 1940s, chemists found other applicabilities for MS from industrial chemistry to biogeochemistry. These applications boosted developments on MS enabling their use as a critical instrument for analytical chemistry.

Certain MS rely on the principle that any charged particle will be deflected by a transversal magnetic field. The resultant (centripetal) force over the particle equals the (magnetic part of the) Lorentz force. Thus, the radius of the curved trajectory of the particle is proportional to the external magnetic field.

$$\vec{F} = q\vec{v} \times \vec{B} = \frac{mv^2}{R}\hat{r} \tag{2.14}$$

where $\vec{F}$ is the magnetic force, q is the charge of the particle, $\vec{v}$ is its velocity, $\vec{B}$ is the external magnetic field, m is the mass of the particle, and R the radius of the trajectory.

As the velocity $\vec{v}$ is perpendicular to the magnetic field in the MS, the magnitude of $\vec{F}$ is qvB. In the non-relativistic approximation ($|\vec{v}| \ll c$[4]), the energy $E = \frac{mv^2}{2}$. Consequently, the radius of the trajectory is proportional to the mass-charge ratio[5] of the particle:

$$R^2B^2 = \frac{2mE}{q^2} \tag{2.15}$$

To determine, for instance, C stable isotope ratio the technique used consisted of separation and measurement of C atoms according to their masses using the conventional MS. However, common MS could not work in further separating radiocarbon

[4] speed of light = 299,792,458 m/s

[5] or relation mass-energy, when charge is selected to a certain value as in the AMS system

atoms. The main reasons are: (i) the abundance of ^{14}C is very small, so a faraday cup (instrument used to measure the currents generated by beams of C stable isotopes in MS) could not measure radiocarbon; and (ii) also due to ^{14}C low abundance, there is a high risk of interference by isobars of ^{14}C, such as ^{14}N, Li_2, ^{13}CH, $^{12}CH_2$ etc.

Radiocarbon dating relied for a few decades since its development on radiometric methods to determine the radiocarbon ages. Radiometric methods for radiocarbon dating englobe any technique whose aim is to estimate the quantity of ^{14}C in a time t based on its emitted beta-radiation.

Developments in metrology, however, overcame the limitations above-mentioned through the so-called accelerator mass spectrometers (AMS). In AMS, ^{14}C atoms are directly counted through a solid state detector and isobars interferences are avoided by a negative ion source and the acceleration stage directly connected to a stripper.

The negative ion source avoids the interference of ^{14}N, an isobar of radiocarbon very abundant in the ambient. Once ^{14}N does not form stable negative ions, already in the source no beam with this isobar can be created. Molecular isobars will be dissociated in a stripper, which consists of a chamber with an inert gas (usually argon or helium). The radiocarbon beam has an energy of a few hundreds keV due to the acceleration stage just before the stripper. Therefore, the collisions with the inert gas will break the molecular bounds, eliminating molecular isobars. Additionally, a certain charge state is selected after the stripper to guarantee only ^{14}C atoms will travel up to the end of the AMS system. In the end, ^{14}C atoms are counted with a sensitive solid state detector, where the charge resulting from the passage of particles through a semiconductor generates a signal. At the same time, the energy is also measured, allowing the further discrimination of radiocarbon against potential insistent interferences.

New generation of AMS include systems with only one stage of acceleration; machines dedicated to radiocarbon quantification. An example is the MICADAS (Figure 2.4), which is the main AMS used in a number of radiocarbon laboratories worldwide, including the ^{14}C-Analytik at Max Planck Institute for Biogeochemistry (MPI-BGC), Jena.

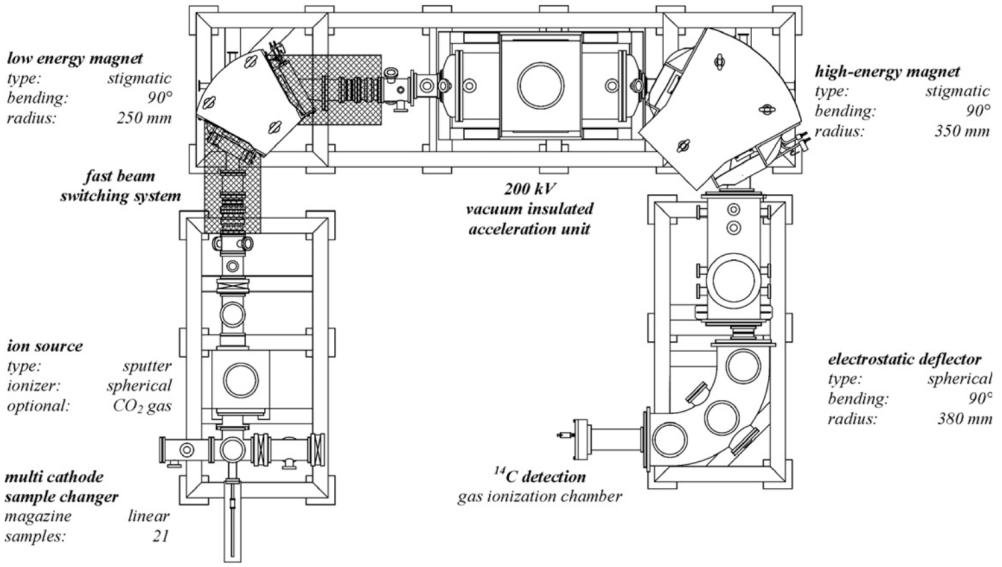

FIGURE 2.4: The layout of the MICADAS system. Actual dimensions of 2.5 m x 3 m (Synal et al., 2007).

Another version of a single stage AMS (SSAMS) system is the one present in the LAC-UFF. It consists of a 250 kV SSAMS system produce by the National Electrostatics Corporation (NEC, USA) (Figure 2.5).

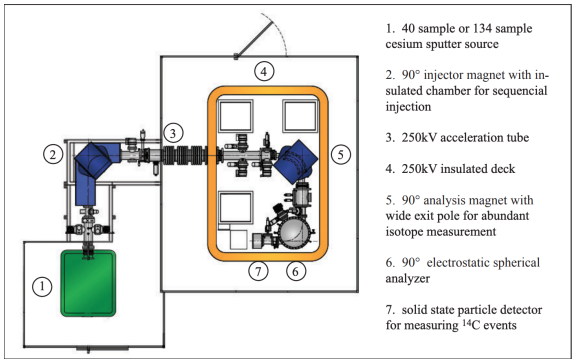

FIGURE 2.5: The layout of the 250 kV NEC SSAMS system with description of the main parts. Scheme from NEC SSAMS manual.

The ion source is a SNICS (Source of Negative Ions by Cesium Sputtering), where cesium (Cs), a heavy alkaline element, produces positive ions and sputters out negative ions from any solid material in the cathode. At LAC-UFF and virtually all the ^{14}C-AMS laboratories worldwide, the target in the cathode is graphite. The stripper gas used at LAC-UFF is helium and the charge state defined is +1.

AMS systems have advantages over radiometric equipments, such as (i) less sample needed (few miligrams instead of grams of material) and (ii) faster measurement for the same resolution, as in AMS the counting time does not depend on the activity or half-life of the radionuclide.

2.5 Gas and Air Samples Purification System - GASPS

The LAC-UFF is the only ^{14}C-AMS facility in South America. LAC-UFF started in 2009 with a preparation laboratory for treating samples for ^{14}C-AMS, including physical and chemical pretreatments, combustion of organic samples, acid hydrolysis of carbonate samples, purification of CO_2 produced by organic and inorganic samples, and conversion to graphite in a variety of materials. In 2012 LAC-UFF has been complemented with the installation of the SSAMS system, becoming independent to perform full analyses of $^{14}C/^{12}C$ ratios by ^{14}C-AMS.

The main materials analysed at LAC-UFF in the past years consisted of charcoal, sediments, soils, shells, otoliths, bones, biopolymers and fuels. The kind of materials analysed and research lines followed in the laboratory correspond to the main requests of scientific collaborations especially from Brazil. The work of this thesis strengthened a new collaboration, through the ATTO project, which in turn requests the analysis of $^{14}CO_2$ from air samples. The main adaptation required to deal with air samples for determination of $\Delta^{14}C$–CO_2 concerns the step of extraction and purification of CO_2 in the sample.

For the routine samples prepared at LAC-UFF, it is necessary to isolate the CO_2 produced from organic or inorganic samples. This is done by releasing the combusted or hydrolyzed sample in a line connected to a vacuum pump. With the pressure difference, the gas travels from the start point in the direction to the pump at the other end of the line. On the path there are cryogenic traps to hold first the water (a dry ice/ethanol mixture at -78 °C) and secondly the CO_2 (with liquid nitrogen at -196 °C), so that the other by-products can be pumped out. The pure CO_2 is transferred to graphitisation tubes (GT), which contain zinc (Zn) and titanium(II) hydride (TiH_2) in the bottom of a larger tube and iron powder (Fe) inside a small tube settled in the larger tube (Figure 2.6).

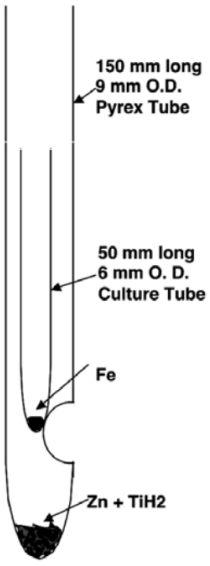

FIGURE 2.6: Pictorial representation of a graphitisation tube (GT) with the reagents for graphitisation. Figure originally in Xu et al. (2007).

Routine samples and standards have a low volume of gas (< 15 mL), which is sufficient to yield 1 mg of C to be targeted in the AMS system. Air samples contain

a mix of several gases (e.g. O_2, N_2, CO_2, water vapour).

Analogously to the vacuum lines for routine samples, the aim with air samples is to isolate the CO_2 to convert it to graphite. Air samples are collected in three-liter flasks with a pressure of ca. 1.6 bar. Yet the principles are the same applied to routine samples, i.e. cryogenically purifying and trapping the CO_2 and transferring it to a GT, caution must be taken to avoid the sample travels too fast in the system. The two main reasons are: the sample might not get trapped and the high volume of gas in a short time might force the turbo molecular vacuum pump, causing an emergency shut-off. Therefore, it is important to control the flux of air being inserted in the line. Controlling the flux manually is risky and not efficient. A mass flow controller (MFC) can do the task more easily. Since it is installed in a high vacuum line, the required specification is a low Δp flow controller, as it guarantees the whole air mass inside the flask is going to be transmitted to the line, even when the pressure difference is low (< 1 mbar).

To avoid compromising the output of samples prepared at LAC-UFF by adapting one of the existing lines for CO_2 extraction from air samples, it was decided to build a new vacuum line dedicated to this purpose. Ideas for the design of the line covering the requirements to successful extraction of CO_2 from air samples were discussed at the Central Radiocarbon Laboratory (CRL) of the Integrated Carbon Observation System (ICOS) network, in Heidelberg. ICOS-CRL performs measurements of $^{14}C/C$ in atmospheric CO_2 from samples all over Europe. At ICOS-CRL a dedicated automated Extraction and Graphitisation Line (EGL) was developed to allow high quality ^{14}C-AMS measurements of up to 1,500 samples per year. The system was thoroughly tested, following high standard quality control. Details, including list of materials and results of quality control measurements, are presented in the astonishing thesis of Dr. Johannes Lux (Lux, 2018). The discussions with Dr. Lux led to the construction of the line named Gas and Air Samples Purification System (GASPS) at LAC-UFF.

However, there is a number of differences between GASPS and EGL. I rank them regarding three points: (i) type of samples; (ii) automation; and (iii) graphitisation procedure. Whereas EGL is designed to extract CO_2 solely from air samples of the ICOS network, GASPS is meant to be more flexible, being enable to purify CO_2 from combusted samples and from inorganic samples hydrolysed with phosphoric acid.

The trade-off of more flexibility is reflected in the need of a more complicated

algorithm to automate the extraction. Moreover, despite automation would be beneficial for saving time in this step of treatment of samples, one needs time to set an efficient software. Unfortunately, it could not be fit in this thesis.

Lastly, the graphitisation procedure is handled differently at ICOS-CRL and LAC-UFF. At ICOS-CRL the graphitisation is done in-line. In a simplified description, the pure CO_2 is inject in reactors where a reaction catalysed by Fe in a hydrogen/water (H_2/H_2O) atmosphere reduces the CO_2 to C (Němec et al., 2010; Lux, 2018). At LAC-UFF the method employed at the graphitisation is the modified zinc reduction, following the procedure described in (Xu et al., 2007), but with certain adaptations to increase the accuracy in the measurements respecting LAC-UFF's set-up (Macario et al., 2015; Macario et al., 2016; Macario et al., 2017). As above mentioned, the pure CO_2 is transferred to GT. The GT containing the reagents and the CO_2 is sealed in the line and baked at 550 °C for 7 hours. The reactions taking place can be summarised as (Verkouteren and Klouda, 1992; Xu et al., 2007; Macario et al., 2016):

$$TiH_2 \xrightarrow{440\ ^\circ C} Ti + H_2 \tag{2.16}$$

$$CO_2 + H_2 \overset{Fe}{\rightleftharpoons} CO + H_2O \tag{2.17}$$

$$CO_2 + Zn \rightarrow CO + ZnO \tag{2.18}$$

$$H_2O + Zn \rightarrow H_2 + ZnO \tag{2.19}$$

$$CO + H_2 \xrightarrow[500-550\ ^\circ C]{Fe} C_{graphite} + H_2O \tag{2.20}$$

$$CO + CO \overset{Fe}{\rightleftharpoons} C_{graphite} + CO_2 \tag{2.21}$$

$$CO + H_2 \overset{Fe}{\rightleftharpoons} C_{graphite} + H_2O \tag{2.22}$$

$$CO + 3H_2 \overset{Fe}{\rightleftharpoons} CH_4 + H_2O \tag{2.23}$$

In principle, the sealed tube reaction prevents a full automation of the line, as the

tube seal is perfomed by the operator. Thus, automating the trapping process might not optimise the process, because the operator has to seal the tubes anyway after the purification. There are alternatives, for instance, with an Automated Graphitisation Equipment (AGE, Wacker et al. (2010)) produced by IonPlus, that could allow a full optimisation of GASPS. However, the extra costs of such adaptations should also be taken into account in future work.

2.5.1 List of materials and technical scheme

The materials used in GASPS are similar to the ones used in EGL. Valves, fittings, MFC, pressure gauges and turbo molecular vacuum pump in both systems have the same specifications. A technical difference occurs in the cooling traps. In EGL a coil of bent 1/4" stainless steel tube is used (Figure 2.7).

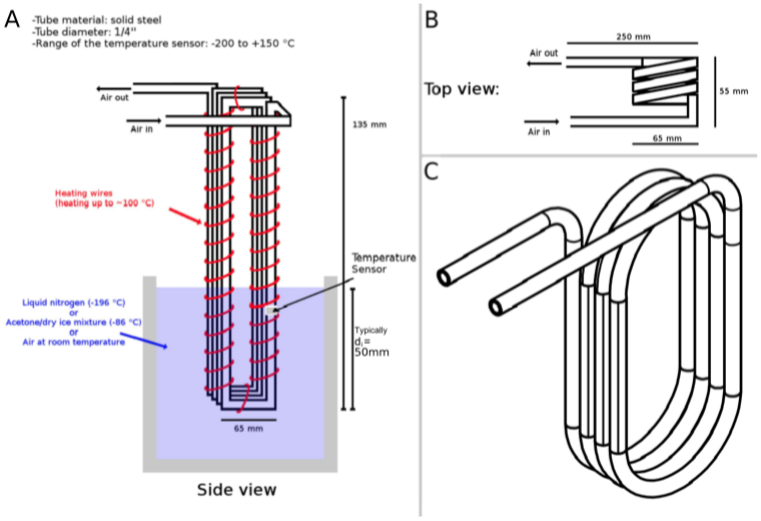

FIGURE 2.7: Schematic view and technical drawing of the cooling trap (coil of bent stainless steel tube) used at EGL. **A**: Side view with heights and width of the trap, on freezing-out immersion depth d_i; **B**: Dimensions of the trap on top view; **C**: Technical 3D drawing of the trap. Figure 3.3 in Lux (2018).

Lux (2018) presented and tested this shape and a configuration where the trap is only partially submerged into the cooling substance, while the top part is heated. He showed this set-up allows a high flow of air with efficient trapping of CO_2, as the CO_2 flakes formed do not obstruct the trap.

Alternatively, glass tube traps with a frit in the connections can avoid this effect, however, with the trade-off that the flow rate in the MFC should be set to 250 ml_n/min instead the high flow used in EGL of 1000 ml_n/min, for the same reasons pointed before, when the sample travels too fast in the system. In GASPS, I opted for a U-shaped glass trap (Figure 2.8).

FIGURE 2.8: Picture of two types of U-shaped glass traps. Picture taken in the ^{14}C-Analytik laboratory at MPI-BGC, Jena. The version on the left side is identical to the ones used in pre-existent purification lines at LAC-UFF. The glass trap with pellets inside (right side) is the version used in GASPS. The pellets increse the surface area with the gas sample.

These U-shaped glass traps are used in other extraction lines already in operation at LAC-UFF and MPI-BGC. They are also used in several laboratories extracting CO_2 from air samples for ^{14}C-AMS (e.g. Turnbull et al., 2007).

The main materials used to build GASPS were:

Mass flow controller Bronkhorst, *F-201DV-ABD-88-V* and
MFC display Bright^{TM} *7.09.200-Bright B2*.

Tubes and fittings Bored-through stainless steel tubes of 1/4" for most of the line and 1/2" in the sections connected to the vacuum pump;
Swagelok connections in stainless steel to stainless steel tubings (1/4" and 1/2");
Ultra-torr connections to glass materials, such as glass tube traps and GT;
Convoluted flexible tubes (3/8" x 6", 1/2" x 6" and 1/4" x 12").

Vacuum pump Pfeiffer, Turbo pump HiCube 80 Eco, *PM-015-888-AT*

Glass traps The U-shaped glass tubes used for cryogenic traps in GASPS were ordered on demand to a German glass company. Therefore, there is no serial number associated to it.

Pressure sensors Pfeiffer, CPT 200, *PT R36 130* and
Pfeiffer, TTR 101, *PT T11 138 310*

The technical scheme of GASPS can be visualised in Figure 2.9.

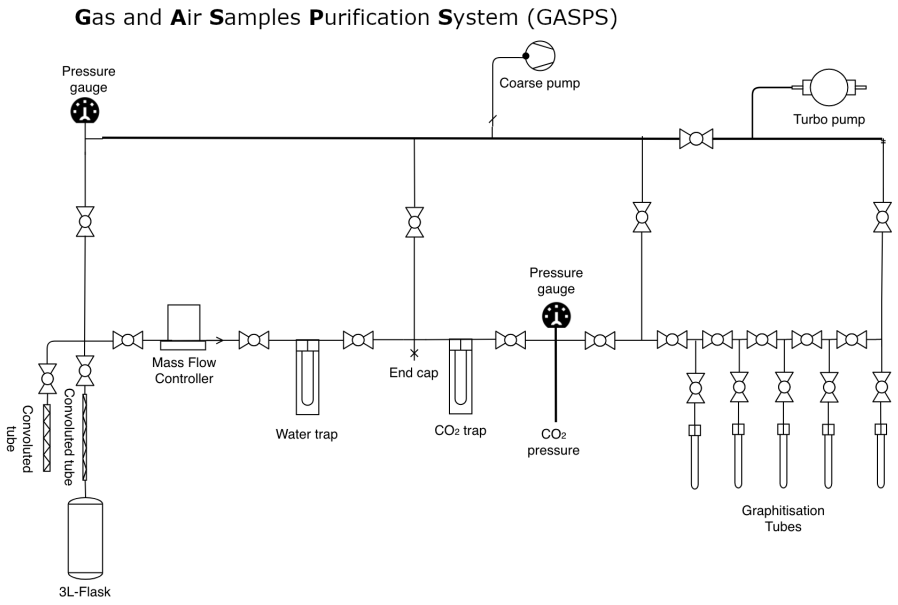

FIGURE 2.9: Technical drawing of GASPS line created on an online software.

Despite the widespread use of radiocarbon in many different scientific fields, it is still not very clear how to use radiocarbon to determine age in open compartmental systems. The numerous advances in theoretical, metrological and experimental aspects of radiocarbon research contribute to tackle this deficit. Analysis of radiocarbon in the output flux of carbon in an open compartmental system would help to determine the mean transit time of carbon, an important system diagnostic time in ecology. To accomplish that, radiocarbon laboratories must process CO_2 from gas mixtures. Therefore, the construction of the dedicated line GASPS at LAC-UFF not only expands the experimental capabilities of the laboratory but also creates the opportunity to constrain more theoretical hypotheses with observations.

Chapter 3

Probability distributions of radiocarbon

Radiocarbon (^{14}C) is a valuable tool for studying dynamical processes in living systems. In particular, radiocarbon produced by nuclear bomb tests in the 1960s has been used in many contexts as a tracer for the dynamics of carbon in different compartments of the global carbon cycle, including the atmosphere, the terrestrial biosphere, and the oceans (Goudriaan, 1992; Jain et al., 1997; Randerson et al., 2002; Naegler et al., 2006; Levin et al., 2010). As a biological tracer, radiocarbon can be used to infer rates of carbon cycling in specific compartments, and to infer transfers among interconnected compartments. Therefore, radiocarbon is used as a diagnostic metric to assess the performance of models of the carbon cycle (Graven et al., 2017), and new datasets are now emerging to incorporate radiocarbon in model benchmarking (Lawrence et al., 2020).

Carbon cycling in biological systems can be represented using a particular class of mathematical models called compartmental systems (Sierra et al., 2018). As carbon enters a system such as the terrestrial biosphere, it is stored and transferred among a network of interconnected compartments such as foliage, wood, roots, soils, and other organisms. Compartmental systems represent the dynamics of carbon as it travels along the network of compartments (Rasmussen et al., 2016; Sierra et al., 2018), and provide information about the time carbon spends in particular compartments and the entire system (Rasmussen et al., 2016; Sierra et al., 2017). Although there seems to be a direct relation between the time carbon spends in a compartmental system and its radiocarbon dynamics, few studies relate both concepts.

An open compartmental system contains inflows and outflows different from zero (Jacquez and Simon, 1993). Timescales in open compartmental systems are

usually characterized by the concepts of *age* and *transit time* (Bolin and Rodhe, 1973; Rasmussen et al., 2016; Sierra et al., 2017). In open systems such as the biosphere, the incorporation and release of carbon occurs continuously, and it is possible to define the concept of *age* as the time elapsed since carbon enters the compartmental system until a generic time. The *transit time* can be defined as the time the carbon needs to travel through the entire system, i.e., the time elapsed between carbon entry until its exit. In order to estimate these time metrics from ^{14}C measurements, a model linking both carbon and radiocarbon dynamics is required. Thompson and Randerson (1999) have used impulse response functions from compartmental models to obtain ages, transit times, and time-dependent radiocarbon dynamics. However, this approach is computationally expensive and can introduce numerical errors if simulations are not long enough to cover the dynamics of slow cycling pools.

Explicit formulas for age and transit time distributions in compartmental systems have been recently developed (Metzler and Sierra, 2018). These formulas do not introduce numerical errors and can describe entire age distributions of carbon for specific pools and for the entire compartmental system. These age distributions suggest that radiocarbon in compartmental systems may consist of a mix of different values, i.e., compartments could be described in terms of radiocarbon distributions that relate the relative proportion of carbon with a particular radiocarbon value. However, until now, radiocarbon is reported and modeled as a single quantity, rather than the mean of an underlying distribution.

Knowledge of the distribution of the isotopic ratio between ^{14}C to ^{12}C in a compartmental system might give important insights on the model structure that better fits existing data. For example, by comparing the signature of radiocarbon in the pools and their outfluxes, we get insights into the size of the compartmental model that better describes ecosystem dynamics (Sierra et al., 2017). Further, empirical knowledge of the radiocarbon distribution of a particular system can play a significant role in determining the most appropriate model to describe a system.

Model-data comparisons using radiocarbon are made more complex by the fact that the quantity of ^{14}C in the atmosphere is continuously changing. This is particularly important after the 1960s when nuclear bomb tests liberated large amounts of thermal neutrons to the atmosphere, contributing to the formation of radiocarbon (bomb or excess ^{14}C). In addition, large quantities of fossil-fuel derived carbon (^{14}C-free) have been emitted to the atmosphere since the beginning of the Industrial Revolution, diluting the atmospheric radiocarbon signal and producing a fast decline

of the radiocarbon isotopic ratio in recent years (Graven et al., 2017). Therefore, we would expect a different radiocarbon distribution for every year in a compartmental system.

However, most studies have focused on estimating the mean isotopic ratio of ^{14}C to ^{12}C in order to evaluate carbon ages and transit times, ignoring its potential underlying distribution. As a tracer, the entire distribution of radiocarbon values are expected to change over time even if the compartmental system is in equilibrium. Thus, obtaining a simple and accurate method to estimate radiocarbon distributions as a function of time (e.g. the year of observation or sample collection) is of great interest for experimental and modeling studies. Therefore, the main objective of this chapter is to introduce a method to obtain distributions of radiocarbon in compartmental systems at steady-state. In particular, we ask the following research questions: (i) How do distributions of radiocarbon in terrestrial compartments change over time as a consequence of changes in atmospheric radiocarbon? (ii) How do empirical data compare to these conceptual radiocarbon distributions? (iii) What insights can these distributions provide for experimental and sampling design for improving model-data comparisons by capturing the entire variability of $\Delta^{14}C$ values?

This chapter is organised as follows: First, we provide the necessary theoretical background to obtain age and transit time distributions from compartmental systems. Second, we describe an algorithm that computes radiocarbon distributions for particular years using an age or a transit time distribution of carbon and an atmospheric radiocarbon curve. Third, we present an application of our algorithm to three compartmental systems addressing the research questions above. Finally, we discuss our results in the context of applications to any general compartmental model and potential new insights from our approach.

3.1 Compartmental systems

Compartmental systems describe the temporal dynamics of matter as it travels through a network of compartments until its final release from the system. A set of compartments is translated mathematically as a set of linear or non-linear ordinary differential equations, whose solutions are the amount of matter in each compartment at a certain time.

We will consider here linear autonomous compartmental systems, characterized by the mass of carbon at time t in m compartments as the vector $\vec{x}(t) \in \mathbb{R}^m$. Additionally, the compartments of the systems considered here are assumed well mixed, which implies that all carbon atoms inside a compartment have the same probability of being transferred to other compartments or to outside the system (Anderson, 1983). This well-mixed property is linked to the fixed rate at which mass is processed inside each compartment. For example, if a compartment i has a process rate k_i, all particles inside the compartment have the same probability of being removed from the compartment at this rate.

The mass of carbon in the compartments changes over time according to the following expression

$$\frac{d\vec{x}(t)}{dt} = \dot{\vec{x}}(t) = \vec{u} + \mathbf{B}\,\vec{x}(t), \qquad \vec{x}(t=0) = \vec{x_0}, \tag{3.1}$$

where the constant vector $\vec{u}$ represents the inputs of carbon into the system, and the $m \times m$ compartmental matrix $\mathbf{B}$ contains constant values of the cycling rates of the compartments in its diagonal entries, while the off-diagonal entries consist of the constant transfer rates among them. In particular, the compartmental matrix in most ecosystem carbon models has an internal structure reflecting transfers between the components (coefficients $\alpha_{i,j}$, representing the proportion of C transferred from compartment j to compartment i) and cycling rates k_i reflecting assumptions of first-order kinetics of loss (at rate k_i) from any given compartment:

$$\mathbf{B} = \begin{pmatrix} -k_1 & \alpha_{1,2}k_2 & \cdots & \alpha_{1,m}k_m \\ \alpha_{2,1}k_1 & -k_2 & \cdots & \alpha_{2,m}k_m \\ \vdots & \vdots & \ddots & \vdots \\ \alpha_{m,1}k_1 & \alpha_{m,2}k_2 & \cdots & -k_m \end{pmatrix}. \tag{3.2}$$

This matrix contains information on the dynamics, structure, and size of a compartmental model. The outflux of carbon from the system can also be obtained from this matrix by summing all column elements; i.e., the outputs from a pool that are not transferred to other pools are assumed to leave the compartmental system.

The information of the amount of carbon entering the system to be partitioned among the compartments is contained in the input vector

$$\vec{u} = \begin{pmatrix} u_1 \\ u_2 \\ \vdots \\ u_m \end{pmatrix}. \tag{3.3}$$

Linear autonomous systems of the form of equation (3.1) have an equilibrium point or steady-state solution $\vec{x}^*$ given by

$$\vec{x}^* = -\mathbf{B}^{-1}\,\vec{u}, \tag{3.4}$$

where the mass of the compartments do not change over time, and inputs are equal to outputs for all compartments.

3.2 Time metrics in ecology

3.2.1 Age distributions

We define age τ in a compartmental system as the time elapsed between the time of carbon entry until some generic time (Sierra et al., 2017). For a time-independent system in steady-state, a probability distribution of ages of carbon in the compartments can be obtained using stochastic methods. According to Metzler and Sierra (2018), the vector of age densities for the compartments (denoted by $\boldsymbol{f_a}(\tau)$) can be obtained as

$$\boldsymbol{f_a}(\tau) = (\mathbf{X}^*)^{-1} \cdot e^{\tau\,\mathbf{B}} \cdot \vec{u} \tag{3.5}$$

where $\mathbf{X}^* = \operatorname{diag}(x_1^*, x_2^*, \ldots, x_m^*)$ is the diagonal matrix with the steady-state vector of carbon stocks as components, and $e^{\tau\,\mathbf{B}}$ is the matrix exponential.

For the whole system (denoted by the function with capital A, $f_A(\tau)$) , the age distribution is given by

$$f_A(\tau) = -\mathbf{1}^\intercal \cdot \mathbf{B} \cdot e^{\tau\mathbf{B}} \cdot \frac{\vec{x^*}}{\|\vec{x^*}\|}, \tag{3.6}$$

where $\|\vec{x^*}\| := \sum_{j=1}^{m} |\vec{x^*}|$ is the 1-norm of the steady-state solution and represents the sum of the masses in the vector.

3.2.2 Transit Time distributions

We define transit time as the time elapsed since carbon enters the compartmental system until it leaves the boundaries of the system (Sierra et al., 2017). The transit time is equivalent, therefore, to the age of the outflux. Metzler and Sierra (2018) also provide an explicit formula to obtain the transit time density distribution for a time-independent system at steady-state as

$$f_{TT}(\tau) = -\mathbf{1}^{\intercal} \cdot \mathbf{B} \cdot e^{\tau \mathbf{B}} \cdot \frac{\vec{u}}{\|\vec{u}\|}. \tag{3.7}$$

The age and transit time distributions are densities and they integrate to 1

$$\int_0^\infty f_A(\tau)\, d\tau = \int_0^\infty f_{TT}(\tau)\, d\tau = 1. \tag{3.8}$$

The derivation of these equations (3.5, 3.6, 3.7) is based on the idea that a deterministic compartmental system of differential equations can be expressed as a continuous-time Markov chain (Metzler and Sierra, 2018). This perspective, allows us to make inferences about the total masses of carbon in a stochastic setting, with explicit formulas for the age of carbon atoms in the system (Azizi-Rad et al., 2021).

3.3 Estimating radiocarbon distributions from compartmental models

We developed an algorithm to convert age and transit time distributions into distributions of radiocarbon expressed as $\Delta^{14}C$ for any given year of observation. We define $\Delta^{14}C$ as

$$\Delta^{14}C = \left[F^{14}C e^{\lambda_C (1950-y)} - 1\right] \times 1000\,[‰] \tag{3.9}$$

where $F^{14}C$ is the Fraction Modern (A_{SN}/A_{ON}), i.e., the sample ratio normalized to $\delta^{13}C$ by oxalic acid standard (OxII), λ_C is the updated ^{14}C decay constant (equals $\frac{1}{8{,}267}\ yr^{-1}$), and y is the year of measurement.

The algorithm works in three main steps, 1) homogenization, 2) discretization, and 3) aggregation (Figures 3.2 and 3.3). We describe these three steps in detail in the sections below using mathematical notation for the system age distribution, but

computations are similar for the transit time distribution, and the age distribution of individual compartments.

3.3.1 Homogenization of input data

The main inputs for the algorithm are an age distribution $f_A(\tau)$, and an atmospheric radiocarbon curve $F_a(t)$ that provides the $\Delta^{14}C$ value of atmospheric CO_2 for a calendar year t. To homogenize the time variable of both $f_A(\tau)$ and $F_a(t)$, we define the year of observation t_0, as the year of interest to produce the radiocarbon distribution. In this way we have f_A and F_a in terms of the same independent variable.

Since we are interested in determining the radiocarbon values of material observed in the system at time t_0, we will look in the radiocarbon curve $-t$ years in the past to obtain the radiocarbon values in the system with an age τ. Therefore, atmospheric radiocarbon can be expressed as a function of age, i.e., $F_a(t_0 - t) = F_a(\tau)$ (Figure 3.2). Now, both the system age distribution $f_A(\tau)$ and the atmospheric radiocarbon curve $F_a(\tau)$ are functions of the continuous variable τ that represents age since t_0.

Several atmospheric radiocarbon datasets can be found in the literature (Graven et al., 2017; Hogg et al., 2013; Hogg et al., 2020; Hua et al., 2013; Hua et al., 2021; Levin et al., 1980; Levin and Kromer, 1997; Levin et al., 2010; Reimer et al., 2013; Reimer et al., 2020). Also forecasts of radiocarbon content in the atmosphere can be found in the recent literature (Graven, 2015; Sierra, 2018). However, these atmospheric radiocarbon datasets do not necessarily have the same resolution in time. Some of them provide predictions or data at an annual or four-monthly time step, while in other datasets, some ranges are spaced by decades. To homogenize the resolution of the $\Delta^{14}C$ and to transform these radiocarbon datasets into a continuous function of τ, we use a cubic spline interpolation to obtain $\Delta^{14}C$ values for any value of τ. After this step, $F_a(\tau)$ can be computed until the last available date in the chosen atmospheric radiocarbon dataset, covered by the range where $f_A(\tau)$ is computed, i.e., for any value of $\tau \in [0, \infty)$.

Atmospheric radiocarbon datasets

For the models studied here, we needed to build two different combinations of atmospheric radiocarbon curves. One for the Northern Hemisphere (NH) to cover the

HFS and Emanuel models, and the second one for the tropics to serve as input for the Porce model (Figure 3.1).

The atmospheric $\Delta^{14}C$ values used for years in the past – e.g., 1965 CE – were obtained by merging the recently released IntCal20 calibration curve (Reimer et al., 2020), which combines radiocarbon data and Bayesian statistical interpolation for the range 55,000 – 0 cal BP (BP = *before present* = 1950 CE), and the records of atmospheric radiocarbon data compiled by Graven et al. (2017), from 1950 to 2015 CE for the NH and for the tropics. Graven et al. (2017) also provides radiocarbon data in one-year resolution on the range 1850 to 1949. However, as in this range there are estimations partially based on the previous NH calibration curve (IntCal13, Reimer et al. (2013)), we decided to subset Graven et al. (2017)'s dataset, starting in 1950 CE.

For the years in the future, such as 2027 CE and 2100 CE, we made use of the forecast simulations computed by Graven (2015), who simulated $\Delta^{14}C$ values in the atmosphere for four Representative Concentration Pathways of fossil fuel emissions: RCP2.6, RCP4.5, RCP6 and RCP8.5. In this work we use the predictions based on the high emissions scenario (RCP8.5), starting in 2016 CE.

The $\Delta^{14}C$ values in all datasets used in this work are written as the deviation from the standard representing the pre-industrial atmospheric ^{14}C concentration. The raw published values are already corrected for fractionation and decay with respect to the standard. It is equivalent to Δ in Stuiver and Polach (1977) (equation (3.9)).

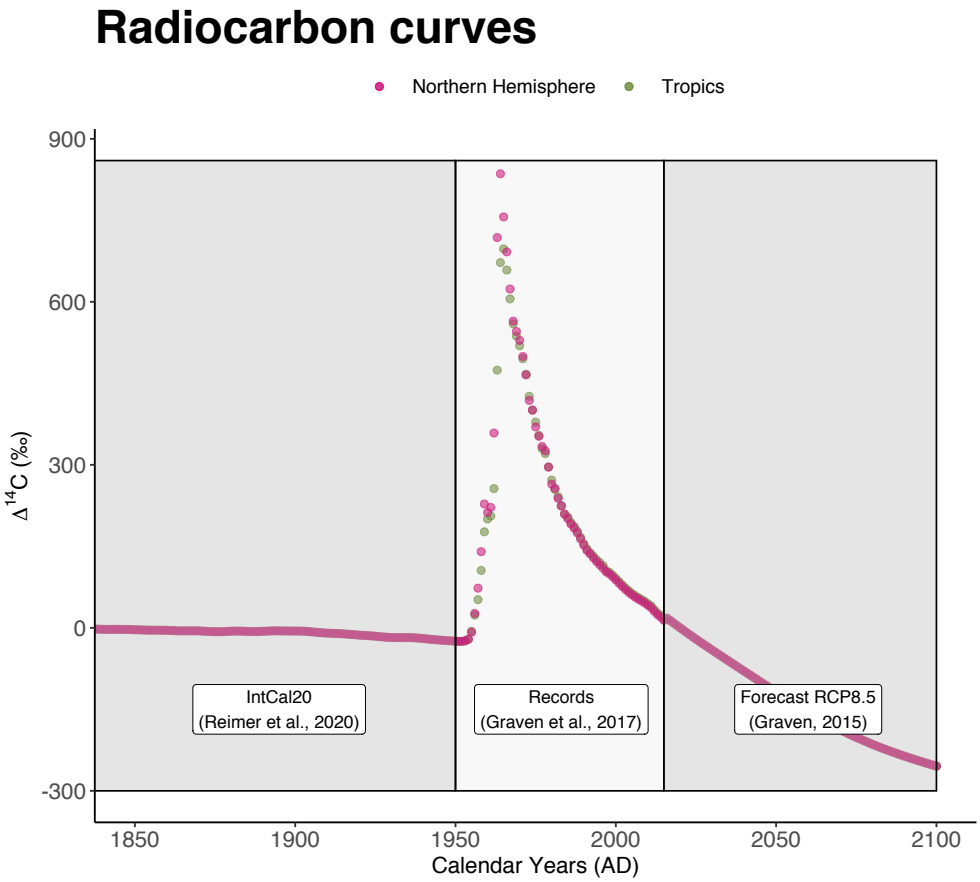

FIGURE 3.1: Scheme of the atmospheric radiocarbon inputs used in the estimation of the probability density distributions of radiocarbon. Before 1950 CE, input radiocarbon data relies on the IntCal20 (Reimer et al., 2020) measurements and modeling; Between 1950 and 2015 it consists of atmospheric $\Delta^{14}CO_2$ records compiled by Graven et al. (2017); From 2016 on, the atmospheric radiocarbon values are based on the predictions of Graven (2015) for the RCP8.5 scenario. The records between 1950 and 2015 comprise values for the atmosphere in Northern Hemisphere (NH) and Tropics. The Tropics records are used as input in the Porce model (section 3.4.2). The NH dataset is used as input in the HFS model and Emanuel model (section 3.4.3).

3.3.2 Discretization

Although we have now the age distribution and the radiocarbon data as continuous functions of age, we need to discretize these functions in intervals of size h. The reason for this discretization is that the probability density function of age $f_A(\tau)$ is a measure of the relative likelihood of an infinitesimal amount of mass having an age τ. But ultimately, we are interested in the probability that a small mass has certain

radiocarbon distribution. Therefore, we need to discretize the probability density function to a probability mass function along a discrete variable $T \in [0, T_{\max}]$. The new discrete probability function of ages can be defined as

$$P_A(\tau \leq T \leq \tau + h) = \int_{\tau}^{\tau+h} f_A(\tau) d\tau. \tag{3.10}$$

From this probability function, we can compute the proportion of total mass in the system with an age T as

$$M(T) = \|\vec{x}^*\| \cdot P_A(T), \tag{3.11}$$

where

$$\begin{aligned} \sum_{T=0}^{T_{\max}} P_A(T) &\approx 1, \\ \sum_{T=0}^{T_{\max}} M(T) &\approx \|\vec{x}^*\|. \end{aligned} \tag{3.12}$$

Equation (3.12) implies that there is an approximation error by discretizing the continuous density function to a finite set of discrete intervals. This approximation error can be minimized by decreasing the size of the intervals h and extending $T_{\max}$ as far as possible.

Once we discretize $f_A(\tau)$ to $P_A(T)$ and obtain discrete proportions of mass with certain age $M(T)$, we proceed to discretize the atmospheric radiocarbon curve with respect to the same discrete interval of ages $T \in [0, T_{\max}]$. This is simply done by computing $F_a(\tau = T)$, which makes the assumption that within each interval $[\tau, \tau + h]$, the atmospheric radiocarbon value is equal to $F_a(\tau)$.

3.3.3 Aggregation

Now we are ready to combine the distribution of mass in the system at discrete age intervals with the atmospheric radiocarbon curve. To do so, we first subdivide the $\Delta^{14}C$ axis of the radiocarbon curve into equally spaced bins (b); for each bin b we take the corresponding radiocarbon content $F_a(T)$ and corresponding intervals of $T \in [0, T_{\max}]$, matching them to the respective values of mass $M(T)$ in the age distribution of carbon. Then, we sum all the masses within the same $\Delta^{14}C$ values (see Figure 3.3 for a better understanding of the aggregation step). The result

can be organized as the amount of carbon mass in discrete intervals of $\Delta^{14}C$; i.e., $M(\Delta^{14}C) = M(F_a(T))$.

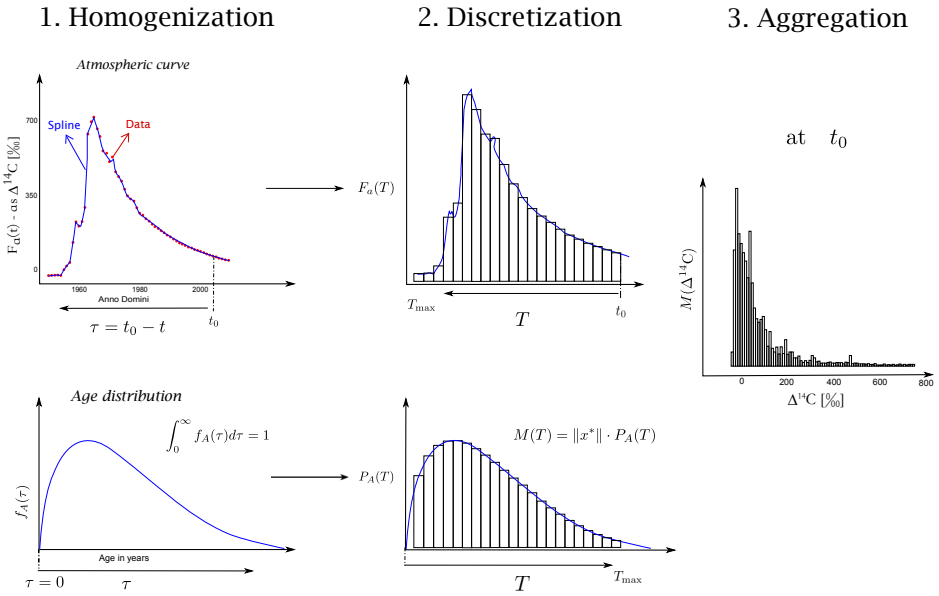

FIGURE 3.2: Graphical visualization of the three main steps for the computation of radiocarbon distributions in a compartmental system using an atmospheric radiocarbon curve of the carbon inputs to the systems, and the age distribution of carbon in a compartmental system. The homogenization step (1.) consists of normalizing the times variables of the atmospheric curve, which is expressed in years of the calendar, and the age distributions, with ages in years. In the step 1, we also apply a spline interpolation to the atmospheric radiocarbon dataset to make sure both curves - atmospheric radiocarbon and age distribution - have the same resolution h. In the discretization step (2.) we divide the continuous curves into discrete intervals, where the masses of carbon will correspond to the probability densities obtained by the computation of the age distribution, multiplied by the steady-state solution of the compartmental system. Finally, in the aggregation (3.) we subdivide the atmospheric radiocarbon curve into intervals with size of the final bin size of the bar-plots, i.e. b, and sum the masses of carbon from the age distribution with the same $\Delta^{14}C$ value they would have in the atmosphere, independent of the age.

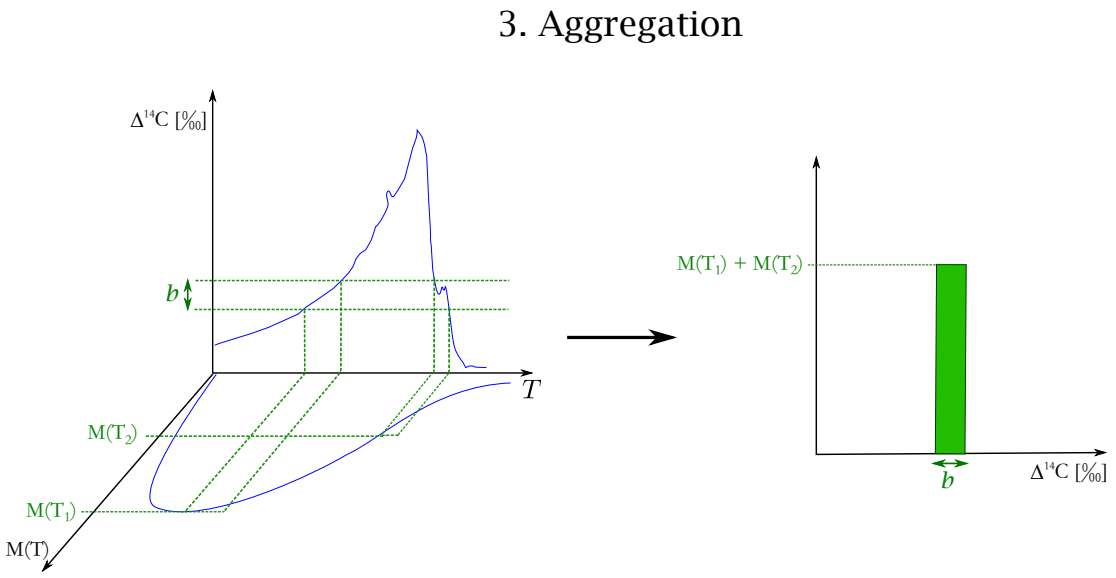

FIGURE 3.3: Third step of the algorithm: aggregation. The radiocarbon curve (atmospheric radiocarbon contents) is subdivide into intervals of size b. Those intervals will correspond to the size of the bins that will generate the bar plots. Inside the range b there is a range of $\Delta^{14}C$ values that will correspond to intervals of ages – or T, in the appropriate normalized time variable from step 1 (homogenization) –, in units of years. The y-axis of the final bar plot will correspond to the sum of carbon masses in the intervals of T. The x-axis of the final bar plot corresponds to the range of $\Delta^{14}C$ values in the atmosphere (and corrected for the decay according to T) defined through the size b.

We implemented these three steps in the R programming language, and used the package SoilR (Sierra et al., 2012a) to obtain the age distribution of the pools, the whole system, and the output flux (equivalent to the transit time) based on equations (3.5), (3.6), and (3.7). The versions used here were R version 4.0.3 and SoilR version 1.1 (Sierra et al., 2014). The link to access the R scripts with the algorithm functions and model results is provided in the Availability Statements.

Since atmospheric ^{14}C concentration for the past 55,000 years is mainly empirically known, generating the radiocarbon curves, we could easily convert age into atmospheric $\Delta^{14}C$. By matching the $\Delta^{14}C$-based-on-age values with the previously estimated densities, we built barplots, gaining insight into the radiocarbon distributions for the models studied in this work. In the algorithm we defined four functions: *PoolRDC*, *SystemRDC*, *TTRDC*, and *C14hist*. The first three functions take the densities outputs, i.e., the carbon contents discretized by age, from built-in SoilR functions, such as *transitTime* and *systemAge*. The densities are subset to build bins

through the *C14hist* function. The logical statements used to construct the bins are based on the atmospheric $\Delta^{14}C$ data and according to user-defined bin size b. This structure allows one to plot histogram-like graphs, where the height of the bars represent the amount of carbon mass with corresponding $\Delta^{14}C$ values. Thus, our algorithm starts with a compartmental matrix, an input vector and a radiocarbon calibration curve, and returns an object containing masses of C and their matching decay-corrected $\Delta^{14}C$ values, estimated for any given year of observation. The match is done by assuming that $\tau = 0$ (age equals zero) at the year of observation t_0. This means that the input radiocarbon signal in past years will correspond to the $\Delta^{14}C$ signal of the atmosphere of those years corrected for the radioactive decay of ^{14}C (average lifetime of 8,267 years, i.e., half-life of 5,730 years) according to the age of the pool, system or outflux.

Besides the radiocarbon distributions for pools, whole system and output flux, one can also compute the expected value of $\Delta^{14}C$ from these distributions in any given year of observation. This is done by computing the mean of $\Delta^{14}C$ weighted by the amount of carbon in $\Delta^{14}C$ bins of size b. The standard deviation of the distribution is obtained as the square root of the difference between the square of the expected value and the expected value of the squares of $\Delta^{14}C$ values.

3.3.4 Set of parameters

As described before, in order to estimate the radiocarbon distributions and expected values of $\Delta^{14}C$, the algorithm needs the following arguments: a compartmental matrix **B**, containing the decomposition and transfer rates within the pools; an input vector $\vec{u}$ containing the input mass to be partitioned among the compartments; the year of observation (equivalent to year of sampling in an experimental framework); the number of years in the past one aims to compute the distributions for; and a set of radiocarbon values in the atmosphere, comprising the year of observation and the number of years chosen. An additional argument is h, the discretization size described above, which has a default value of 0.1 years, but could be modified according to user preferences.

For the HFS model, **B** is the matrix in equation (3.13), with the form of equation (3.2), and $\vec{u}$ is the numeric vector in the same equation (3.13), with similar form as equation (3.3). We estimated the radiocarbon distributions for different years of observation, in order to address different research questions raised in this work. In

the results and Supplementary material of chapter 3 we present the distributions for the pools and total outflux of all the three models for the years 1965, 2027 and 2100. Additionally, in the supporting material we provide the non-stacked radiocarbon distributions of individual pools for the same mentioned years (Figures A.3 – A.11). Videos with the radiocarbon distributions for the total outflux and whole system for all the years between 1955 and 2100 (Videos S1 – S6, respectively) can be found in Chanca et al. (2022). Radiocarbon distributions of the outflux in the HFS model are also presented for the years 1996, 1998, 2002, and 2008, as for those years we also have independent $\Delta^{14}C$ data from soil CO_2 efflux in the Harvard Forest to compare to our estimations (Sierra et al., 2012b). For all those estimations, the number of years of computation was 1,000 years. The bin size b for plotting the histograms was set as 10 ‰ for most of the radiocarbon distributions, except for the year 1965, where it was set up to 40 ‰, avoiding gaps on the x-axis.

3.4 Application in ecological compartmental models

3.4.1 Harvard Forest soil model

Our approach can be used to obtain radiocarbon distributions for linear compartmental models of any size representing carbon cycling processes at different scales and for different biological systems. We discuss here the probability distributions of radiocarbon obtained for three different carbon cycle models. Despite the method described throughout this work may not be limited to these examples, the approach is particularly useful for interpretation of radiocarbon measurements in ecosystems in the future. Nevertheless further applications might include carbon dynamics in aquatic systems, molecular transformations of carbon in organisms, among others.

In the following sections we focus on a model that represents the dynamics of soil organic carbon in a temperate forest, which we call here the Harvard Forest Soil (HFS) model. In the appendix, we describe two other carbon models, hereafter called Porce model and Emanuel model. The Porce model represents the carbon cycle of a tropical forest in the Porce region (Colombia) through seven interconnected compartments (Sierra et al., 2021). The Emanuel model describes the global carbon cycle through a 5-box model (Emanuel et al., 1981).

The pools of the HFS model were operationally defined, which means they were based on methods to separate organic matter performed on samples from the Harvard Forest in Massachusetts, USA (Gaudinski et al., 2000; Sierra et al., 2012b). Soil samples collected in O-horizon, corresponding to 0 – 8 cm depth, and A-horizon (8 – 15 cm depth) were separated into seven soil fractions corresponding later to each of the compartments of the model (Figure 3.4); one pool corresponds to *dead roots* x_1. Pools x_2, x_3, and x_4 correspond, respectively, to fractions from the O-horizon here called *Oi*, *Oe/a L*, and *Oe/a H*. We keep the pool names given in Gaudinski et al. (2000) and Sierra et al. (2012b), but these fractions are equivalent to leaf litter (*Oi* fraction), recognizable root litter (*Oe/a L* fraction), and humified fraction, i.e., organic matter that has been transformed by microbial action (*Oe/a H*). Pools x_5, x_6, and x_7 correspond, respectively, to fractions from the A-horizon here called *A, LF (>* 80 *μm)*, *A, LF (<* 80 *μm)*, and *mineral associated*. The A-horizon pools were fractionated by density (1 g cm^{-3}), with the low-density portion being further subdivided by sieving into recognizable leaf larger than 80 μm (*A, LF (>* 80 *μm)* fraction, pool x_5) and smaller than 80 μm (*A, LF (<* 80 *μm)* fraction, pool x_6). Details about the methods employed to fractionate the samples can be found in Gaudinski et al. (2000).

The HFS model was built by fitting empirical radiocarbon data from the above described soil fractions. Details about the use of the data to build the compartmental model are presented in Sierra et al. (2012b). For the same sites, independent data (i.e., data not used for estimating the compartmental matrix) are available (Sierra et al., 2012b). The independent data used in this work consists of $\Delta^{14}C$ measurements on total soil CO_2 efflux collected between 1996 and 2010 (with exception for the year 2005). We used these data to compare the representativity of the mean $\Delta^{14}C$ measurements to the expected $\Delta^{14}C$ values obtained through our algorithm. In the results we present the probability distributions of radiocarbon for the years 1996, 1998, 2002, and 2008. The number of samples measured corresponding to the respective years was n = 12, 28, 23, and 10. We also estimated the expected value of $\Delta^{14}C$ for the remaining years and these values can be seen in the Figures A.1 and A.2 of the supporting information material.

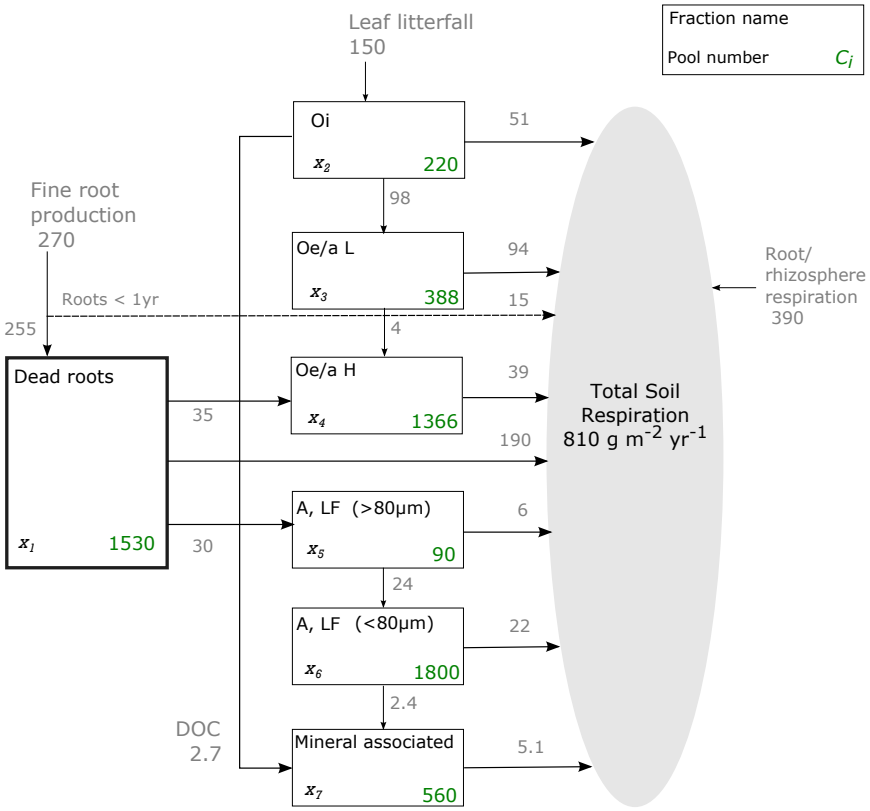

FIGURE 3.4: Scheme of Harvard Forest soil model stocks (C_i) and fluxes among compartments (adapted from Sierra et al. (2012b)). All the fluxes are in units of gC m^{-2} yr^{-1} and stocks in gC m^{-2}. Pool x_1 corresponds to *dead roots*; in the O-horizon we have pools x_2: *Oi* (leaf litter), x_3: *Oe/a L* (recognizable root litter), and x_4: *Oe/a H* (humidified OM). In the A-horizon, we have pools x_5: *A, LF (> 80μm)* (less dense, i.e., density < 1 g cm^{-3}, fraction with particles $> 80\mu$m), and x_6: *A, LF (< 80 μm)* (less dense fraction passing through an 80 μm sieve). The seventh pool x_7 represents the dynamics of the *mineral associated* fraction (density > 1 g cm^{-3}).

The set of ordinary differential equations for the HFS model can be expressed in compartmental form as

$$\begin{pmatrix} \dot{x}_1 \\ \dot{x}_2 \\ \dot{x}_3 \\ \dot{x}_4 \\ \dot{x}_5 \\ \dot{x}_6 \\ \dot{x}_7 \end{pmatrix} = \begin{pmatrix} 255 \\ 150 \\ 0 \\ 0 \\ 0 \\ 0 \\ 0 \end{pmatrix} + \begin{pmatrix} -255/1530 & 0 & 0 & 0 & 0 & 0 & 0 \\ 0 & -150/220 & 0 & 0 & 0 & 0 & 0 \\ 0 & 98/220 & -98/388 & 0 & 0 & 0 & 0 \\ 35/1530 & 0 & 4/388 & -39/1366 & 0 & 0 & 0 \\ 30/1530 & 0 & 0 & 0 & -30/90 & 0 & 0 \\ 0 & 0 & 0 & 0 & 24/90 & -24/1800 & 0 \\ 0 & 2.7/220 & 0 & 0 & 0 & 2.4/1800 & -5.1/560 \end{pmatrix} \begin{pmatrix} x_1 \\ x_2 \\ x_3 \\ x_4 \\ x_5 \\ x_6 \\ x_7 \end{pmatrix}. \tag{3.13}$$

In the HFS model, for the whole system in 1965 CE (Figures 3.5b and A.3), the distribution of radiocarbon aggregates the contributions of the different pools, which results in different peaks in the overall distribution. The mode (i.e., the $\Delta^{14}C$ with highest mass density) is below 0 ‰ because a large portion of the total amount of carbon is contributed by the *mineral associated* pool that is predominantly still pre-bomb carbon with little contribution from carbon fixed after 1964. In addition, other pools that cycle fast, contribute relatively small amounts of bomb ^{14}C to the overall distribution.

The radiocarbon distribution in the output flux of the HFS model in 1965, i.e., the radiocarbon distribution that corresponds to the transit time distribution for this year (Figures 3.6b – blue bars – and A.3) has three distinct peaks in the distribution. In the soil model, the distribution of the outflux is very similar to that of the *dead roots* pool (Figure A.3), which is the main contributor to the total respiration flux. However, other pools also contribute to the respiration flux with their radiocarbon signatures and emphasize fluxes from the fastest cycling pool (*Oi*) and respiration of carbon that was present in other pools before the bomb peak.

The shapes of the distributions change dramatically for subsequent years after the bomb spike (Figures 3.6b). For 2027 CE, the expected $\Delta^{14}C$ values of fast pools drop considerably, in parallel with atmospheric ^{14}C, compared to 1965 CE (Figure A.4). These fast pools do not store much radiocarbon from the bomb period, and their radiocarbon signatures reflect recent carbon from the atmosphere. In contrast, slow cycling pools in 2027 had relatively high $\Delta^{14}C$ values, mostly because they still contain radiocarbon from the bomb period. In the output flux (Figures 3.6b - green bars - and A.4), as expected, since the respiration flux is dominated by the faster-cycling pools such as *dead roots* and *Oi* for HFS model, most of the radiocarbon is narrowly distributed around the recent atmospheric $\Delta^{14}CO_2$ value in 2027 ($\Delta^{14}CO_2$ = -28.8 ‰) (Graven, 2015), with almost no contributions from bomb ^{14}C.

By the year 2100, the atmospheric $\Delta^{14}CO_2$ values have dropped to -254.5 ‰ (Graven, 2015), reflecting the Suess effect. In all the models studied here, the distributions of most pools show a lower $\Delta^{14}C$ variability in 2100. Faster-cycling pools have dropped to reflect negative $\Delta^{14}C$ in the atmosphere over the 73 years since 2027, while the slow pools still show a wide range of $\Delta^{14}C$ values that includes C fixed during the bomb period (now ∼150 years previously). The latter pattern can be observed for *mineral associated* (x_7), *A, LF (< 80 µm)* (x_6) and *Oe/a H* (x_4) pools in the HFS model (Figure A.5).

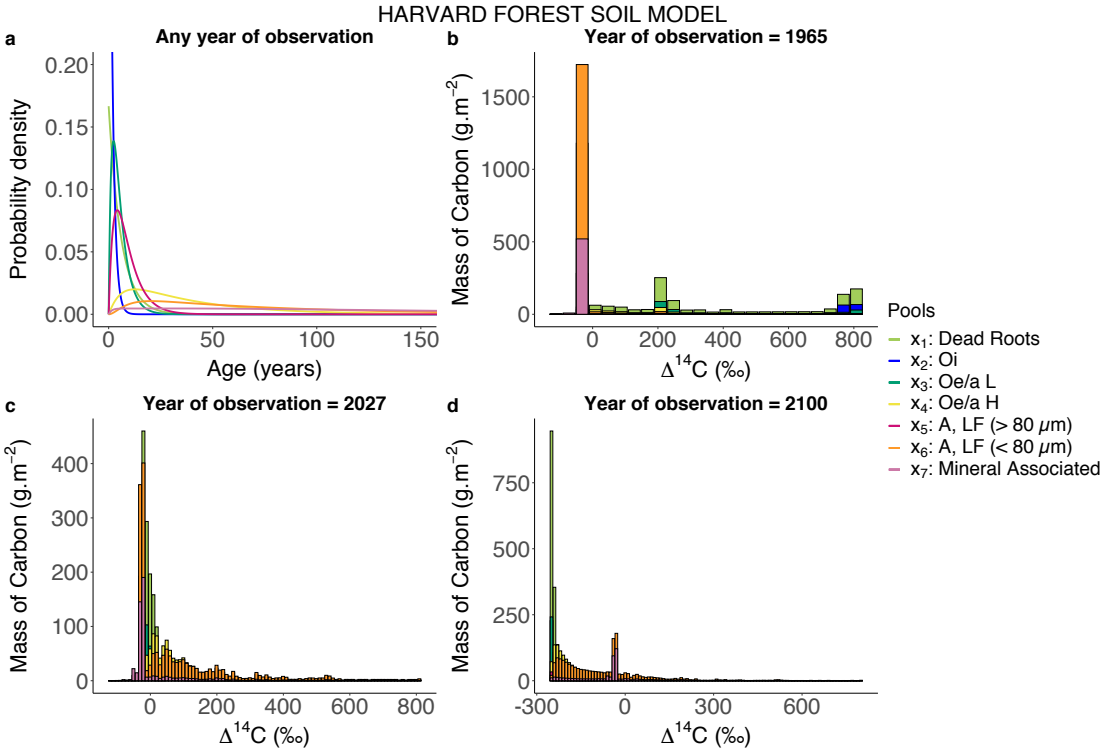

FIGURE 3.5: **(a)** Pool age distributions for the Harvard Forest Soil model computed in a span of 1,000 years with a resolution of 0.1 year. Mean system age is 50.9 years. Mean pool ages vary from 1.5 yrs (for *Oi* pool) to 150 yrs (for *mineral associated* pool). **(b)** Mass density distribution of radiocarbon in 1965 – just after the ^{14}C bomb peak in 1964. Distribution was computed over 1,000 years, discretized by 0.1 yrs. Bin size $b = 40‰$. The expected Δ^{14}C and standard deviation (sd) of the whole system in 1965 is 141 $\pm$ 280 ‰. **(c)** Mass density distribution of radiocarbon in 2027. Distribution was computed over 1,000 years, discretized by 0.1 yrs. Bin size $b = 10‰$. The expected Δ^{14}C and sd of the whole system in 2027 is 54 $\pm$ 144 ‰. **(d)** Mass density distribution of radiocarbon in 2100. Distribution was computed over 1,000 years, discretized by 0.1 yrs. Bin size $b = 10‰$. The expected Δ^{14}C and sd of the whole system in 2100 is -147 $\pm$ 146 ‰.

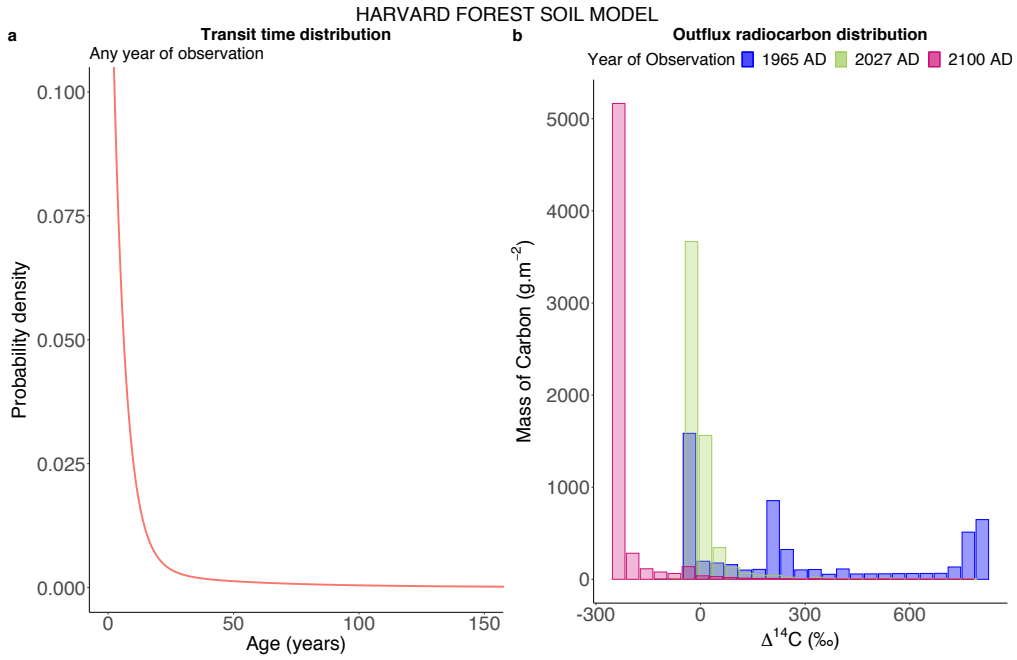

FIGURE 3.6: **(a)** Transit time distribution for the Harvard Forest Soil model computed in a span of 1,000 years with a resolution of 0.1 year. Mean transit time is 14.7 years. **(b)** Mass density distributions of radiocarbon for the output flux (total respiration) in the years 1965, 2027 and 2100. Distribution was computed over 1,000 years, discretized by 0.1 yrs. Bin size $b = 40‰$ for all the years of observation. The expected $\Delta^{14}C$ values and standard deviations of the outflux are: 334 ± 333 ‰ in 1965; 9 ± 81 ‰ in 2027; and -223 $\pm$ 78 ‰ in 2100.

Radiocarbon measurements of total soil CO_2 efflux at the Harvard Forest compared relatively well with the theoretical distributions of radiocarbon in the output flux obtained from our approach. Total soil CO_2 efflux includes both decomposition sources predicted by the model and root respiration, estimated by Gaudinski et al. (2000) to be $\sim$ 55% and to have $\Delta^{14}C$ values equal to the atmosphere in any given year.

In the model, for all the years presented in this section (1996, 1998, 2002, and 2008) the mode represents a mass of respired carbon equivalent to $\sim 10^3$ gC m^{-2}. We refer also to smaller peaks, hereafter secondary peaks, where the mass of respired carbon is equivalent to values larger than 100 gC m^{-2} but lower than 1 kgC m^{-2} in one bin size (b) range. For all the theoretical distributions in this section $b = 10$ ‰, however, as one could anticipate, the size of the b has not effect on the expected value. The measurements were always within the expected range of $\Delta^{14}C$ estimated

through the algorithm (Figure 3.7, Table 3.1). In all cases, the average of the measurements was relatively close to the expected value of the theoretical distributions. However, the variance of the observations was smaller than the expected variance from the model (Figure A.2 and Video S7). In particular, the expected values were systematically higher in ^{14}C than the average of the observations for years 1996, 1998, 2002, and 2008 by 23.5 ‰, 21.8 ‰, 15.1 ‰, and 10.8 ‰, respectively (Figure 3.7). The standard deviation of the observations were 17.3 ‰, 26.2 ‰, 8.4 ‰, and 13.6 ‰ for the years 1996, 1998, 2002, and 2008, respectively, which are smaller than the expected standard deviation of the distributions, which were 107.6 ‰, 103.3 ‰, 96.3 ‰, and 89.7 ‰ for the corresponding years, as a consequence of the larger spread of the theoretical distributions.

For the year 1996 (Figure 3.7a), the 12 measurements of soil CO_2 efflux ranged from 104.3 ‰ to 167.3 ‰ (σ = 17.3 ‰). The mode of the theoretical distribution also falls in this interval: (112, 122] ‰. Secondary peaks fall in a range with magnitude of one bin size below 0 ‰, starting in $\Delta^{14}C$ values of -28 ‰ and in a wide range of $\Delta^{14}C$ above the mode, ranging from 122 ‰ to 212 ‰ (Table 3.1).

For the year 1998 (Figure 3.7b), the 28 measurements of soil CO_2 efflux ranged from 66.4 ‰ to 193.9 ‰, (σ = 26.2 ‰). The mode of the theoretical estimation fall in the range from 102 ‰ to 112 ‰ (Table 3.1), while secondary peaks are observed in the ranges (-28,-18], (92,102], and (112, 202].

For the year 2002 (Figure 3.7c), the 23 measurements of soil CO_2 efflux range from 88 ‰ to 117.9 ‰, (σ = 8.4 ‰). The theoretical mode falls partially in the range of the observations: (81, 101] ‰. The theoretical estimations include the range observed in the empirical data – (102, 152] ‰ – however, with probability density one order of magnitude smaller than the mode. Moreover, the theoretical distribution has a secondary peak in the range of (71, 81], which is not observed in the measurements.

Finally, in the year 2008 (Figure 3.7d), the ten measurements of soil CO_2 efflux range from 60.8 ‰ to 104.7 ‰, (σ = 13.6 ‰). The peaks (carbon masses over 100 gC m^{-2}) of the theoretical distributions for this year are concentrated in the range (41, 121], with the mode in the bin (51, 61] ‰.

For all the years, secondary peaks falling in the negative part of the $\Delta^{14}C$ axis (Table 3.1), comprising values between -29 or -28 ‰ and -19 or -18 ‰, are not captured in the soil $\Delta^{14}CO_2$ efflux measurements.

TABLE 3.1: $\Delta^{14}C$ ranges with masses of carbon above 100 gC m^{-2} according to our estimations; $\Delta^{14}C$ expected values according to weighted mean of mass distribution of radiocarbon; and observed $\Delta^{14}C$ mean values of soil CO_2 efflux.

	$\Delta^{14}C$ [‰]			
Year	Mode[a]	Secondary Peaks[b]	Expected value[c]	Mean value[d]
1996	(112, 122]	(-28, -18], (102, 112], (122, 212]	153 ± 107.6	129.5 ± 17.3
1998	(102, 112]	(-28,-18], (92, 102], (112, 202]	139.4 ± 103.3	117.6 ± 26.2
2002	(81, 101]	(-29,-19], (71, 81], (101, 151]	115.9 ± 96.3	100.8 ± 8.4
2008	(51,61]	(-29, -19], (41, 51], (61, 121]	85 ± 89.7	74.8 ± 13.6

a Carbon masses $\sim 10^3$ gC m^{-2};
b Carbon masses between 100 gC m^{-2} and 1 kgC $^{-2}$;
c Expected value of theoretical radiocarbon distribution of the outflux (weighted mean);
d Mean value of the $\Delta^{14}C$ values measured on soil CO_2 efflux from the Harvard Forest.

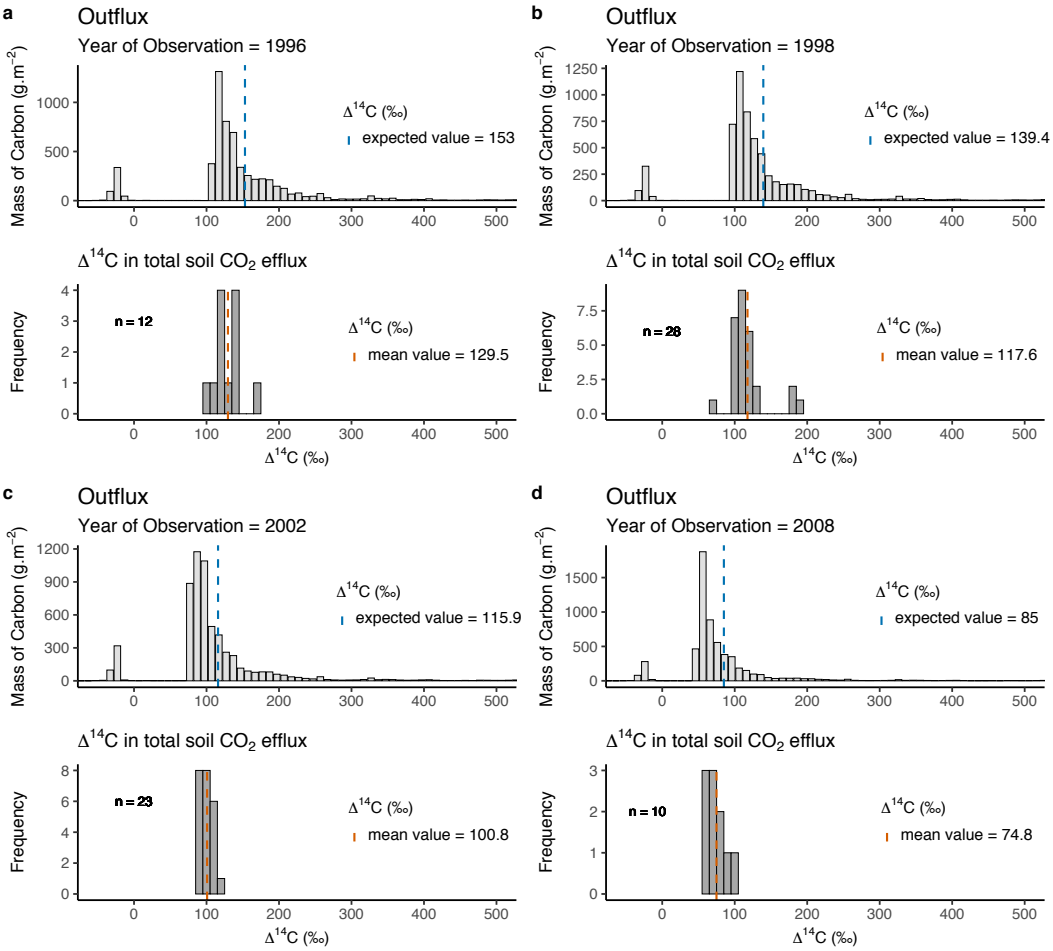

FIGURE 3.7: Comparison between theoretical radiocarbon distribution and independent empirical data for the corresponding years of observation. **(a)** Year of observation = 1996 CE = Year of sampling and number of observations $n = 12$; **(b)** Year of observation = 1998 CE = Year of sampling and number of observations $n = 28$; **(c)** Year of observation = 2002 CE = Year of sampling and number of observations $n = 23$; **(d)** Year of observation = 2008 CE = Year of sampling and number of observations $n = 10$.

In this work, we also computed the radiocarbon distributions for two additional compartmental models. One model represents the carbon cycle of an old-growth tropical forest ecosystem based on measurements made at the Porce region in Colombia. The model parameters were obtained through a data assimilation procedure on the empirical data. We denote it here as the Porce model (Sierra et al., 2021). Another model represents the global carbon cycle, and it is based on the simple model described by Emanuel et al. (1981). We refer to it here as the Emanuel

model.

3.4.2 Porce Model

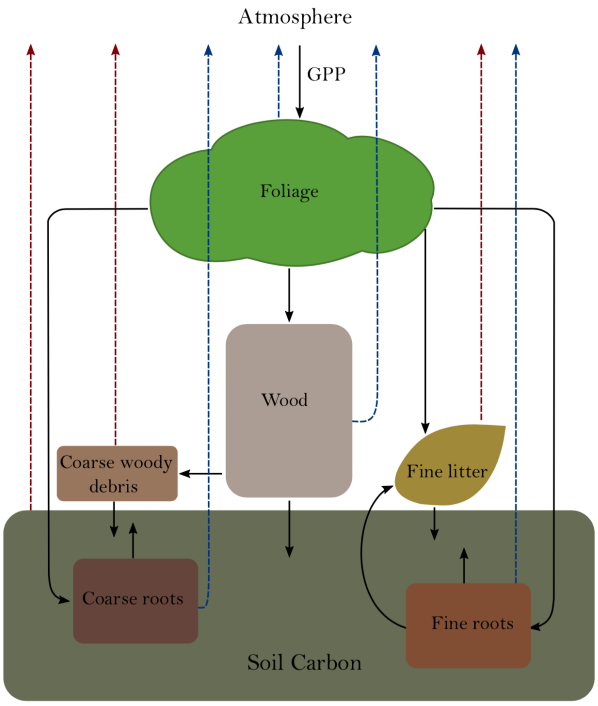

FIGURE 3.8: Scheme representing the connection between compartments in Porce model (Sierra et al., 2021). The pools are identified as x_1: *Foliage*, x_2: *Wood*, x_3: *Fine roots*, x_4: *Coarse roots*, x_5: *Fine litter*, x_6: *Coarse woody debris*, and x_7: *Soil carbon (0 – 30 cm)*. Pools $x_1 - x_4$ are live biomass pools, while dead biomass and soil pools correspond to compartments x_5, x_6, and x_7.

The Porce model consists of seven compartments representing x_1: *Foliage*, x_2: *Wood*, x_3: *Fine roots*, x_4: *Coarse roots*, x_5: *Fine litter*, x_6: *Coarse woody debris*, and x_7: *Soil carbon (0 – 30 cm)*. Carbon enters the *foliage* compartment in the form of gross primary production, with an average value of 23.7 MgC ha^{-1} yr^{-1}. From the *foliage* (x_1), carbon is transferred to the *wood* and root pools (x_2, x_3, x_4), and from these live biomass pools, carbon is subsequently transferred to the dead biomass and soil pools (x_5, x_6, x_7). A pictorial structure of this compartmental system can be visualized on the Figure 3.8. In compartmental form, the Porce model can be expressed as the equation (3.14).

$$\begin{pmatrix} \dot{x}_1 \\ \dot{x}_2 \\ \dot{x}_3 \\ \dot{x}_4 \\ \dot{x}_5 \\ \dot{x}_6 \\ \dot{x}_7 \end{pmatrix} = \begin{pmatrix} 23.74 \\ 0 \\ 0 \\ 0 \\ 0 \\ 0 \\ 0 \end{pmatrix} + \begin{pmatrix} -2.98 & 0 & 0 & 0 & 0 & 0 & 0 \\ 0.47 & -0.03 & 0 & 0 & 0 & 0 & 0 \\ 0.03 & 0 & -0.03 & 0 & 0 & 0 & 0 \\ 0.09 & 0 & 0 & -0.02 & 0 & 0 & 0 \\ 0.75 & 0 & 0.03 & 0 & -2.6 & 0 & 0 \\ 0 & 0.009 & 0 & 0.00002 & 0 & -0.52 & 0 \\ 0 & 0 & 0 & 0 & 0.66 & 0.51 & -0.02 \end{pmatrix} \begin{pmatrix} x_1 \\ x_2 \\ x_3 \\ x_4 \\ x_5 \\ x_6 \\ x_7 \end{pmatrix}. \tag{3.14}$$

The age and transit time distributions of this compartmental model can be observed in the Figures 3.9a and 3.10a, respectively. Additionally, from the age and transit time distributions, we have also computed the radiocarbon distributions for the years 1965, 2027 and 2100 (Figures 3.9b–d, 3.10b, A.6, A.7 and A.8), as well as the radiocarbon distributions of the whole system and its total outflux for the period between 1955 and 2100 (Videos S3 and S4). The arguments of the functions used to compute the theoretical radiocarbon distributions are the same ones used for the HFS model, following the section 3.3.4. Therefore, the bin size b of the distributions for the year 1965 is $b = 40$ ‰, while for 2027 and 2100 it is set as $b = 10$ ‰.

As observed in the HFS model, the probability distribution of radiocarbon for the whole system has the mode on $\Delta^{14}C$ values of the main contributor, a slow-cycling pool: *Soil carbon (0 – 30cm)* (Figures 3.9b–d, and A.6 – A.8). Moreover, for the year 2100, where the atmospheric $\Delta^{14}CO_2$ will most likely have largely dropped due to the Suess effect (Graven, 2015), the distribution of radiocarbon of slow pools is wide.

In the outflux of the Porce model (Figure 3.10b, A.6, A.7 and A.8), the peaks are related to the fast dynamics of pools, such as *foliage* and *fine litter*. The expected $\Delta^{14}C$ values in the year of observation of the fast pools will change according to the atmospheric radiocarbon signals detected for the contemporaneous years of sampling (Figures A.6, A.7 and A.8).

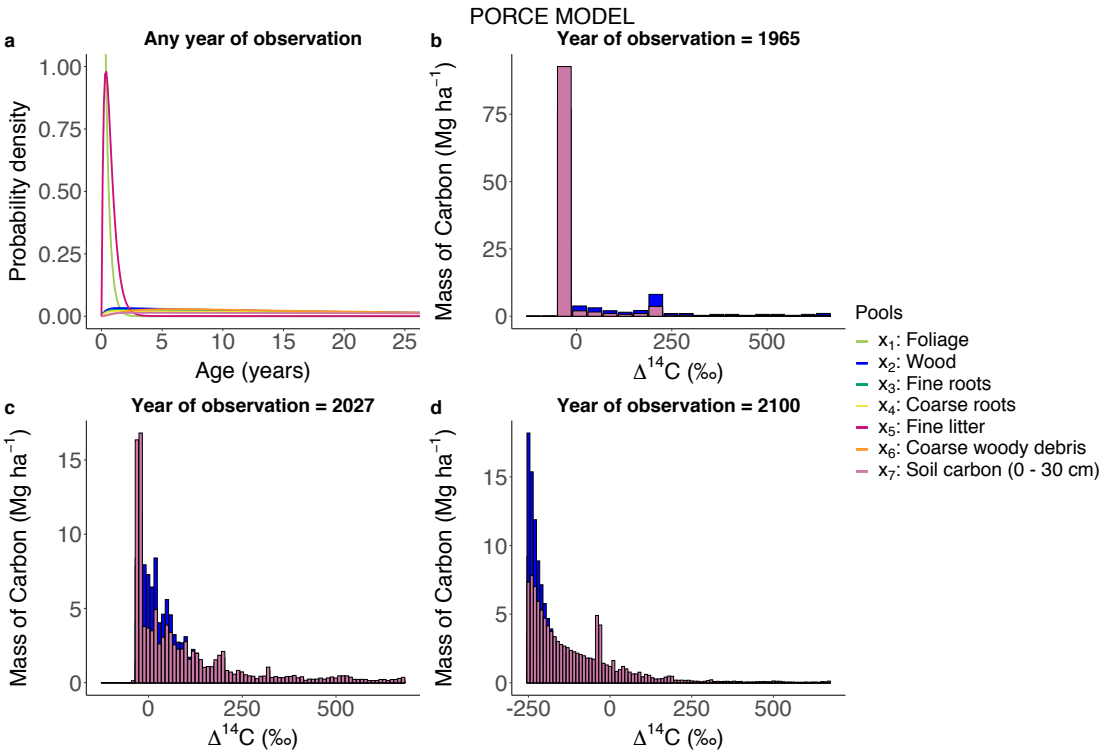

FIGURE 3.9: **(a)** Pool age distributions for the Porce model computed in a span of 1,000 years with a resolution of 0.1 year. Mean system age is 40.7 years. Mean pool ages vary from 0.3 yrs (for *Foliage* pool) to 55.3 yrs (for *Soil Carbon* pool). **(b)** Mass density distribution of radiocarbon for 1965 – just after the ^{14}C bomb peak in 1964. Distribution was computed over 1,000 years, discretized by 0.1 yrs. Bin size b = 40 ‰. The expected Δ^{14}C and standard deviation (sd) of the whole system in 1965 is 62.3 $\pm$ 193 ‰. **(c)** Mass density distribution of radiocarbon for 2027. Distribution was computed over 1,000 years, discretized by 0.1 yrs. Bin size b = 10 ‰. The expected Δ^{14}C and sd of the whole system in 2027 is 85.4 $\pm$ 151 ‰. **(d)** Mass density distribution of radiocarbon for 2100. Distribution was computed over 1,000 years, discretized by 0.1 yrs. Bin size b = 10 ‰. The expected Δ^{14}C and sd of the whole system in 2100 is -147.9 $\pm$ 131 ‰.

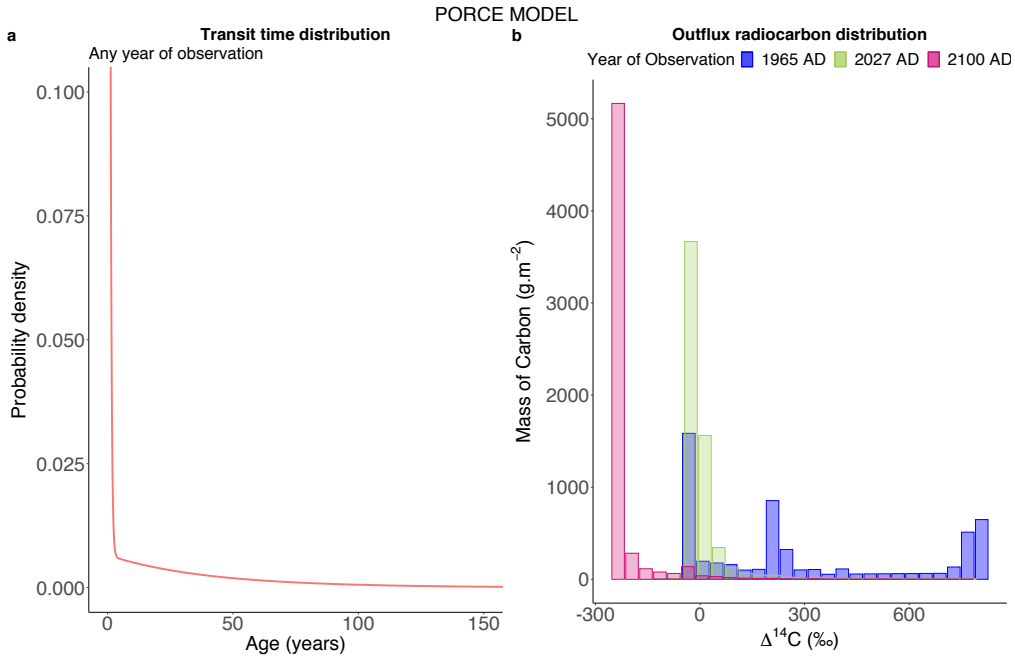

FIGURE 3.10: **(a)** Transit time distribution for the Porce model computed in a span of 1,000 years with a resolution of 0.1 year. Mean transit time is 11.3 years. **(b)** Mass density distributions of radiocarbon for the output flux (total respiration) in the years 1965, 2027 and 2100. Distribution was computed over 1,000 years, discretized by 0.1 yrs. Bin size $b = 40‰$ for all the years of observation. The expected $\Delta^{14}C$ values and standard deviations of the outflux are: 532 ± 292 ‰ in 1965; 1.1 ± 90 ‰ in 2027; and -227 $\pm$ 80 ‰ in 2100.

3.4.3 Emanuel Model

The Emanuel model was published in 1981 and consists of a 5-box model of the global terrestrial carbon cycle. The boxes represent the pools x_1: *Non-woody tree parts*, x_2: *Woody tree parts*, x_3: *Ground vegetation*, x_4: *Detritus/Decomposers*, and x_5: *Active soil carbon*. There are inputs from the atmosphere to two pools (x_1 and x_3). From x_1 carbon is partitioned into pools x_2 and x_4. Carbon from x_3 partition into pool x_5, which also receive the transfers from pools x_2 and x_4. All the stocks (in PgC) and transfers among the compartments (in PgC yr^{-1}) can be visualized in the scheme on the Figure 3.11. In compartmental form, the Emanuel model is represented by equation (3.15).

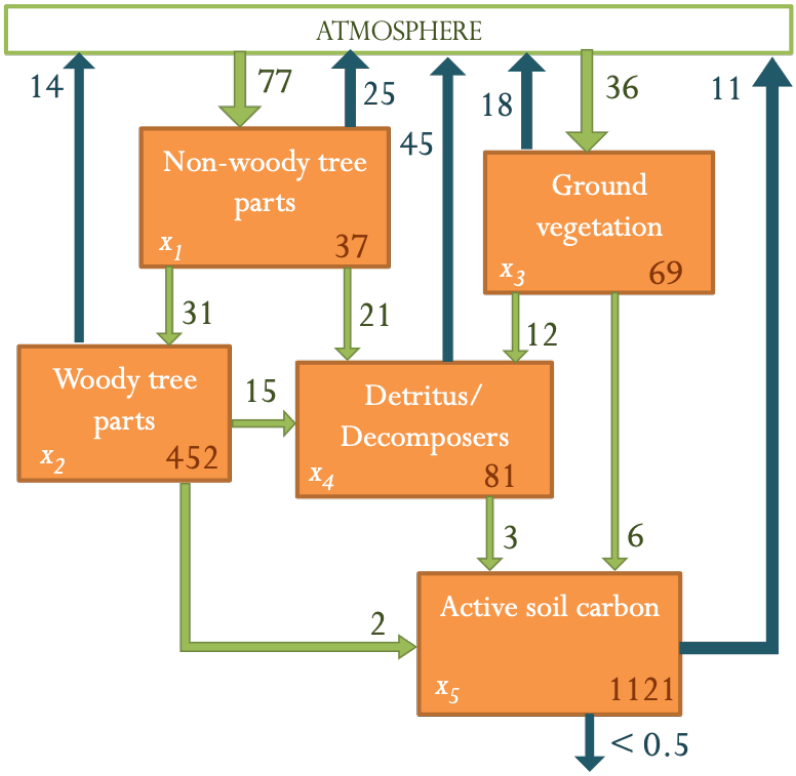

FIGURE 3.11: Scheme representing the stocks (in PgC) and fluxes (in PgC yr^{-1}) among compartments in Emanuel model (adapted from Emanuel et al. (1981)). Pools are numbered as x_1: *Non-woody tree parts*, x_2: *Woody tree parts*, x_3: *Ground vegetation*, x_4: *Detritus/Decomposers*, and x_5: *Active soil carbon*.

$$\begin{pmatrix} \dot{x}_1 \\ \dot{x}_2 \\ \dot{x}_3 \\ \dot{x}_4 \\ \dot{x}_5 \end{pmatrix} = \begin{pmatrix} 77 \\ 0 \\ 36 \\ 0 \\ 0 \end{pmatrix} + \begin{pmatrix} -77/37 & 0 & 0 & 0 & 0 \\ 31/37 & -31/452 & 0 & 0 & 0 \\ 0 & 0 & -36/69 & 0 & 0 \\ 21/37 & 15/452 & 12/69 & -48/81 & 0 \\ 0 & 2/452 & 6/69 & 3/81 & -11/1121 \end{pmatrix} \begin{pmatrix} x_1 \\ x_2 \\ x_3 \\ x_4 \\ x_5 \end{pmatrix}, \tag{3.15}$$

As pointed out by Emanuel et al. (1981), the *active soil carbon* compartment x_5 has a turnover time much smaller than 1,000 years. Therefore, the choice of *nyears* parameter equals to 1,000 years is plausible and sufficient for the coverage of the entire variability in the computation. The radiocarbon data used to initialize the algorithm was the same used for the HFS model, discussed in the subsection 3.3.1. The arguments of the functions used to compute the theoretical radiocarbon distributions are

the same ones used for the HFS and Porce models, following the subsection 3.3.4. Particularly for the aggregation step, it means the bin size b of the distributions for the year 1965 is $b = 40$ ‰, while for 2027 and 2100 it is set as $b = 10$ ‰.

The age and transit time distributions of this compartmental model can be observed in the Figures 3.12a and 3.13a. Moreover, from the age and transit time distributions, we have also computed the radiocarbon distributions for the years 1965, 2027 and 2100 (Figures 3.12b–d, 3.13b, A.9, A.10 and A.11), as well as the radiocarbon distributions of the whole system and its total outflux for the period between 1955 and 2100 (Videos S5 and S6).

As observed for the other two models, slower pools also show a wider $\Delta^{14}C$ distribution in the Emanuel model. The widest distributions are from *woody tree parts* and *active soil carbon* (Figure A.9, A.10 and A.11). This might reflect the slow incorporation of the input radiocarbon signal to those pools.

In the Emanuel model, the largest outflux back to atmosphere comes from the *detritus/decomposers* pool (45 PgC yr^{-1}) (Figure 3.11). Analogously to the HFS model, the Emanuel model has its outflux radiocarbon distribution (Figure 3.13b) similar to the distributions of the fast-cycling pools, such as *detritus/decomposers* (Figures A.9, A.10 and A.11), however, the expected $\Delta^{14}C$ values are evidently different (Figures A.9, A.10 and A.11).

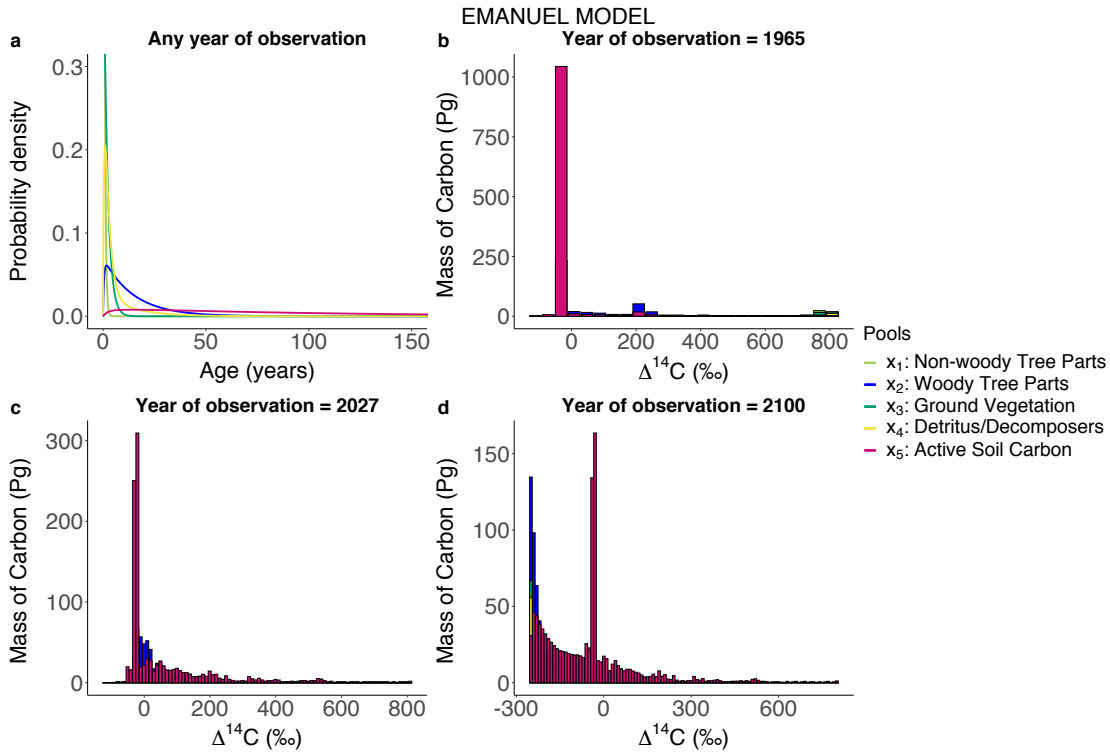

FIGURE 3.12: **(a)** Pool age distributions for the Emanuel model computed in a span of 1,000 years with a resolution of 0.1 year. Mean system age is 72.8 years. Mean pool ages vary from 0.5 yrs (for *Non-woody Tree Parts* pool) to 108 yrs (for *Active Soil Carbon* pool). **(b)** Mass density distribution of radiocarbon for 1965 – just after the ^{14}C bomb peak in 1964. Distribution was computed over 1,000 years, discretized by 0.1 yrs. Bin size b = 40 ‰. The expected $\Delta^{14}C$ and standard deviation (sd) of the whole system in 1965 is 98 $\pm$ 255 ‰. **(c)** Mass density distribution of radiocarbon for 2027. Distribution was computed over 1,000 years, discretized by 0.1 yrs. Bin size b = 10 ‰. The expected $\Delta^{14}C$ and sd of the whole system in 2027 is 53 $\pm$ 146 ‰. **(d)** Mass density distribution of radiocarbon for 2100. Distribution was computed over 1,000 years, discretized by 0.1 yrs. Bin size b = 10 ‰. The expected $\Delta^{14}C$ and sd of the whole system in 2100 is -116 $\pm$ 161 ‰.

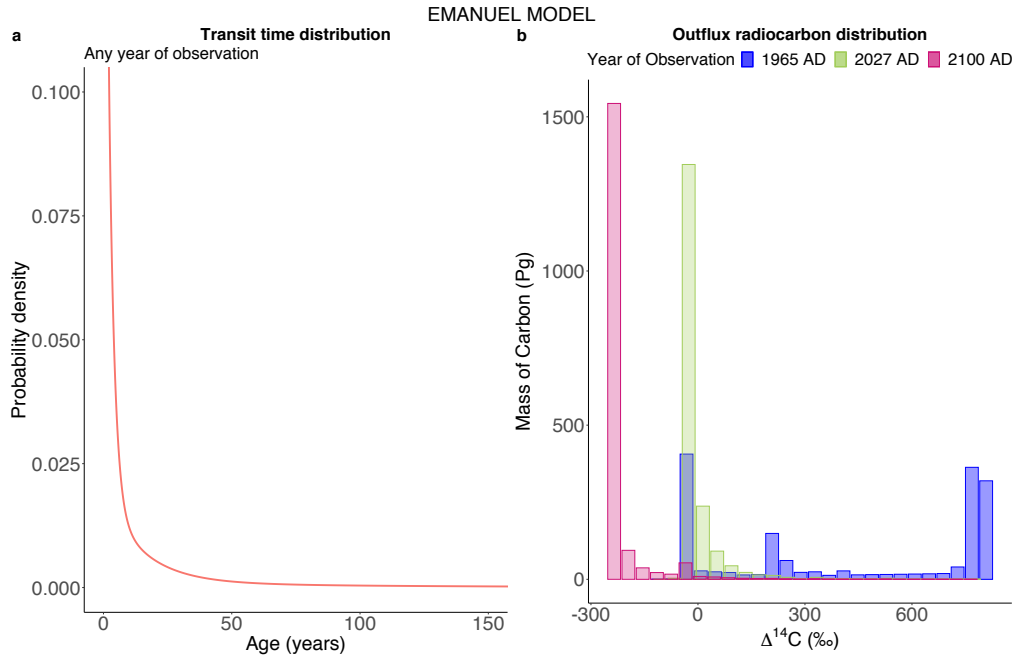

FIGURE 3.13: **(a)** Transit time distribution for the Emanuel model computed in a span of 1,000 years with a resolution of 0.1 year. Mean transit time is 15.6 years. **(b)** Mass density distributions of radiocarbon for the output flux (total respiration) in the years 1965, 2027 and 2100. Distribution was computed over 1,000 years, discretized by 0.1 yrs. Bin size $b = 40‰$ for all the years of observation. The expected $\Delta^{14}C$ values and standard deviations of the outflux are: 467 ± 354 ‰ in 1965; 2.2 ± 78 ‰ in 2027; and -225 $\pm$ 80 ‰ in 2100.

3.5 Discussion

Overall, our results show that even though the age and transit time distributions for the compartmental systems at steady-state are static (Figures 3.5a, 3.6a, 3.9a, 3.10a, 3.12a and 3.13a), the radiocarbon distributions are highly dynamic and non-normal (e.g. Figures 3.5b–d, 3.9b–d, 3.12b–d, Videos S1–S6). They change dramatically over time as the atmospheric CO_2 source is affected by the bomb spike and the Suess effect (Suess, 1955), i.e., the effect of the dilution of radiocarbon in the atmosphere due to the emission of fossil fuels (^{14}C-free). Pools that cycle fast, i.e., pools with sharp age distribution peaks, such as *dead roots* and *Oi* in the HFS model or *foliage* in the Porce model, followed most closely the radiocarbon dynamics in the atmosphere, while pools that cycle slowly showed a wide range of values. Consequently, the expected $\Delta^{14}C$ values also vary largely.

The distributions we obtained for the compartments of all models show very unique shapes for different years and the $\Delta^{14}C$ values are not normally distributed. In 1965, just after the peak of excess ^{14}C in the atmosphere due to nuclear weapon tests, pools that cycle fast had a wide $\Delta^{14}C$ range with high probability, due to the incorporation of radiocarbon values that changed rapidly over the period 1955 – 1964 CE. Compartments that cycle slowly have a narrower distribution with their modes corresponding to negative $\Delta^{14}C$ values, as they represent pre-bomb atmospheric signals that varied less.

3.5.1 How do distributions of radiocarbon change over time as a consequence of changes in atmospheric radiocarbon?

Our results clearly showed that distributions of radiocarbon in a compartmental system at steady-state change considerably over time, despite the stationarity of the age and transit time distributions for such systems, where the total mass of carbon does not change over time. These changes reflect recent and expected dramatic changes in the carbon isotopic signature of the inputs originating in the atmosphere, including the bomb spike and the Suess effect, which acts as tracer of the global carbon cycle.

In the non-steady-state case, the age and transit time distributions become also time dependent. There are methods for obtaining age distributions of carbon in compartmental systems out of equilibrium (Metzler et al., 2018), however, the additional complexity that would be incorporated to the algorithm is outside the scope of this manuscript. We expect, nevertheless, that the topic of radiocarbon distributions for non-linear and non-autonomous systems can be discussed in future work.

For fast cycling pools, we expect changes to match that of the radiocarbon content in the atmosphere. Consequently, the radiocarbon distributions for fast cycling pools present peaks in $\Delta^{14}C$ values similar to those from the contemporary atmospheric radiocarbon. That is an effect of the fast response of highly dynamic pools to the variations in the isotopic composition of the system inputs. As fast pools are the major contributors to the output flux, the total respiration also has similar narrow distributions close to the atmospheric $\Delta^{14}C$ in the year of observation t_0. For slow cycling pools that receive carbon from other pools, we expect wider distributions that include contributions from C fixed decades to centuries in the past. Thus,

excess ^{14}C takes a longer time to be observed in the radiocarbon distributions of slow cycling pools.

As a consequence of fossil fuel (^{14}C-free) emissions to the atmosphere, the dilution of atmospheric radiocarbon (Suess effect, Suess (1955)) affects radiocarbon distributions, without affecting, however, the dynamic equilibrium (steady-state) of the compartmental system. This further widens distributions in slow cycling pools, and causes fast cycling pools to have lower $\Delta^{14}C$ values than slow cycling pools. The Suess effect becomes particularly relevant in the distributions for future years, as shown in the distributions of radiocarbon based on the forecast of atmospheric $\Delta^{14}CO_2$ values. The $\Delta^{14}CO_2$ in the atmosphere is estimated to achieve values as low as ca. -254 ‰ in 2100 for the RCP8.5 scenario (Graven, 2015). Such low values can emerge in the radiocarbon distributions of the pools with relatively high density in two cases: (i) if the pool cycles fast but the $\Delta^{14}C$ values in the atmosphere present high dilution (as in 2100), or (ii) with natural or bomb, however non-diluted, $\Delta^{14}C$ values in the atmosphere, but in very slow cycling pools (i.e., >2,500 yrs of carbon age). The latter case reflects sufficient time for radioactive decay to reduce radiocarbon ratios in the carbon residing in the system. In experiments, this could result in an inability to distinguish faster and slower cycling pools using $\Delta^{14}C$ average values. Thus, one advantage of using these radiocarbon distributions is to get insight into the dynamics of transfers in the compartmental system, highlighting when these become less meaningful in the future years. Such issues can begin as soon as in 2027, when the atmospheric $\Delta^{14}CO_2$ values start to decline to values never observed before by natural processes (i.e., without the anthropogenic effects such as the fossil fuel emissions). In the forecast for central Europe (Sierra, 2018), this transition year occurs as soon as 2022. This underlines the urgency of measurements in the current situation and the use of archived samples from the last decades, to emphasize the difference between fast pools that will track the changing atmosphere and slower pools that adjust more gradually and retain bomb ^{14}C signals even in future decades.

3.5.2 How do empirical data compare to these conceptual radiocarbon distributions?

Measurements of radiocarbon in the output flux of a soil system suggest that field measurements capture the mean value of the distributions, but not necessarily the

variance of its distribution. The observations tend to be around the mean value with a fairly small standard deviation. Conversely, the estimate of $\Delta^{14}C$ values from the model show that for slow cycling pools, the spread of the $\Delta^{14}C$ distributions can capture almost all the atmospheric $\Delta^{14}CO_2$ history.

Although we do not have independent observations available for specific pools to compare with our model predictions, we expect that for fast cycling pools the measurements will fall in a narrow range of $\Delta^{14}C$ values, as can be observed in experiments assessing the fossil fuel CO_2 distribution by measurements of $\Delta^{14}C$ on deciduous leaves (Santos et al., 2019). For slow cycling pools, we would expect that the variability of $\Delta^{14}C$ experimental data will be broader.

Carbon pools that cycle slowly can be very important for climate change mitigation, since they could store carbon for a longer time. Therefore, an accurate understanding of their dynamics is crucial. A valuable tool to assess these dynamics is using radiocarbon as a tracer to further constrain models. However, based on our results and interpretations, we believe that future research work should attempt at better capturing the spread of radiocarbon values in such pools.

We recognize that the variability in the observations includes measurement uncertainty in addition to the expected variability due to the age distribution of carbon and the atmospheric radiocarbon history. Nevertheless, the comparison of the variability between measurements and the theoretical distributions help to contextualize the origin of the observed variance and interpret measurements performed in different years.

3.5.3 What insights can these distributions provide for experimental and sampling design for improving model-data comparisons by capturing the entire variability of $\Delta^{14}C$ values?

Overall, our results have implications for the interpretation of measured radiocarbon data. The radiocarbon distributions computed here can also give useful insights for the design of empirical studies. The number of samples required to adequately represent the internal variability in radiocarbon depends on the year of observation and the particular compartment of interest. Our results suggest that fast cycling pools can have their $\Delta^{14}C$ mean determined with a low sample size. For example, this would be the case for *dead roots* and *Oi* pools in the HFS model; *foliage* and *fine litter* in the Porce model; and *non-woody tree parts* and *ground vegetation* in the Emanuel

model. A priori, determining exact sample sizes may be a suitable approach for future studies. For samples already collected, caution must be taken in interpreting the results, since a bulk measurement may not capture the whole distribution of possible radiocarbon values.

Our study opens up new opportunities to empirically determining radiocarbon distributions in compartmental systems. For example, this could be achieved by sampling designs that are representative of the compartments with higher variance, making sure the number of samples catches the entire potential variability. This way, it should be possible to determine empirical radiocarbon distributions. Consequently, empirical determination of radiocarbon distributions in compartmental systems could be used to obtain age and transit time distributions using inverse statistical methods. This offers tremendous opportunities for accurate estimations of time metrics, incorporating the complexity of biological systems through multiple interconnected compartments. However, more research is still needed to determine whether radiocarbon distributions map to unique age and transit time distributions. To guarantee the uniqueness of the age and transit time distributions from compartmental systems, one should be able to assure that only one combination of rates in the compartmental matrix builds the estimated distributions.

Moreover, as pointed out by Gaudinski et al. (2000), limited information about the cycling rates are obtained by ^{14}C measurements of bulk SOM made at a single point in time. Therefore, being able to compute radiocarbon distributions for different years of observation could improve the interpretations of the time-evolution of carbon in compartmental systems.

3.6 Conclusions

We introduced here a new method to obtain probability distributions of radiocarbon in open compartmental systems based on previous knowledge on the age distribution of carbon and the time history of atmospheric $\Delta^{14}CO_2$. By applying this method to different models, we were able to infer potential shapes of radiocarbon distributions in compartments that strongly change over time and depend on how fast carbon cycles within each compartment.

Radiocarbon distributions (formally distributions of $\Delta^{14}C$) cannot be interpreted directly as distributions of age of carbon. Distinctively to age, $\Delta^{14}C$ values in a pool do not increase/decrease monotonically; in addition, the $\Delta^{14}C$ mean value changes

over time due to inputs from the atmospheric signal and mixing inside and among compartments even for systems at steady-state – in contrast to age distributions, which do not change with the year of observation for such systems. This implies that we can have two or more different calendar years with the same $\Delta^{14}C$. Therefore, despite age and transit time distributions for systems in steady-state being static, radiocarbon distributions' shape, expected value, mode, and variance are expected to vary greatly over time, especially since the beginning of the Anthropocene epoch.

Radiocarbon distributions can be used together with the known changes in atmospheric $\Delta^{14}CO_2$ to evaluate how models predict the changing distributions of radiocarbon in each compartment and its output over the last decades. This provides a reliable and consistent method to test models against observations of systems in equilibrium and to refine model representations of C dynamics in soils and ecosystems.

3.7 Availability Statements

Data availability The atmospheric $\Delta^{14}CO_2$ datasets used in this research are available through Graven (2015), Graven et al. (2017), and Reimer et al. (2020) or http://intcal.org. Data on the compartmental model presented in this research as HFS model, including the independent $\Delta^{14}C$ data used for comparisons with our estimations are available through Sierra et al. (2012b). The coefficients used for the Porce model are available in Sierra et al. (2021). The global carbon cycle compartmental model used here, namely Emanuel model, can be accessed in Emanuel et al. (1981).

Code availability The algorithm developed to estimate the radiocarbon distributions in the individual compartments, the whole system and the outflux, as well as an R script to plot the distributions and calculate the expected values of the distributions have been permanently archived in Zenodo with the digital object identifier https://doi.org/10.5281/zenodo.6373329 (Chanca, 2022) as well as a public GitHub repository through the link: https://github.com/ingridchanca/RDCDistributionOpenComp.git.

Chapter 4

Measuring carbon isotopes in the central Amazon

Tropical forests, when undisturbed, are believed to have strong carbon uptake rates (Stephens et al., 2007). It has also been estimated that tropical forests can store approximately 46 % of the carbon in living terrestrial reservoirs worldwide (Soepadmo, 1993), and for this reason, they may have an important role in mitigating global warming, even though they account only for ca. 13 % of the ice-free land on the Earth's surface (Saugier et al., 2001). The vegetation and soil in tropical forests not only store but also cycle huge amounts of carbon through two main processes: photosynthesis and respiration. These two processes are responsible for the major fluxes between the terrestrial biosphere and the atmosphere. While photosynthesis produces carbohydrates using atmospheric CO_2 in a photochemical reaction, respiration follows the inverse path by breaking down glucose into CO_2 and breathing it back to the atmosphere.

Special attention should be reserved to tropical rainforests, as they proved to be important in regulating climate, maintaining biodiversity, and sequestrating carbon (Fu et al., 2018). An important forest in this category is the Amazon rainforest. It is estimated based on checklists of tree taxa for the Amazon forests that they account for ca. 11 % to ca. 20 % of the estimated number of the world's tree species (Ter Steege et al., 2016; Cardoso et al., 2017). Besides its large species diversity, it contains as well a remarkable diversity of ecosystem types such as *Terra-Firme*, *Várzea*, *Igapó*, *Campina*, Savanna, and *Campinarana* (Villa Zegarra, 2017). This large diversity is, however, a source of complexity and uncertainties on the major fluxes of carbon between the Amazon rainforest and atmosphere. A high variety of plant and animal species, and a range of environmental features such as soil composition,

atmospheric carbon dioxide concentration, relative humidity, wind, light, temperature and nutrients, contribute to the complexity of the carbon dynamics within these different ecosystems. Therefore, finding proxies for estimating the potential C sequestration of the forest in an experimentally manageable way and that takes such complexities implicitly is of great interest. A pivotal diagnostic metric for characterising the potential of terrestrial ecosystems in the land C sequestration is the C transit time, defined as the mean age of carbon mass in the ecosystem respiration (Rasmussen et al., 2016; Sierra et al., 2017; Lu et al., 2018). Particularly radiocarbon can be used to trace the carbon dynamics of different ecosystems, different compartments and as a tool to estimate the C transit time of the ecosystem.

The main objective of this chapter is to estimate the average time carbon stays in a central Amazon primary forest using radiocarbon as a tracer. To do so, the questions addressed in this chapter are (i) can we observe differences in the cycling rates between *campinarana* and *terra-firme* using $\Delta^{14}C$ measurements alone? (ii) how do $\Delta^{14}C$ values give us insights into the cycling rates of different compartments? (iii) how long does carbon take to be respired by a *terra-firme* ecosystem in central Amazon?

4.1 Theoretical background

The major uncertainties of the carbon cycle balance are linked to the poor comprehension of the feedbacks between processes in the terrestrial ecosystems and concentrations of carbon dioxide in the atmosphere (Pataki et al., 2003; Stephens et al., 2007). Whereas photosynthesis consists of one main process, the assimilation of CO_2 by primary producers, the ecosystem respiration flux is the result of the metabolism of many different biological components (e.g. woody and non-woody tissue, soil microorganisms). Ecosystem respiration is commonly conceptualized as the sum of two main components, respiration from autotrophic organisms (mostly plants) and respiration from heterotrophic organisms (fungi and bacteria).

Given the complexity of the respiration process, there is still a large uncertainty in the partitioning of ecosystem's respiration, which affects the ability to understand carbon-climate feedbacks. The relative contribution of different sources to the ecosystem respiration can be estimated by several approaches, ranging from techniques that might disturb the conditions of the system such as root exclusion and component integration (Lalonde and Prescott, 2007; Sapronov and Kuzyakov, 2007)

to less invasive and disruptive methods such as the determination of isotopic carbon (stable and unstable) ratio (Hardie et al., 2009). Hence observations of carbon isotopic ratios in the ambient CO_2 and in the respiration flux can help to disentangle the different processes involved in ecosystem respiration.

The carbon isotopic ratio in terrestrial ecosystems is altered by fractionation effects caused during photosynthesis and respiration. Photosynthesis tends to select $^{12}CO_2$ molecules over heavier C isotopologues from the atmosphere as they will react faster due to their lower mass. Consequently, the C isotopic ratio on the respired CO_2 will be depleted (less heavier C isotopes, i.e. more negative C signal) when compared to the C ratio in the free-atmosphere. Hence observing the variation of this signal in the atmospheric air within and above the canopy is a tool for understanding the carbon cycle balance. Moreover, since C isotopes are subjected to mass-dependent fractionation effects, it is important to take into account potential effects of *de novo* assimilation on the interpretation of C isotope ratios. For instance, in forests, CO_2 released from the soil can be reassimilated by the foliage, especially at lower heights within the canopy, where also the light intensity is lower. The 'recycling' of CO_2 contribute to a more depleted $\delta^{13}C$ on leaves. This effect is known as the *canopy effect* (Van Der Merwe and Medina, 1991, and references therein) and it is particularly strong in dense forests.

As discussed in chapter 2, nuclear weapon tests in the atmosphere during the 1960s produced a large number of thermal neutrons that led to the production of excess ^{14}C. After the Limited Test Ban Treaty in 1963, the concentration of radiocarbon in the atmosphere started to decline due to its incorporation in the biosphere (terrestrial reservoirs and ocean). Thus, the ratio ^{14}C to C[1] works as tracer of the fate of carbon in the atmosphere-biosphere cycle path.

The partition of C isotopes after biogeochemical processes due to fractionation effects allows one to determine the sources of the C isotope signal. However, in this chapter, the $\Delta^{14}C$ (corrected for mass-dependent fractionation effect, section 2.1.2) is used to estimate the time C takes to transit the system, as the internal processes occur at varied rates. Especially during the course of slow-cycling processes, some ^{14}C might decay. The ^{14}C-to-C ratio of the ecosystem respiration is used to infer the mean (transit) time that carbon takes from the moment of assimilation through photosynthesis to the moment of release through respiration.

[1] Total C = N(^{12}C) + N(^{13}C) + N(^{14}C) $\approx$ N(^{12}C) + N(^{13}C)

There is some evidence in the past 20 years that a large fraction of carbon from respired CO_2 in forests comes from carbohydrates recently metabolized (Waring et al., 1998; Malhi et al., 1999; Trumbore, 2000; Chambers et al., 2004; Sierra et al., 2021). The remaining fraction can take orders of magnitudes longer to be decomposed, generating a distribution of transit times. This distribution of transit times is reflected in a distribution of radiocarbon values at the output flux, as shown in chapter 3. However, as also shown in the previous chapter, the expected value of this underlying distribution of radiocarbon is close to the experimental mean values of $\Delta^{14}C$ in steady-state conditions. Thus, the estimate of the mean transit time based on a mean value of $\Delta^{14}C$ in the ecosystem respiration, despite not intrinsically accurate, can be a good estimation of the order of magnitude of this quantity.

4.1.1 The Keeling plot method

Carbon stable isotopes can provide information on the sources composing the observed signal of atmospheric CO_2 within a forest canopy. Carbon stable isotopic signals are the result of the integration of diverse fractionation processes, each with a different footprint. In order to estimate the origin of the composed signal, mixing models can be used. This idea was used by Charles D. Keeling when developing a method to identify isotopic sources in air samples (Keeling, 1958; Keeling, 1961). The same approach could be used for the ratio of radioactive carbon and stable carbon ($\Delta^{14}C$), to obtain insights on the transit time of carbon, i.e. the age of carbon in the respiration source (Phillips et al., 2015).

The basis of the Keeling plot method is the conservation of mass (Equation 4.1) and of the product of CO_2 concentration and the C ratio (Equation 4.2, Tans (1980)), which leads to the requirement that the background signal does not change over time (Keeling, 1958; Keeling, 1961). The CO_2 in the air within the canopy of a forest is a mix of the CO_2 from the troposphere with the CO_2 from ecosystem respiration. The carbon isotopic ratio of these elements can be combined in a simple mixing model as

$$[CO_2]_{canopy} = [CO_2]_{trop} + [CO_2]_{ER} \tag{4.1}$$

where *trop* stands for *troposphere* and *ER* for *ecosystem respiration*. The corresponding equation for isotopic ratios Δ of the ^{13}C or ^{14}C isotopes can be expressed as

$$\Delta_{canopy}[CO_2]_{canopy} = \Delta_{trop}[CO_2]_{trop} + \Delta_{ER}[CO_2]_{ER}. \quad (4.2)$$

Considering that $[CO_2]_{canopy}$ is simply the sum of the concentration of the ecosystem respired CO_2 ($[CO_2]_{ER}$) and of the CO_2 in the troposphere ($[CO_2]_{trop}$), equation (4.2) can be reduced to:

$$\Delta_{canopy} = \frac{[CO_2]_{trop}}{[CO_2]_{canopy}}(\Delta_{trop} - \Delta_{ER}) + \Delta_{ER} \quad (4.3)$$

The equation (4.3) has a linear relation of the form $y = ax + b$, where:

- the independent variable x is $\frac{1}{[CO_2]_{canopy}}$,
- y is the C isotopic ratio in the canopy, i.e. Δ_{canopy},
- $a = (\Delta_{trop} - \Delta_{ER})[CO_2]_{trop}$, and
- b, or hereafter the y-intercept, is Δ_{ER}, i.e. the C isotopic ratio of CO_2 respired by the whole ecosystem.

4.1.2 Miller-Tans mixing model

The Miller-Tans model is a two-member mixing model, as the Keeling plot approach. The underlying assumptions made by Miller and Tans (2003) are the same applied by Keeling (1958). However, by a rearrangement of the equations (4.1) and (4.2), the Miller-Tans model becomes suitable for cases where both background CO_2 concentration and isotopic composition change over time. This method consists of a canopy-minus-background approach and the mixing model is described as:

$$\Delta_{canopy}[CO_2]_{canopy} - \Delta_{trop}[CO_2]_{trop} = \Delta_{ER}([CO_2]_{canopy} - [CO_2]_{trop}), \quad (4.4)$$

where Δ represents the C isotope ratio (i.e. $\delta^{13}C$ or $\Delta^{14}C$). In equation (4.4), the C isotopic ratio of CO_2 respired by the whole ecosystem (Δ_{ER}) corresponds to the slope of the linear equation.

4.2 Study area

This study was performed in locations inside the ATTO (Amazon Tall Tower Observatory) site. The ATTO site is situated in the Uatumã Sustainable Development Reserve (in portuguese: *Reserva de Desenvolvimento Sustentável do Uatumã*, RDS-Uatumã), ca. 150 km NE of the city of Manaus, Amazonas, Brazil. Besides permanent research plots, the ATTO site maintains three research towers equipped with instruments for measurements related to diverse fields of study, such as greenhouse gases, micrometeorology, and aerosols, among others. One tower is what names the Brazilian-German project ATTO and stands for Amazon Tall Tower Observatory. The ATTO tower is 325 m high and was installed in 2015 in the ATTO site. Two other towers were built in 2010 and 2011. One of them is an 80 m heavy-duty guy-wired walk-up tower (Instant UpRight, Dublin, Ireland, henceforth *instant tower*) and the second one is an 81 m triangular mast tower, essential for the pilot measurements in the ATTO site (Andreae et al., 2015).

The Amazon Basin, delimited by the Amazon river and its tributaries, occupies ca. one-third of South America. The Amazon Basin contains several types of ecosystems, including heath forests (in smaller and taller facies), lowland evergreen rainforests and savannah. In the RDS-Uatumã, several of those ecosystems are found. Especially in the surroundings of the ATTO site, there are research plots in the heath forests, known in Brazil by the Tupi language names *campina* (meaning 'dry and low little forest') and the ecotone *campinarana* (*-rana* means false, giving to *campinarana* the sense of *false campina*), as well as plots and research towers on the locally called *terra-firme*. More specifically, the three research towers of the ATTO site are located in the plateau of the *terra-firme* ecosystem, ca. 120 m above sea level (Andreae et al., 2015).

The ecosystems *campinarana* and *terra-firme* are distinct particularly in terms of their floristic composition, structure and soil type, despite they can be found separated by only a few kilometres. Among the several ecosystems in the Amazon Basin *campinaranas* are one of the less productive ecosystems and compared to *terra-firme* forests, they are about four times less productive (Villa Zegarra, 2017; Chambers et al., 2001b). These two ecosystems were chosen for the measurements, because they present accentuated carbon cycling differences, driven especially by the differences in the soil characteristics, but simultaneously they share the same compartments

and vegetation type (C3 plants). The *campinas* are a more distinct ecosystem regarding carbon cycling when compared to *terra-firme*, however, the absence of accumulation of litter and the major presence of shrubs would prevent the comparison of the same compartments in both ecosystems.

Campinarana is one of the types of the so-called white-sand ecosystems (WSE), that include also the *campina*. The WSE cover approximately 5 % of the Amazon Basin (Adeney et al., 2016). *Campinarana* is a ecotone marked by sandy soils with a continuous vegetation, whose canopy can be 5 – 25 m high (Figure 4.1**a**). This ecosystem faces episodes of extremes from very low to very high in terms of its soil water content. However, it does not get seasonally flooded as other ecosystems in the Amazon rainforest, such as *igapós*.

FIGURE 4.1: Vegetation in **(a)** open forested *campinarana*, as in plot C3; **(b)** *terra-firme*, similar to plot TF1. Picture **(a)** from Demarchi et al. (2022). Picture **(b)** taken by Sebastian Brill at ATTO site.

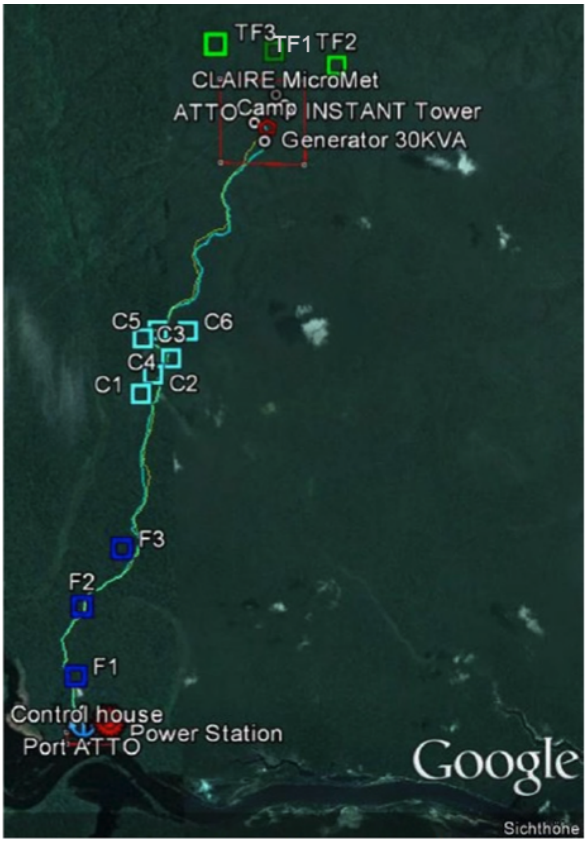

FIGURE 4.2: Map of the study area showing the existing permanent plots, including the ones where samples of this work were collected, and the instant tower. **TF** are plots in the *terra-firme* plateau, **C** stands for *campinas* and *campinaranas* and **F** refers to forests of an old riparian area. Figure from PELD-MAUA project.

Terra-firme is a local nomenclature for non-flooded lowland evergreen tropical rainforest and it is the dominant ecosystem in the Amazon Basin. It is an ecosystem characterised by clayey soils, tall trees (canopy $\sim$ 35 m high, with emergent trees achieving 45 m), high biodiversity, among other ecophysiological features (Figure 4.1**b**). The dense *terra-firme* forests in central Amazon can be subdivided according to topography into plateau, slope and valley.

For this chapter a number of samples was collected, especially to overcome the lack of radiocarbon data in the literature. Samples of tree leaves, fine litter, dead wood and stems representing respectively four compartments (foliage, fine litter, coarse woody debris and wood) and atmospheric air were collected in the plot TF1 (1.0 ha) and on the instant tower (Andreae et al., 2015), both locations in the *terra-firme* (non-flooded) plateau ecosystem. Additionally, samples from the same compartments were collected in the plot C3 (0.5 ha), located in the *campinarana* ecosystem (Figure 4.2).

4.3 Collection of samples

Tree leaves were collected in two conditions in the *terra-firme* ecosystem: in a vertical profile around the instant tower and in a random sampling on trees in the plot TF1. Leaf samples in both conditions were collected on the same day in May of 2018 (wet season) as well as the leaves collected in the *campinarana* (plot C3). Leaf samples in a vertical profile were collected a few centimetres from the edges of the instant tower

at different heights. In total, leaves from 30 heights from the highest level of the canopy next to the tower to forest ground (base of the instant tower) were collected. The plots TF1 and C3 have an area of 1 hectare and, to perform the sampling, the plots were subdivided into 10 random points of collection. For each point, a few leaves were cut with gardening scissors from the closest tree. Each set of leaves was immediately stored into a zip lock bag and received a sample ID on the bag.

Fine litter, the decomposing fallen leaves close to trees, was collected also in the TF1 and C3, right next to the tree from where leaf samples were cut off. Thus, the points of collection of litter samples were the same ones of the leaf samples. The few grams of litter collected around each tree of the points of collection were individually stored in zip lock bags and identified by a unique sample number.

Dead wood was also sampled in TF1 and C3. For each point of collection, there was at least one fallen or decomposing tree, representing the coarse woody debris compartment. Chunks of the fallen tree were removed with a machete and stored in an identified zip lock bag. Additional information as the species or age of the tree were not available. The texture of the wood varied among the samples, with some being more soft while others were dense and hard.

In each point of collection on TF1 and C3 there was one standing tree. The trees varied in size and species. In order to obtain the random variability of $\Delta^{14}C$, trees were not pre-selected by size or species. However, trees with identification tags were prioritized as more relevant information could be later obtained for those. The samples representing the wood compartment consisted of stem cores sampled with an increment borer of 5 mm diameter. The length of each sample varied according to the tree width. In contrast with stem core samples collected for routine dendrochronological studies, the stem cores collected here did not aim for the distance between the center of the tree and the bark, as the center cannot be easily determined in the field. The stem cores were stored in plastic straws and closed with lids for transportation. The increment borer was cleaned with pure alcohol and rinsed with water between each sampling.

From all the compartments, the main aim was to determine the $\Delta^{14}C$ value of the individual samples. Additionally, the leaves collected in a vertical profile had their $\delta^{13}C$ values determined by isotope ratio mass spectrometry (IRMS).

Atmospheric air was collected for the determination of $\Delta^{14}CO_2$ and $\delta^{13}CO_2$, besides greenhouse gases concentrations. The samples of air were collected in a vertical profile below the canopy ($\sim$ 35 m high), corresponding to heights of 4 m and 24

m above ground level (agl). To obtain a reference signal of the troposphere, samples of air were also collected at the top level of the instant tower, at 79 m agl. Those samples were collected in October 2019, during the dry season, every ca. two hours for 24 hours. They were collected each time with alternation of the heights, with three samples corresponding to the reference height. In this way, the number of samples summed up to 24 flasks.

The samples of air were collected in flasks made of borosilicate glass and with a volume of three liters (hereafter 3-L flasks, Figure 4.3, Lux (2018)). The 3-L flasks were prepared beforehand, being filled with transport air (dry ambient air with a well-known composition) with an overpressure of 1.6 bar. Atmospheric air was collected through a portable sampler that contains a pump enabling the air coming from an inlet to be pressurized inside the volume of the flask (Figure 4.4). Each 3-L flask was flushed with air for 15 minutes. Maintaining the flow rates at around 1.2 L/min and pressures at ca. 0.8 bar above atmospheric pressure, the samples likely represent the air of the last minute of sampling.

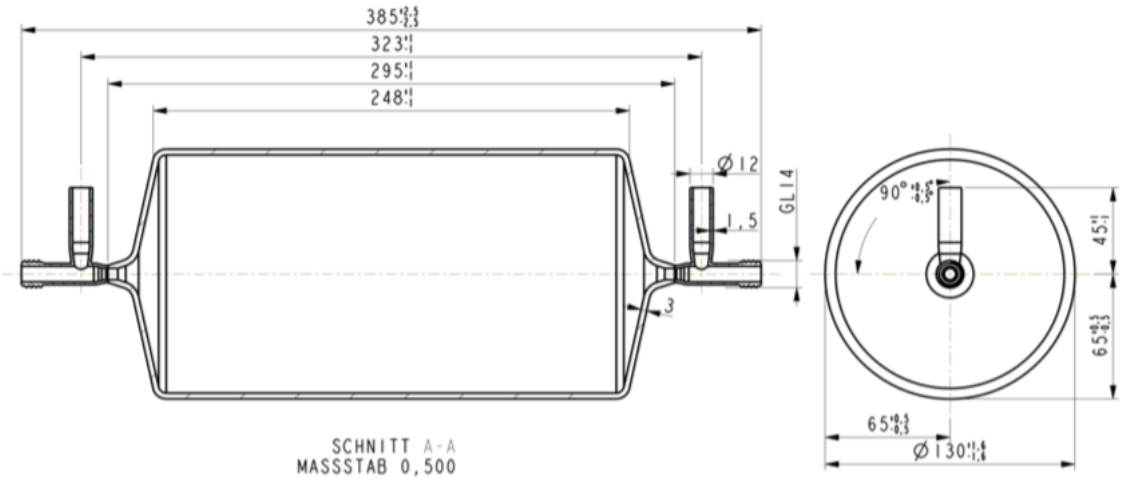

FIGURE 4.3: Technical drawing of 3L-flasks of ICOS made by Stephan Baum; Figure from Lux 2018 (thesis).

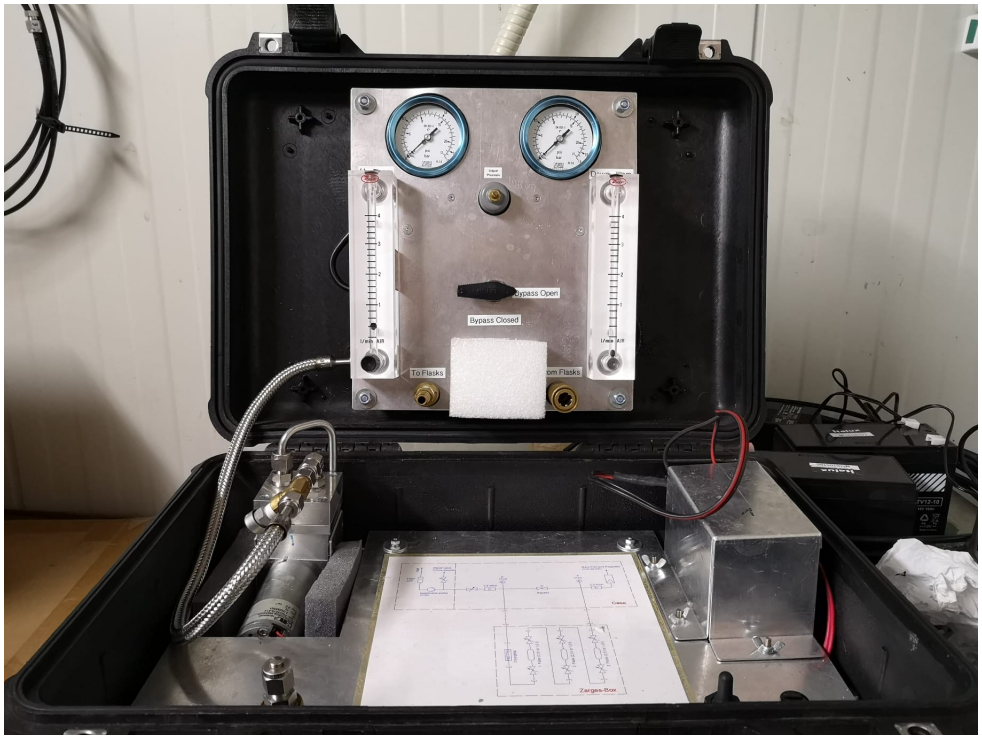

FIGURE 4.4: Picture of the portable sampler used to collect air samples in 3L-flasks at the instant tower (80 m) in ATTO site.

The air collected in 3L-flasks at the instant tower in 2019 had their CO_2 concentrations measured in the Gas laboratory at the MPI-BGC. In order to check how representative these samples were in the time of sampling, the CO_2 concentrations measured in the laboratory after ca. 20 days of the collection were compared to *in-situ* measurements performed with equipments based on the cavity ring-down spectroscopy technique (G1301 and G1302 analyzers [Picarro Inc., USA], hereinafter short-named as *Picarro*), which measures the concentrations of the CO_2/CH_4/CO continuously on the instant tower at the heights of 4 m, 24 m, 38 m, 53 m and 79 m agl (Andreae et al., 2015). The *in situ* instruments provide average values of CO_2 concentrations for every half hour throughout the year.

4.4 Preparation of samples for ^{14}C-AMS

Radiocarbon preparation and measurements were performed in four different radiocarbon laboratories. Preparation of solid (leaf, litter, dead wood and stem core) samples was performed at the LAC-UFF (Radiocarbon Laboratory at Fluminense

Federal University), in Niterói, Brazil and measured in the MICADAS (MIni CArbon DAting System) of the ^{14}C-Analytik, MPI-BGC (Radiocarbon Laboratory at Max Planck Institute for Biogeochemistry), in Jena, Germany. Carbon dioxide from air samples extracted at the ICOS-CRL (Integrated Carbon Observation System – Central Radiocarbon Laboratory) at Heidelberg University, in Heidelberg, Germany had its $\Delta^{14}CO_2$ measured at the CEZA (Curt-Engelhorn Zentrum Archäometrie) ^{14}C-AMS facility, in Mannheim, Germany.

The pretreatment of solid samples brought to LAC-UFF included: rinse with ultrapure water, drying in furnace at 40 °C, and crushing (ultra small leaves could not be crushed into powder). Large chunks of dead wood were broken into smaller pieces and rinsed several times to eliminate small insects that were still living inside the deeper parts of the sample. Additionally, stem cores were sanded before crushing. For $\Delta^{14}C$ determination, the pretreated samples were further combusted in quartz tubes containing cupric oxide (60 – 70 mg) and a silver wire at 900 °C for 5 hours. After combustion, the CO_2 was extracted through a purification line under vacuum (< 1 mTorr) by cryogenic traps (dry ice/ethanol and liquid nitrogen). The dry ice/ethanol mixture achieves -78 °C and traps the water produced during the combustion of the sample. Liquid nitrogen has a temperature of -196 °C, freezing the CO_2. The other gases, mainly N_2 and O_2, could be pumped out of the line. The pure CO_2 was transferred to graphitization tubes, which are borosilicate tubes containing TiH_2, zinc and iron powder; the latter settled inside a smaller tube to avoid contact with the other reagents. The graphitization tubes were brought to the oven at 550 °C for 7 hours, to become graphite by TiH_2/Zn reduction. For the determination of $\delta^{13}C_{leaf}$ from leaves collected in the vertical profile, a small aliquot of each sample pretreated at LAC-UFF was measured in an IRMS (Isotope Ratio Mass Spectrometer) coupled to an EA (Elemental Analyzer).

Several analyses were performed in the air of the 3L-flasks. The 3L-flasks were first shipped to the ICOS facility in Jena for measurements of the concentrations of CO_2, H_2, CO, CH_4, N_2O, and SF_6. An aliquot was also used for determination of $\delta^{13}CO_2$, and $\delta^{18}O$ of CO_2 by IRMS. After the measurements in Jena, the remaining air samples in 3L-flasks were shipped to the ICOS-CRL facility in Heidelberg, where CO_2 was extracted and converted to graphite in the line as described on the thesis of Lux (2018). The $\Delta^{14}C$ of the samples was measured at the CEZA laboratory in Mannheim. The extraction line of ICOS-CRL is similar to the one built at LAC-UFF (section 2.5), however, GASPS was not used for those samples as it was still under

tests.

4.5 Carbon isotopes in terrestrial compartments

Through the measurement of radiocarbon in samples representing slow-cycling pools (coarse woody debris and wood) and fast-cycling pools (foliage and fine litter), it was possible to observe the variability of $\Delta^{14}C$ values corresponding to each compartment (Figure 4.5). The observations show large variances of $\Delta^{14}C$ of slow-cycling pools, whereas fast-cycling pools have a much smaller variability, even in a vertical profile (leaves in *terra-firme*) or small sample size (fine litter). Table 4.1 summarises the observations of $\Delta^{14}C$ for each compartment in each ecosystem. Errors in $\Delta^{14}C$ determinations were around 2.5 ‰.

TABLE 4.1: $\Delta^{14}C$ values of samples (leaf, fine litter, dead wood and stem core) representing four different compartments (foliage, fine litter, coarse woody debris and wood) in two different ecosystems (*campinarana* and *terra-firme*) in the central Amazon, ATTO site.

Ecosystem	Type	n	mean	sd	median	min	max
Campinarana	Dead Wood	5	118.1	63.0	91.7	52.7	213.2
Campinarana	Leaf	5	19.3	3.5	19.1	14.5	24.1
Campinarana	Fine Litter	6	23.5	8.1	22.3	16.0	38.4
Campinarana	Stem Core	6	50.6	86.3	13.6	-16.2	202.6
Terra-firme	Dead Wood	7	90.4	40.5	95.6	29.6	143.5
Terra-firme	Leaf	28	17.8	10.1	16.9	-4.5	42.9
Terra-firme	Fine Litter	6	26.0	4.7	26.9	17.6	30.7
Terra-firme	Stem Core	7	125.4	112.4	118.8	28.3	353.9

In a confidence interval of 94-95 %, a one-way analysis of variance (ANOVA) shows that the interaction of type of compartment and ecosystem to which it belongs plays a role on the observed differences in $\Delta^{14}C$ values ($F = 2.67$), however, those differences are better explained by the type of compartment ($F = 14.01$).

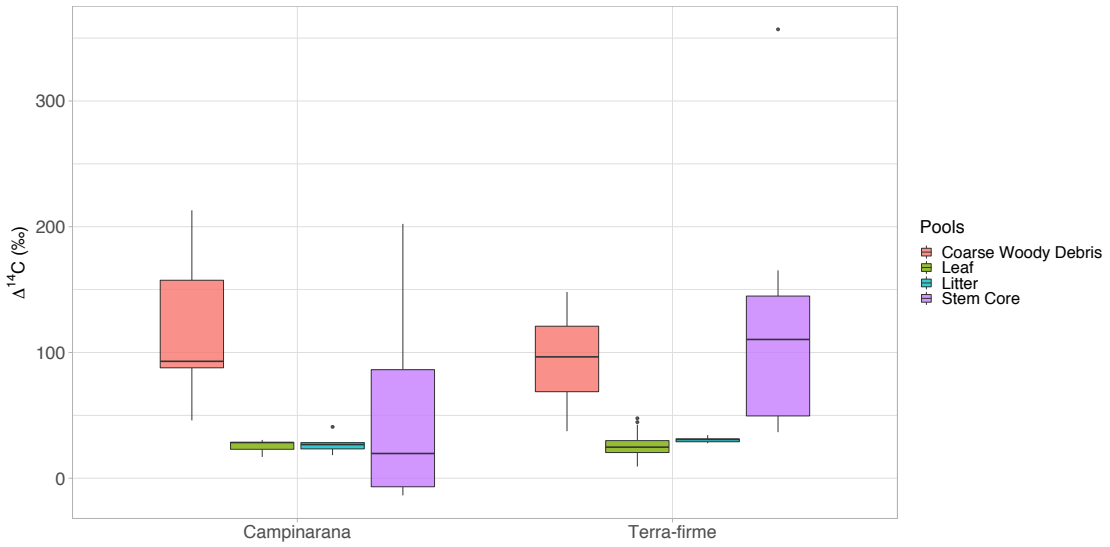

FIGURE 4.5: Boxplots of the radiocarbon contents in samples collected in 2018 from four different compartments in two different ecosystems in the ATTO site. The whiskers mark the minimum and maximum values (with a few values outside marked as dots); the first quartile Q1 is the lower part of the box and represents the 25th percentile; the line in the middle of the box is the median (Q2); and the third quartile Q3 is the upper part of the box, representing the 75th percentile. The number of measurements of each box corresponds to *n* in Table 4.1.

Significant differences on $\Delta^{14}C$ between the ecosystems *campinarana* and *terra-firme* were not observed (Kruskal-Wallis, $p > 0.05$; Games-Howell post-hoc test and Dunn's test, non-significant adjusted p-value). The only compartment with significant differences in $\Delta^{14}C$ between the ecosystems is the wood, represented by stem core samples. The $\Delta^{14}C$ of stem cores from *campinarana* range from negative values, i.e. before the radiocarbon bomb period, to large positive $\Delta^{14}C$ values (maximum value = 202.6 ‰). In the *terra-firme* plateau the positive values span up to a value of $\Delta^{14}C$ = 353.9 ‰, but the range does not cover negative values.

4.6 Carbon isotopes in atmospheric CO_2

Pataki et al. (2003) suggest that, in general, to obtain a low standard error (< 1 ‰) in $\delta^{13}C_{ER}$ (stable C isotope ratio of ecosystem respired CO_2) through the Keeling plot method ($\delta^{13}C_{ER}$ = y-intercept), one should aim for CO_2 concentration ($[CO_2]$) ranges larger than 75 ppm in air. The air samples collected at the instant tower in October 2019 have a $[CO_2]$ range of ca. 112 ppm, if we take both day-time and

night-time observations, and ca. 78 ppm for only night-time. Despite it is likely that gas exchange between ecosystem and troposphere are not at equilibrium, which could be seen as a violation of the assumptions underlying the Keeling method and Miller-Tans model, it is reasonable to assume in a first order approximation that equilibrium is a met condition in regional scales and for only C3 ecosystems as it is the case of this study in the *terra-firme* forest (Pataki et al., 2003; Buchmann and Kaplan, 2001).

In the Figure 4.6 it is possible to check the high agreement (R^2 = 0.98) between both independent measurements of CO_2 concentrations (*Picarro* and laboratory). The same figure is a good illustration of the uptake/outflux of CO_2 by the ecosystem. The lowest values of [CO_2], in ppm, occur around mid-day, where the maximum of the photosynthesis occurs at the Equator. This represents the process when the forest is assimilating CO_2 for producing energy at its maximum. The minimum [CO_2] at 24 m during the days of collection corresponds to ca. 390 ppm. The counterpart of this process occurs during the night, when in the absence of solar radiation, plants do not perform photosynthesis and the major contribution of the ecosystem to the atmosphere is through (dark) respiration, increasing the [CO_2] in the canopy air to a maximum. At the height of 24 m, this maximum in [CO_2] in the days of measurements occurs at 7:00 am (local time, AMT = UTC – 4 = BRT – 1) and is equivalent to ca. 501 ppm (slightly lower than the observation at 4 m, which corresponds to 530 ppm around the same time). The mean background [CO_2] according to the Mauna Loa station in October 2019 is $\approx$ 409 ppm (data public available in GML NOAA Data Page, file created on 7 March, 2022 and accessed on 7 April, 2022).

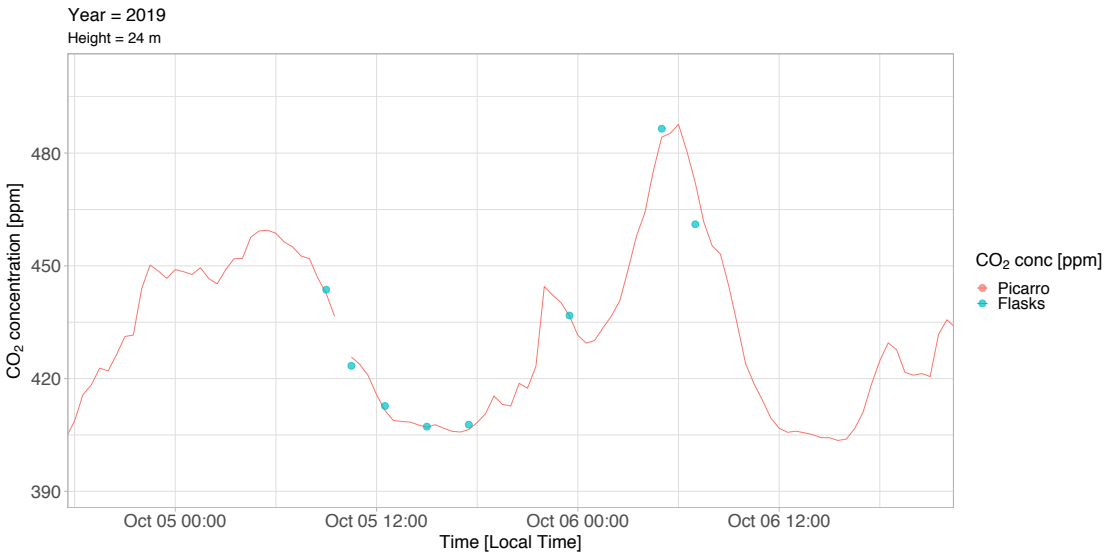

FIGURE 4.6: Comparison between CO_2 concentrations measured through inlets at 24 m height in the instant tower (80 m) with a Picarro instrument and measured at the laboratory from air samples collected in 3L-flasks.

The Keeling plot method was applied to the $\Delta^{14}CO_2$ measurements of the 3L-flasks, including all the heights sampled, i.e. 4 m, 24 m, and 79 m agl (Figure 4.7). The obtained regression line had relatively good fit, with an R-squared of 0.4 and a significant intercept (p-value) of 0.003. According to the Keeling plot method (equation 4.3), this intercept can be interpreted as the radiocarbon signature of the respired CO_2 flux from the ecosystem.

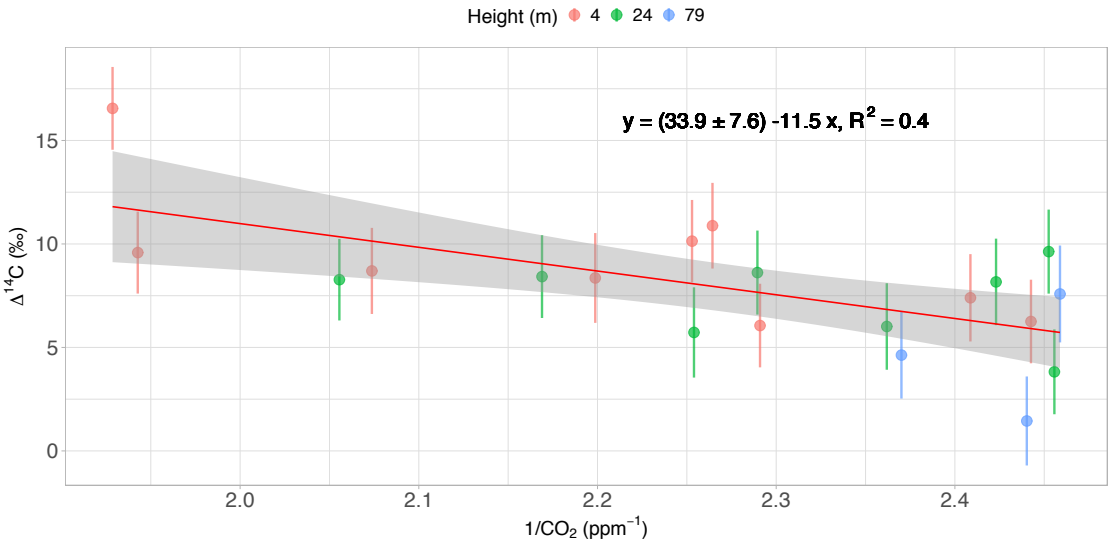

FIGURE 4.7: Keeling plot of $\Delta^{14}CO_2$ from air samples collected in the ATTO site in a vertical profile at the 80 m walk-up tower.

Additionally, the Miller-Tans mixing model was applied to the $\Delta^{14}CO_2$ results, estimating a $\Delta^{14}C_{ER}$ of 32.0 $\pm$ 7.44 ‰ (Figure 4.8). The fit with the regression line in this case was slightly better than when the Keeling plot method was applied (R^2 = 0.55 instead of 0.4; $p < 0.001$).

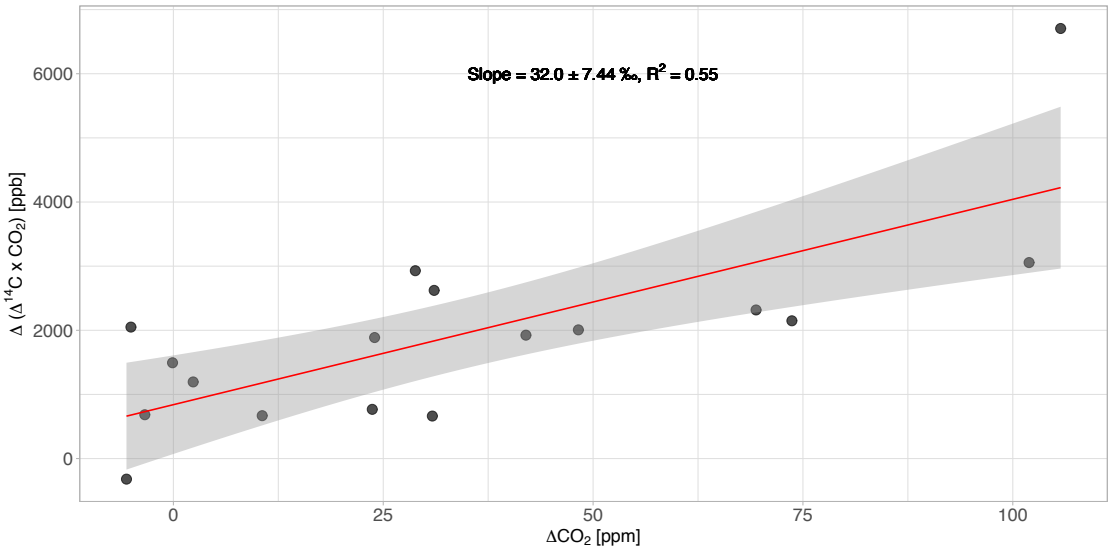

FIGURE 4.8: Miller-Tans mixing model based on the $\Delta^{14}CO_2$ from atmospheric air collected in a vertical profile at the instant tower in ATTO site during the dry season in 2019.

4.7 Comparison between $\Delta^{14}C$ in the canopy air and fast pools

All the analyses in this section are on the *terra-firme* observations. While $\delta^{13}C$ of leaves show a linear correlation with height and $\Delta^{14}C$ does not show any pattern correlated to height at all in leaves, when we take into account only the C isotopes in the CO_2 from flasks in a vertical profile, we can observe a very different relationship. The $\Delta^{14}C$ of CO_2 has a better (despite still weak, $R^2 = 0.29$) statistically significant relationship with height, while for $\delta^{13}C$ in CO_2 this relationship with height is even smaller ($R^2 = 0.19$) and not statistically significant. If we consider only night-time measurements for the flasks samples, the relationship of $\Delta^{14}C$ with height increases to $R^2 = 0.77$, while for $\delta^{13}C$ we obtain virtually the same result ($R^2 = 0.24$, $p = 0.26$) (Figure 4.9).

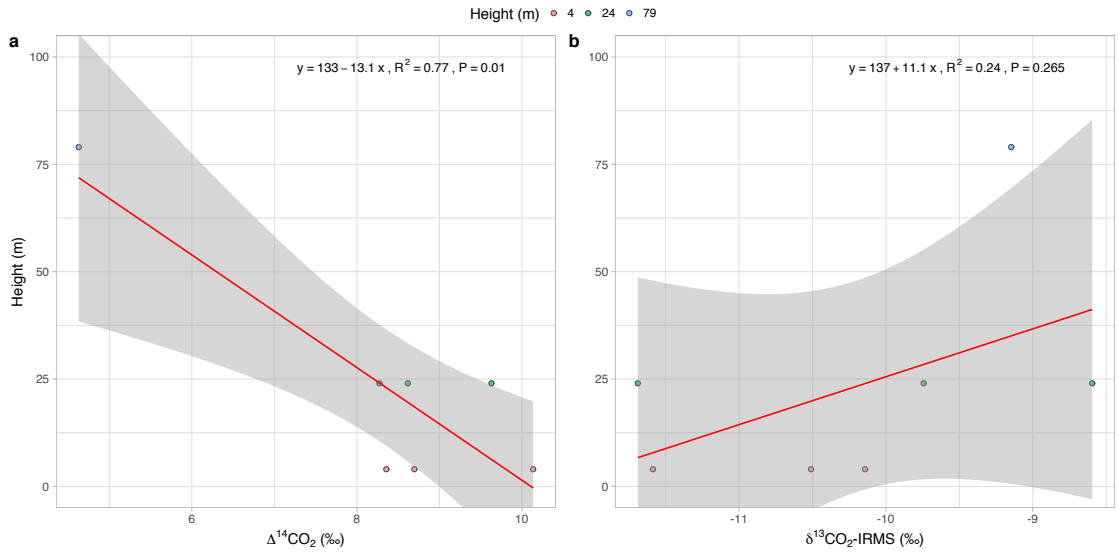

FIGURE 4.9: Relationship of $\Delta^{14}CO_2$ and $\delta^{13}CO_2$ from air samples with the height above ground level in metres. Measurements corresponding samples collected during the night.

The $\Delta^{14}C$ from atmospheric CO_2 and fine litter or foliage are statistically different (Tukey pairwise post-hoc test as well as Games-Howell post-hoc test). Statistical significant ($p < 0.05$) differences were found between the groups: Leaf – CO_2 and Litter – CO_2. Statistically significant differences were observed in the group fine litter – leaf using Games-Howell post-hoc test, however, this test could be limited for a sample size smaller than six (as it is the case for fine litter samples; Table 4.1). No

statistical significant difference was found between fine litter and leaf using Tukey pairwise post-hoc test.

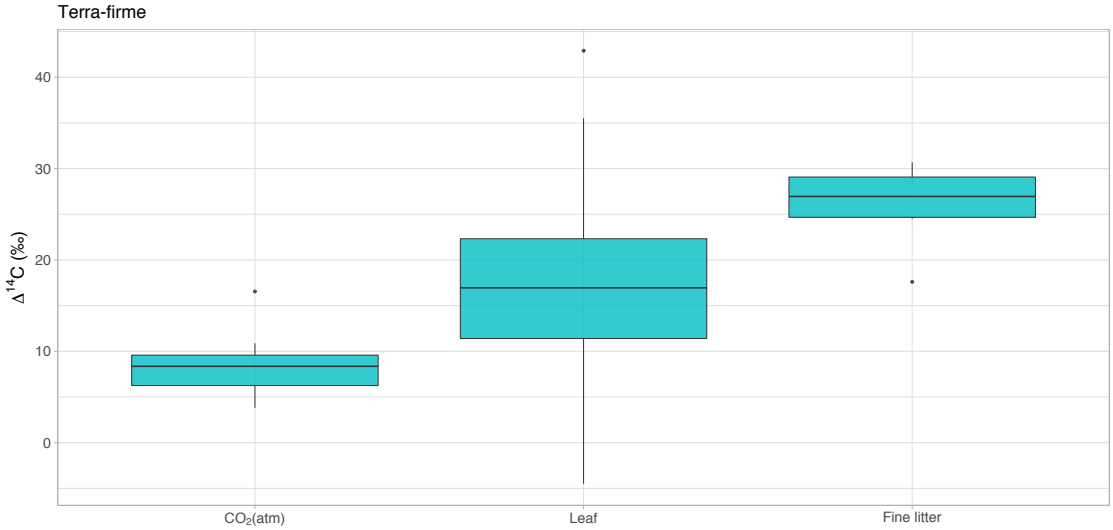

FIGURE 4.10: $\Delta^{14}C$ of samples from different compartments and $\Delta^{14}CO_2$ of atmospheric air in *terra-firme*. Samples of the compartments were collected in May 2018 (wet season), whereas air samples were sampled in October 2019 (dry season).

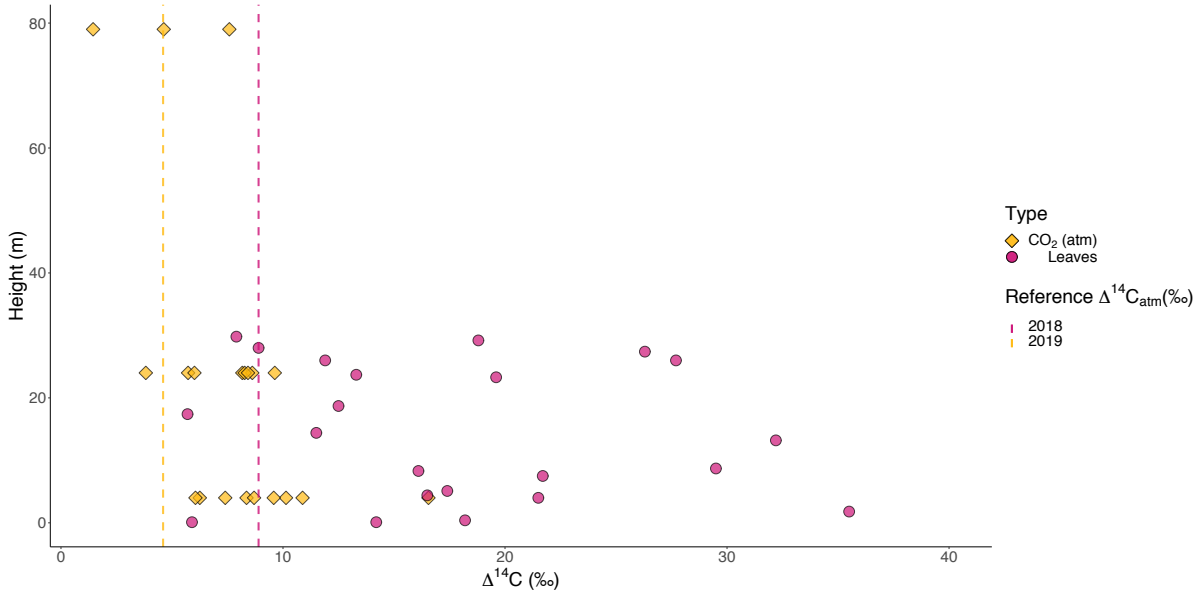

FIGURE 4.11: $\Delta^{14}C$ values of leaves and atmospheric CO_2 in a vertical profile collected at the 80 m walk-up tower (instant tower) in ATTO site. Leaf samples were collected in 2018 and air samples in 2019.

In the figure 4.11, the reference values of $\Delta^{14}C$ in the atmosphere come from the simulations in the RCP8.5 scenario performed by Graven (2015). The yellow diamond dots represent the $\Delta^{14}CO_2$ measurements (samples collected in 2019), while the pink circles are the $\Delta^{14}C$ measurements on the leaves in a vertical profile collected in 2018.

As $\Delta^{14}C_{leaf}$ has no correlation with height, instead varying from 6 ‰ to 35 ‰ within the whole profile, no correlation between $\Delta^{14}C_{leaf}$ and $\Delta^{14}CO_2$ in the *terra-firme* could be found in this study. When compared to slow-cycling compartments such as coarse woody debris and wood, foliage presents a fairly narrow variability of $\Delta^{14}C$ values, however, not as small as the variability observed for $\Delta^{14}CO_2$ values in the ambient air (below and above the canopy).

4.8 Discussion

4.8.1 Can we observe differences in the cycling rates between *campinarana* and *terra-firme* using $\Delta^{14}C$ measurements alone?

The absence of statistically significant differences in the $\Delta^{14}C$ of same pools in different ecosystems suggests that radiocarbon alone is not able to constrain information about the carbon cycling difference between ecosystems in the Amazon, particularly for transition ecosystems. It does not mean, though, that it could not still be used with success as a benchmark tool, especially for compartmental models.

It is important to notice that the number of samples included in this work is not large (Table 4.1) (except for the foliage pool in *terra-firme* – n = 28), therefore, the analysis and interpretations could be limited by the small sample size. As showed in the previous chapter, for slow-cycling pools, the estimated underlying distribution of radiocarbon is wide, which indicates the need of a larger number of samples in order to capture the whole variability of $\Delta^{14}C$ values.

Campinarana is an ecosystem characteriscally slower than *terra-firme* concerning the carbon dynamics, however, with $\Delta^{14}C$ alone in the four compartments studied, it was not possible to observe this difference. It could be due to the fact that most of the carbon stored in *campinaranas* is in the roots (Villa Zegarra, 2017), a compartment not measured in this study. Therefore, it is expected that roots would show statistically significant differences in their $\Delta^{14}C$ when compared to the roots in *terra-firme*.

The slow pools in this study, namely coarse woody debris and wood, showed the expected high variability on $\Delta^{14}C$ values as suggested from the previous chapter. The stem cores in the *campinarana* captured even negative values of $\Delta^{14}C$, which would correspond to atmospheric $\Delta^{14}CO_2$ values before the bomb spike. A potential explanation could rely on the assumption that the *campinarana*, being a less productive environment, has a slower rate of increment of its tree stems; thus, the trees could stand in the ecosystem for a longer time than the trees with the same diameter at breast height (DBH) in *terra-firme*, storing in this way the C with radiocarbon signals from an older atmosphere. However, direct comparisons between the mean annual increment (MAI) of stems in *campinarana* and *terra-firme* plateau in simultaneous studies could not be found. In fact, sparse studies on the growth rates of trees in the two ecosystems provide similar averaged values for adult trees with DBH > 50 cm. It is worth noting that the MAI is related to the growth of the diameter of the stems and does not take the height of the trees into account. Considering that the trees in *terra-firme* are about two times higher, the previous hypothesis could still hold. However, if only the similarities of the growth in diameter of stems (i.e. MAI = 1 – 3 mm yr^{-1}) of both ecosystems are considered, an alternative interpretation is that the trees in *campinaranas* could be using older carbon, for example from the roots, to built the stem biomass as a consequence of the limitation of macronutrients as phosphorus (P) and nitrogen (N) in sandy soils (Luizão, 1995; Villa Zegarra, 2017; Campos, 2017).

Dead wood is a relevant reservoir of carbon, as its development is related to mortality and damage of trees. Coarse litter, which comprises trunks and large (> 10 cm diameter) branches, composes ca. 30 % of the total surface litter inputs in the central Amazon (Chambers et al., 2001a). In this study, the smallest $\Delta^{14}C$ values observed in dead wood samples were 29.6 $\pm$ 2.4 ‰ and 52.7 $\pm$ 2.6 ‰ for *terra-firme* and *campinarana*, respectively, while the maximum values were 143.5 $\pm$ 2.4 ‰ and 213.2 $\pm$ 2.4 ‰ (Table 4.1). The minimum $\Delta^{14}C$ observed in *terra-firme* would correspond to the $\Delta^{14}CO_2$ in the atmosphere of 2012, 2013 CE (33.3 ‰ and 27.2 ‰ respectively, Graven et al. (2017)), which equates 6 years until the year of collection. For the minimum $\Delta^{14}C$ of dead wood in *campinarana*, two atmospheric $\Delta^{14}CO_2$ in different parts of the bomb curve have similar values (Graven et al., 2017): 1957 CE ($\Delta^{14}CO_2$ = 51.9 ‰) and 2008 CE ($\Delta^{14}CO_2$ = 52.3 ‰). These calendar years are equivalent to C ages of 62 and 11 years, respectively. Using the same approach, the maximum values would correspond to carbon ages of 28 years and 35 years, respectively to *terra-firme* and

campinarana. It is important to keep in mind that the interpretation of radiocarbon contents in dead wood might be more problematic. The main reason is that the C input of coarse woody debris pool (especially the fallen and standing dead trunks) comes from live trees, which also show a high variability of C ages and $\Delta^{14}C$ values. Therefore, the observed mean $\Delta^{14}C$ in dead wood is not simply related to the turnover time of C, but also linked to the age of the original tree. This could lead to a 'pre-aging' of the dead wood that cannot be easily estimated from radiocarbon measurements alone.

In summary, these results showed that there are limitations in the use of radiocarbon to observe differences in cycling rates among ecosystems. Especially for interconnected slow-cycling pools (e.g. stems and dead wood), additional information on the age of the sampled compartment might become crucial to estimate time lags and to disentangle atmospheric $\Delta^{14}CO_2$ from the rising or falling part of the bomb curve.

4.8.2 How do $\Delta^{14}C$ values give us insights into the cycling rates of different compartments?

Based on estimations of C turnover times, stock of C as biomass and physicochemical characteristics of soil, nutrients and so forth, it is known that different compartments cycle C at different rates. Results from chapter 3 suggested that the cycling rate of a pool could influence the mean $\Delta^{14}C$ observed in the compartment, as a consequence of the shape of the underlying distribution of radiocarbon in multi-compartmental open systems at steady-state, such as the old-growth forest in the ATTO region. It was estimated that slow-cycling pools would generate wide probability distributions of $\Delta^{14}C$, while fast-cycling pools would show narrow distributions and mean values of $\Delta^{14}C$ close to the contemporaneous atmospheric $\Delta^{14}CO_2$.

The atmospheric $\Delta^{14}CO_2$ in the free-atmosphere (79 m agl, ca. 2 times higher than the canopy level) shows almost no variability within measurements taken in different times of the day and has a median $\Delta^{14}CO_2$ of 4.6 ‰ (Figure 4.11). This value matches exactly the median $\Delta^{14}CO_2$ value forecasted by Graven (2015) in the RCP8.5 (or *business-as-usual*) scenario of fossil fuel emissions, which is the most dramatic scenario among the four Representative Concentration Pathway (RCP) scenarios presented by the IPCC fifth assessment report (AR5) in 2014 (IPCC, 2014b). This result is remarkable, while potentially worrying, given that the ATTO site is

located in an old-growth primary forest far from major cities, so that local fossil contamination is unlikely.

Nevertheless, this observation also agrees with the atmospheric $\Delta^{14}CO_2$ value that would be obtained by applying the decline rate observed by Levin et al. (2013) of 3 ‰ yr^{-1} to the last record for the tropical region reported by Graven et al. (2017). The last data point of Graven et al. (2017) is in 2015 and corresponds to an atmospheric $\Delta^{14}CO_2$ = 16.7 ‰. The decline rate of 3 ‰ yr^{-1} in the 4 years between 2015 and 2019 (year of collection of air samples in ATTO) returns an atmospheric $\Delta^{14}CO_2$ = 4.7 ‰. A direct observation that seems to agree with the $\Delta^{14}CO_2$ at 79 m in the ATTO site is provided by Levin et al. (2021). $\Delta^{14}CO_2$ from samples collected at Alert station (82.45° N, 62.52° W, 185 m asl, Canada - Arctic) average 3.4 ‰ (σ = 3.7 ‰) in 2018 and 0.2 ‰ (σ = 4.6 ‰) in 2019 (Data in ICOS-ERIC Carbon Portal). The value observed in Alert in 2018 seems to match the one observed in ATTO, considering that the expected variation in $\Delta^{14}CO_2$ from high northern latitudes to the tropics is less than 1.5 ‰ (Levin et al., 2021) and that the atmosphere takes about one year to mix from North to South. However, an additional direct observation, in principle, diverges from the $\Delta^{14}CO_2$ observed in ATTO in 2019. Based on tree rings and atmospheric radiocarbon contents, Hua et al. (2021) estimate a $\Delta^{14}C$ of 12 ‰ for the region surrounding ATTO (SH zone 3). This latitude has, however, a small complication. ATTO is located around the border of the zones 3 in the SH and NH, as the transition is defined to be the Equator. Therefore, there is a chance that the NH zone 3 curve is more adequate or an average between SH and NH zone 3. NH zone 3 has a mean $\Delta^{14}C$ of 0 ‰ in 2019 (Hua et al., 2021). The average of both SH zone 3 and NH zone 3 would correspond to 6 ‰, which approaches the observation at ATTO.

The agreement between the $\Delta^{14}CO_2$ at 79 m in the ATTO site and the estimations cited suggests that this height is adequate as a reference of the background $\Delta^{14}CO_2$ for an extended region. This background results from an atmospheric mixing that have reduced inter-hemispheric differences since the 1970s associated to the tropical low pressure belt (Ancapichún et al., 2021).

Fast pools such as foliage and fine litter have a much narrower variance, in accordance with the predictions presented in the previous chapter. However, when compared to the $\Delta^{14}CO_2$ in ambient air, the dispersion of $\Delta^{14}C$ values in fast pools is 2 – 3 times larger. It was noted as well that the leaves in a vertical profile present no correlation of their $\Delta^{14}C$ values with their height in the canopy. Hitherto it seems

not to exist a consensus on whether a positive or negative correlation should be expected or not. Hypothetically, there is no reason to believe such correlation would take place, as the canopy effect is a consequence of the multifold fractionation effect led by the recycling of CO_2. Once $\Delta^{14}C$ notation removes the mass-dependent fractionation on radiocarbon by normalising it as 0.975 of the ^{13}C fractionation in the photosynthesis (the latter obtained through $\delta^{13}C$), the canopy effect observed on $\delta^{13}C_{leaf}$ disappears in the $\Delta^{14}C_{leaf}$.

On the other hand, a correlation between $\Delta^{14}CO_2$ in the canopy air and the sample height was found in this study (Figure 4.9). First, this suggests that the CO_2 closer to the ground level has a higher proportion of older carbon and this proportion gets smaller in the direction of the troposphere. In this case, a potential structure describing the interconnection between foliage, wood and soil could be serial without feedbacks, as flux feedbacks could increase the mix of C masses with different $\Delta^{14}C$. Thus, this additional mix would be reflected in the $\Delta^{14}CO_2$ because of the respiration and decomposition, and most likely the correlation of ambient $\Delta^{14}CO_2$ with height agl would disappear. However, it is necessary to check this hypothesis with data that includes the $\Delta^{14}CO_2$ of respiration from individual compartments, such as foliage and wood, and soil efflux, besides ambient CO_2 from more heights.

Secondly, the apparent correlation arises the question whether the leaves at lower heights are assimilating older carbon and, therefore, getting an apparent older age. Measuring the radiocarbon of leaves at lower heights that are monitored, so that the actual age of the leaf can be inferred, can test the latter hypothesis. Nevertheless, the distinction between the leaf age and the age of the carbon in the leaf should be always kept in mind, as they might be divergent. Soter (2011) observed that a pronounced version of this effect could largely impact the chronologies of ancient sites based on ^{14}C dating of short-lived organic materials, such as seeds. On one hand, considering the respired CO_2 from soils is only about a decade old, the described effect would be negligible on leaves, as a modern radiocarbon signal would not greatly shift the $\Delta^{14}C_{leaf}$. On the other hand, if a difference between the leaf age and the carbon age based on ^{14}C is observed, this could work as an additional information on the C transit time of soils; or could be an indicative of a higher contribution from a pool respiring older carbon, such as tree stems under C source limitation (Herrera-Ramirez et al., 2020) or coarse woody debris. Alternatively, leaves at different heights might grow using different sources of carbon, not necessarily linked to the ambient CO_2.

According to one of the post-hoc statistical tests, there are significant differences between leaf and fine litter $\Delta^{14}C$ values. This difference implies a time lag between these two pools. In general, in tropical forests, fine litter is expected to decompose in less than a year, whereas carbon may stay in living plant tissues such leaves for a few years. Therefore, the observed $\Delta^{14}C$ of fine litterfall in fact might be accounting for the carbon fixed a few years before the collection, as a result of the time spent in the foliage. A similar interpretation was given in the page 7 of the final report of the "Carbon dynamics in vegetation and soils" (LBA-ECO Team CD-08 Phase I) (Trumbore et al., 2005).

The two slow-cycling pools studied here, represented by dead wood and stem core, presented a large variability of $\Delta^{14}C$ values. This result also resonates with the predictions from the previous chapter. The live wood itself presents a wide range of $\Delta^{14}C$ values in the *terra-firme*, but this variability is not statistically different from the one observed in the dead wood in *terra-firme*. This could be due to the fast growth rate of standing trees – if not only the diameter, but also the height is taken into account – and the fast decomposition rate enabled by the *terra-firme* soils in the plateau, especially during the rainy season. Thus, in a multi-compartmental model based on *terra-firme* observations, it is expected that the decomposition rates corresponding to wood and coarse woody debris pools would be similar, but differences could be related to their respective stocks or fluxes within adjacent pools. Since *terra-firme* is the dominant ecosystem in the Amazon Basin ($\approx$ 65 %), such model would probably approach accurately the dynamics of carbon for the whole central Amazon region. The differences coming from other ecosystems (e.g. *campinarana*, where stem core and dead wood are significantly distinct) could be applied through a weighted contribution to an overall model for the central Amazon or could be modelled separately to address ecosystem-scale research questions.

4.8.3 How long does carbon take to be respired by a *terra-firme* ecosystem in central Amazon?

So far, literature values of $\Delta^{14}C$ for Amazonian soil efflux and plant respiration are lacking. Such values could provide a better orientation about the sources and proportions driving the integrated $\Delta^{14}CO_2$ of the canopy air.

The estimation based on the Miller-Tans mixing model for the *terra-firme* plateau on ATTO site gives a $\Delta^{14}C_{ER}$ of 32.0 $\pm$ 7.4 ‰. This value is in agreement with the

atmospheric $\Delta^{14}CO_2$ for the year 2012 CE ($\Delta^{14}C$ = 33.3 ‰, Graven et al. (2017)) and corresponds to a mean transit time of 7 to 9 years (2019 CE minus 2012 CE for the mean), assuming a one-pool model where the input is the atmospheric CO_2 radiocarbon and the output is the $\Delta^{14}CO_2$ of the ecosystem respiration. Several years BCE have similar atmospheric $\Delta^{14}CO_2$ in Graven et al. (2017), however, it would imply that the mean transit time of the ecosystem respiration is in the order of thousand of years, which is not in accordance with estimations of mean C transit times based on other proxies. However, according to the compilation of Hua et al. (2021), the year 1957 would also agree with this $\Delta^{14}C_{ER}$, which leads to a mean transit time of 63 years. Nevertheless, considering the records of Graven et al. (2017) and simulations of Graven (2015) were in closer agreement with the $\Delta^{14}CO_2$ observations at 79 m in ATTO, the discussion will continue exploring the first mean transit time (7 – 9 years).

Despite the large standard error of the $\Delta^{14}C_{ER}$ estimated through both Keeling method and Miller-Tans model (ca. 7 ‰) when compared to common standard errors obtained for $\delta^{13}C_{ER}$ (< 1 ‰), the standard deviation in years for the estimate of mean transit time is not large, as the atmospheric $\Delta^{14}CO_2$ declines at about the same rate (5 ‰ yr^{-1}, Graven et al. (2017)). For the background $\Delta^{14}CO_2$ based on measurements in western Europe (e.g. Jungfraujoch station), this decline for the late 2010s occurs at a slower rate of ca. 3 ‰ yr^{-1} (Levin et al., 2013). The decline estimated for the central Amazon region based on observations around 2012 CE was 4.3 ‰ yr^{-1} (Muhr et al., 2018).

An estimation of the global carbon mean transit time lays between 19 and 30 years (95 % confidence interval), however the mean turnover time in latitudes near the Equator is estimated to be around 15 years (Carvalhais et al., 2014). Yet for a tropical forest in Colombia, the estimation of the mean transit time of the ecosystem based on a linear 7-pool model (Porce model of chapter 3) corresponds to 11.2 ± 1.2 years (Sierra et al., 2021). Incubation experiments of soil samples from a *terra-firme* slope in the Colombian Amazon, when modelled as an homogeneous pool model, returns a mean transit time of 9 to 13 years for the soil ($\Delta^{14}CO_2$ of soil respiration = 85 ± 12 ‰ for samples collected in 2011) (Sierra et al., 2013).

In spite of three completely different approaches to estimate the mean transit time in fairly close (< 2,000 km) regions (namely the one in Sierra et al. (2021), the incubations from Sierra et al. (2013) and this study), the values obtained are similar. Yet the one-pool-based estimation of the mean transit time in central Amazon in

this study is 2 – 4 years lower than the one obtained through the Porce model (7 pools). However, assuming both environments have a similar mean transit time, this difference at the ATTO site could be related to missing internal processes overlooked in a simpler model. At the current state of data, it is not possible to infer whether the negligence of the fluxes of carbon between vegetation and soil in this region could indeed change the mean transit time of the central Amazon region to a higher or even lower value.

An additional difference between the mentioned approaches relates to the carbon transit time distributions. Through a multi-compartmental model as the Porce model, it is possible to estimate the underlying distribution of the transit time, taking into account the different ages of carbon in different compartments. In one-pool model approaches, the estimation is limited to the mean of an unknown underlying distribution as the distribution of ages in the system is unknown. Sometimes it is simplified to the turnover time, defined either as the stock over flux of carbon or the inverse of the decomposition rate. The knowledge of the distribution of transit time of carbon is relevant to accurately interpret the behaviour of the system. The transit time distribution of the whole ecosystem is usually skewed, influenced by the distribution of carbon ages from slow-cycling pools that, in general, have a long tail. Thus, the respired CO_2 of a ecosystem might have a mean transit time of a few years to decades because a high proportion of carbon is respired in a few years, but the mean value does not allow to infer the proportion, if any, of carbon that is respired later, after a few decades. In the Porce model (Sierra et al., 2021) it was estimated that 50 % of carbon, given by the median of the transit time distribution, is respired by the ecosystem in ca. half a year, while 95 % of carbon take up to 70 years to be respired.

Future research should aim to better constraining the different pools and their interconnections, in order to more accurately model the carbon ages and transit times, especially focussing on their underlying distributions. Carbon isotope mixing models are powerful considering their mathematical simplicity, however, they rely on robust data, that should be encouraged to be obtained, especially for the radiocarbon isotope. Additionally, sampling strategies can be improved. A deeper discussion in the latter is given in section 5.1.

4.9 Conclusions

The carbon cycle in the Amazon rainforest can vary largely, as a consequence of the high diversity of species and ecosystems. Radiocarbon can be useful to trace the dynamics of carbon in different C pools and ecosystems. Moreover, radiocarbon can be measured in the field and modelled, providing an estimation of the mean transit time of C in the ecosystem.

This study used radiocarbon to address three research questions related to how can $\Delta^{14}C$ distinguish cycling rates of slow and fast pools in different ecosystems and what the ecosystem's C transit time estimated from it.

The main findings can be summarized as:

(i) According to the $\Delta^{14}C$ there are no significant differences between the cycling of aboveground carbon in the *campinarana* (a white sand ecotone) and *terra-firme* (lowland evergreen rainforest). This suggests that despite the age of carbon masses in different compartments might vary, on average the aboveground carbon has similar radiocarbon values.

(ii) The $\Delta^{14}C$ values in different compartments within a single ecosystem are distinguishable. These differences can be related to the individual cycling rates of C pools, further describing their dynamics as fast or slow.

(iii) Based on a two end-member mixing model on ambient air samples in a vertical profile in *terra-firme* it was possible to estimate the $\Delta^{14}C$ of the CO_2 respired by the whole ecosystem. The $\Delta^{14}C_{ER}$ value obtained estimates a mean C transit time of 7 to 9 years, in accordance to a study in a tropical forest in Colombia.

Despite there are no clear differences between the aboveground C cycle in *campinarana* and *terra-firme*, the cycling differences could be prominent in the belowground carbon. This suggests these two ecosystems might use different strategies of carbon allocation, at the same time, compensating for the particular limitations in each of them: lack of nutrients in *campinarana* forest soils and competition for light by plants in the dense *terra-firme* forest.

It is virtually impossible to directly measure the C transit time of an ecosystem. However, $\Delta^{14}C$ of C pools might be extremely useful to estimate mean transit times and to disentangle cycling mechanisms. Moreover, coupling radiocarbon measurements with the theory of compartmental dynamical systems is a step towards accurate estimations of ecosystem's time metrics. Therefore, investment of resources

and research onto both the experimental and theoretical aspects of radiocarbon as an environmental tracer may not be overlooked.

Chapter 5

General Conclusion

This doctoral thesis was motivated by the need to better understand the carbon cycle in one relevant, yet one of the most threatened biomes in the world: the Amazon rainforest. One way to accomplish that is by quantifying accurately the time carbon spends in the ecosystem. Since it is not trivial to measure time-related quantities such as the age of carbon in an ecosystem pool or the transit time of carbon moving through the entire ecosystem, a tracer becomes very useful for this purpose.

Radiocarbon is a very useful tracer of the carbon cycle in ecosystems because it decays on timescales that are much longer than most ecosystem processes. However, for long it is known that the concentrations of radiocarbon in the atmosphere and, consequently, in the biosphere, change over time. Several factors contribute to the variations of radiocarbon contents in the atmosphere. These factors can be natural variations linked to changes on the geo- and solar magnetic fields or anthropogenic effects impelled by burning of fossil fuels and nuclear weapon tests. Independent of the factors leading to the variation of radiocarbon contents in the atmosphere, those alterations are well-documented thanks to records of the past carbon isotope signals on several materials. In the last century, also the contemporaneous changes could be successfully recorded through monitoring of air samples. The documentation and modelling to fill the gaps on actual data builds the radiocarbon history in the atmosphere up to 55,000 years ago. This information is crucial for the calibration of archaeological samples, but in this thesis we focussed on modern samples, that are linked to the information collected especially since the fifties and predictions up to 2100 CE.

The records and predictions of radiocarbon in the atmosphere were crucial to fulfil the goal of this thesis. This goal was to better understand the variations of radiocarbon contents in terrestrial ecosystems, including an estimation of the time

carbon takes to be release by a central Amazon primary forest. The specific objectives related to the general goal of this thesis were ranked in the introduction.

The main objectives of this thesis were addressed in three chapters. Objective 1 was related to the development of a theoretical approach to use radiocarbon distributions in open compartmental systems to better understand C cycling in ecosystems.

In environmental studies using radiocarbon as a tracer of biogeochemical processes within the terrestrial ecosystems it is common to emphasise the mean values of $\Delta^{14}C$ on samples. The samples represent C-pools that can vary in stock and cycling rate of carbon. In chapter 3, I presented a simple algorithm developed to estimate the underlying distribution of radiocarbon in interconnected compartments with continuous exchange of carbon with the surroundings in a dynamical equilibrium state. Undisturbed soils and old-growth forests fall in this category and it was found that for such systems there is a correspondence between the speed of cycling of a C-pool and its radiocarbon distribution.

As a consequence of the non-monotonic increase or decrease of atmospheric $\Delta^{14}C$ values, the radiocarbon distributions vary according to the year of observation. This behaviour is contradictory to the carbon age distributions, which are static at steady-state. This distinction is relevant when one tries to obtain a carbon age from a radiocarbon measurement. An open system at steady-state will always have the same carbon age or transit time distribution, hence it will return the same mean carbon age or transit time. On the other hand, as the radiocarbon distributions change over time, the mean $\Delta^{14}C$ will also vary according to the year of observation. Thus, a same mean system age might correspond to different mean $\Delta^{14}C$ values depending on when the samples were collected.

Fast-cycling pools tend to present a narrow distribution of $\Delta^{14}C$ values with the mode around the values of the contemporaneous atmospheric $\Delta^{14}CO_2$. Conversely, slow-cycling pools have a wider distribution of radiocarbon values, in some cases presenting multiple peaks.

It was also observed that a mean value of $\Delta^{14}C$ of soil CO_2 efflux is close to the expected value of an underlying distribution of radiocarbon that has probability densities of $\Delta^{14}C$ values weighted by the carbon masses. These results indicated that the theoretical radiocarbon distributions presented can help the interpretations of radiocarbon contents obtained in experiments as long as they are under dynamical equilibrium.

Additionally, the results of chapter 3 provided insights into sampling design for an improved model-data comparison of radiocarbon measurements. It was suggested that slow-cycling pools need more samples than fast-cycling pools, when one aims to capture the whole variability of $\Delta^{14}C$ values. The minimum sample size may also depend on the year of collection. Moreover, the radiocarbon distributions in open compartmental systems at steady-state offer opportunities to better incorporate the complexity of terrestrial ecosystems in the estimation of system diagnostic times.

Towards the end of the 21^{st} century, especially in the most dramatic scenario of emissions of greenhouse gases, the use of radiocarbon as a tracer might be severely impaired. This lamentable outcome could also be observed through the radiocarbon distributions obtained in chapter 3. The unique natural labelling promoted by the bomb ^{14}C might become less meaningful already in the near future, when the atmospheric $\Delta^{14}CO_2$ cross values never observed in the well-documented history of atmospheric radiocarbon.

However, while this alarming fate does not arrive, it is important to use the full potential of the radiocarbon as a tracer in environmental studies. Objective 2 of this thesis aimed for the collection of samples representing the C compartments and ambient air in the highly complex Amazon rainforest. In contributing to this objective, I constructed a dedicated vacuum line to purify the samples before conversion to graphite at LAC-UFF. This process was detailed in section 2.5, where the line called GASPS (Gas Samples Purification System) is compared to the extraction and graphitisation system of ICOS-CRL at Heidelberg University. GASPS has the flexibility of extracting CO_2 from air samples and purifying pre-combusted organic samples without changing its set-up. GASPS is not an automated system, however, for the purposes of this thesis such automation would not optimise the whole procedure, as at LAC-UFF the samples are graphitised in sealed tubes and the latter requires human operation in the current set-up of LAC-UFF. The construction of GASPS contributed to LAC-UFF by expanding the types of samples that can be prepared in this laboratory.

In chapter 4, I presented results of $\Delta^{14}C$ in C-pools of two primary forests in the central Amazon. Via measurements of $\Delta^{14}CO_2$ in the canopy of the dominant ecosystem in Amazon (*terra-firme*) and background measurements performed at heights two times above the canopy level, it was also possible to estimate the mean transit time of the ecosystem. These results tackled objective 3 of this thesis.

Firstly, the radiocarbon measurements of paired compartments in the two distinct ecosystems in the central Amazon (*campinarana* and *terra-firme*) have not presented significant differences. This result suggests that radiocarbon measurements alone might not provide sufficient information on the C cycling of different ecosystems. The only significant difference observed between ecosystems occurred for the wood pool (represented by stem cores), indicating a much slower C cycling of this compartment in *campinarana*.

However, the significant differences of $\Delta^{14}C$ on aboveground C-pools in these two very distinct ecosystems allowed us to conclude that radiocarbon can provide consistent and measurable differences between compartments.

Lastly, a two end-member mixing model (Miller-Tans model) was applied to the observations of $\Delta^{14}CO_2$. By comparing the $\Delta^{14}C$ of the ecosystem respiration estimated by the Miller-Tans model with the atmospheric $\Delta^{14}CO_2$ records, a mean transit time of 8 years was estimated for carbon passing through a central Amazon forest. This estimation is consistent with mean transit times obtained by diversified approaches performed by other studies in tropical forests close to the Equator and in the Eastern Amazon.

5.1 Future research

Through this work we addressed questions of significant relevance for the radiocarbon community. At the same time, it is recognised that gaps still exist and more work is necessary to address the new questions emerging from the studies presented here. Upgrades to all presented studies might be performed to enhance the accuracy of the estimations and their interpretations.

Experimental aspects at LAC-UFF introduced by this thesis can be improved, allowing higher throughput of samples prepared without affecting the accuracy of the measurements. The vacuum line installed at LAC-UFF in the course of this thesis (GASPS) could incorporate a more efficient cooling trap, allowing higher mass flow rates of the gas samples. Additionally, a combination of GASPS with an automated graphitisation equipment (e.g. AGE, IonPlus) could optimise the extraction of CO_2 and graphitisation process. Any adaptations have to be thoroughly tested with control samples and are encouraged for future work.

Chapter 3 dealt with radiocarbon distributions in open systems that are under steady-state conditions. Future research can profit of the insights into radiocarbon

distributions of interconnected multi-compartmental systems to benchmark models. However, in order to accommodate more realistic systems, an algorithm incorporating time dependencies on the inputs and the matrix exponential of the system should be developed. Additionally, taking into account systems out of equilibrium in future works on theoretical radiocarbon distributions could allow comparisons of models describing disturbed ecosystems.

The radiocarbon measurements of C-pools in the central Amazon presented in this thesis might improve our comprehension of carbon cycling in this biome. The estimation of the mean transit time of carbon based on mixing models of $\Delta^{14}C$ and CO_2 concentrations could be improved by more frequent analyses of air samples in a vertical profile that incorporate more heights within the canopy. In addition, measurements of the $\Delta^{14}CO_2$ in the free-atmosphere would provide a more accurate radiocarbon value for the background signal. The latter has been addressed recently, during the course of this thesis, with the installation of an integrated air sampler and an auto-sampler for 3L-flasks, both collecting samples at the height of 321 m at the ATTO tower. The first batch of those samples should be analysed in the near future.

An alternative to the two end-member mixing model approach performed in this thesis is the estimation of C transit time distributions. To obtain such distributions, a compartmental model describing the ecosystem could be implemented, analogously for instance to the Porce model (Sierra et al., 2021). Such compartmental model may be derived from estimations of stocks of carbon and its fluxes among different vegetation and soil C-pools.

Additionally, improving the strategy for radiocarbon sampling by expanding it to belowground pools and the efflux of $^{14}CO_2$ of the different pools individually might offer insights into the number of compartments and the interaction among them. In the context of the central Amazon, this strategy is to be implemented. Firstly, data on carbon stocks and fluxes reported in different studies is being put together. Further, measurements on the $\Delta^{14}C$ of belowground pools (roots, bulk soil and soil fractions) is to be performed complementing the $\Delta^{14}C$ of these compartments in the central Amazon published elsewhere. Lastly, future measurements on the $\Delta^{14}CO_2$ of the respiration of individual pools supplement the few reported data for this region.

Despite the relevance and benefits that could be provided by estimations based on such a model and radiocarbon measurements, this strategy demands time and resources that could not fit this doctoral thesis. Nevertheless, it is highly encouraged

for future research in the central Amazon.

The use of radiocarbon as tracer of the carbon dynamics in terrestrial ecosystems is a powerful tool. However, radiocarbon research in such context needs synergy, especially in areas of high dynamical complexity as the Amazon rainforest. When aiming to couple the radiocarbon results with the theory of dynamical compartmental systems, this task becomes even more challenging, because the collaboration becomes crucial in order to understand and represent the right processes leading carbon through atmosphere – biosphere – atmosphere.

Appendix A

Supplementary material of chapter 3

Contents of this file

1. Figures A1 to A11

Introduction

This supporting material contains twelve additional figures.

Figures A.1 and A.2 show respectively the evolution over time of the expected values of $\Delta^{14}C$ and the comparison of these values with empirically obtained $\Delta^{14}C$ values in the total soil CO_2 efflux for the years between 1996 and 2010 (with exception of 2005) in the Harvard Forest, USA. Nine figures show the distributions of radiocarbon separately for each pool, the total outflux and whole system. Three of them (Figures A.3, A.4, and A.5) were produced for the Harvard Forest Soil model, referred as HFS model in the main manuscript; additional three figures (Figures A.6, A.7, and A.8) represent the same estimations for the Porce model; the last three figures (Figures A.9, A.10, and A.11) correspond to radiocarbon distributions for the Emanuel model. The radiocarbon curve, model parameters and methods employed to produce these figures are the same described in the main manuscript (section 3: Methods) and code and scripts can be accessed in the public GitHub repository through: https://github.com/ingridchanca/RDCDistributionOpenComp.git.

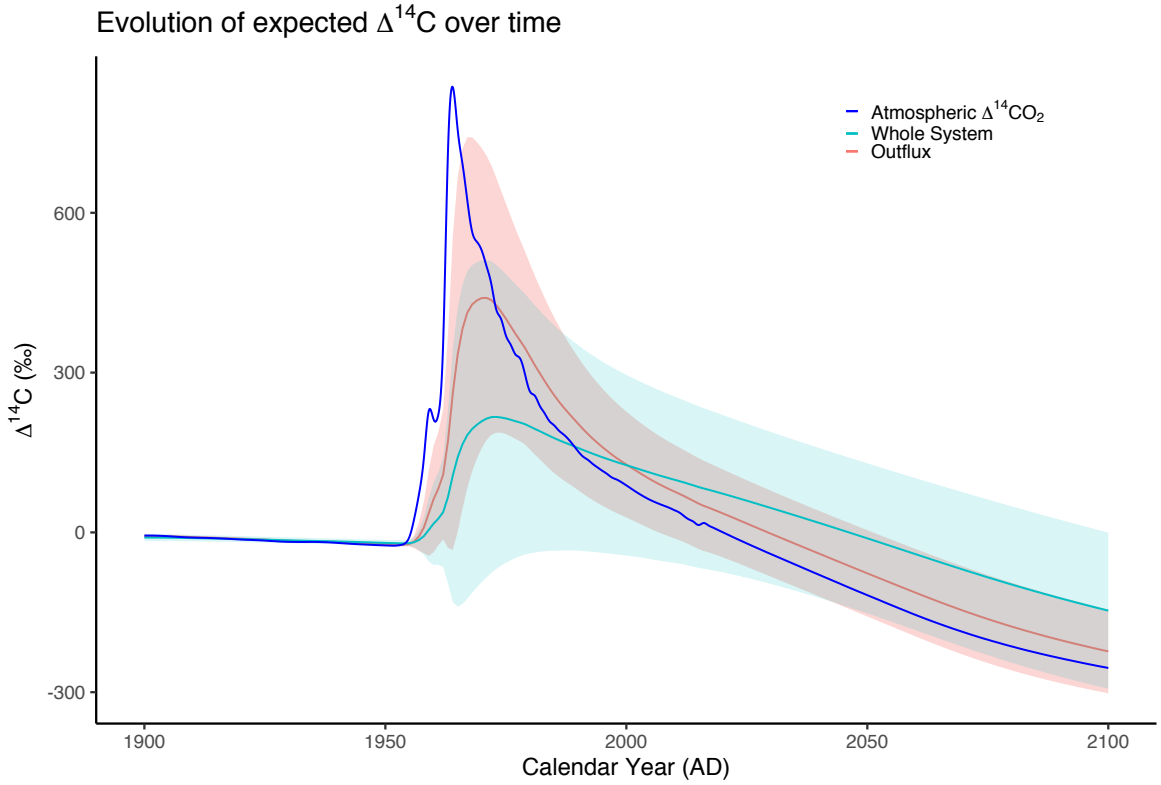

FIGURE A.1: Evolution of the expected $\Delta^{14}C$ values of outflux (red) and whole system (light blue) for the HFS model between the years 1900 and 2100. The ribbons are the standard deviation of the expected values of $\Delta^{14}C$ predicted by the model through a weighted mean.

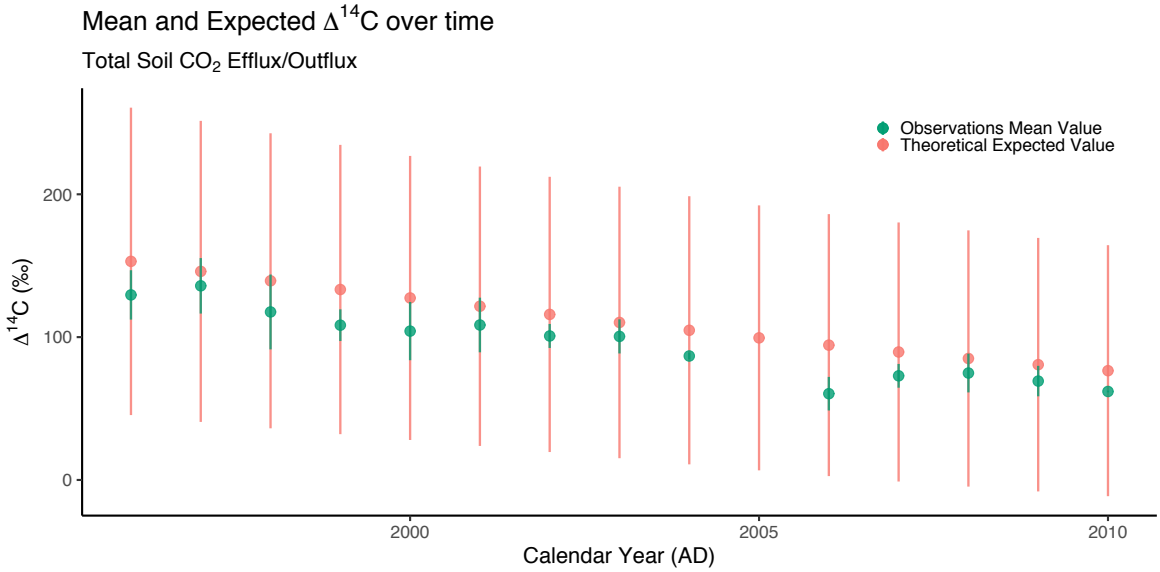

FIGURE A.2: Change over time (AD 1996 - 2010) of the expected $\Delta^{14}C$ values (orange) and of the mean $\Delta^{14}C$ values of observations (green) from samples of total soil CO_2 efflux in the Harvard Forest (HFS model). There are no measurements on samples of soil efflux for the year 2005, therefore, for this year, only the theoretical estimation is provided. Error bars represent the standard deviation of the expected $\Delta^{14}C$ values (orange) and the uncertainty of the observations of $\Delta^{14}C$ (green).

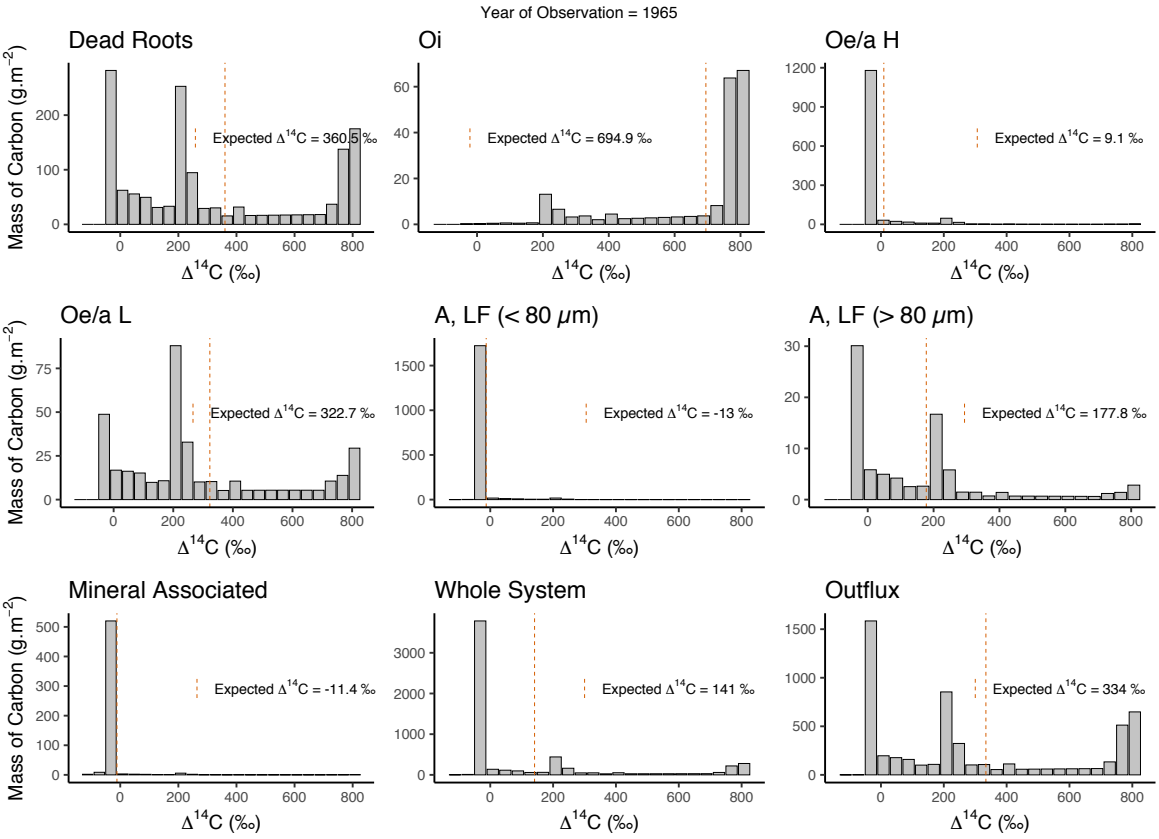

FIGURE A.3: $\Delta^{14}C$ distributions of the HFS model for each of the seven pools, outflux, and whole system . The year of observation is 1965 – just after the bomb peak in 1964 – and the distributions are computed over 1,000 years, with discretization $h = 0.1$. The bin size b is equal to 40 ‰.

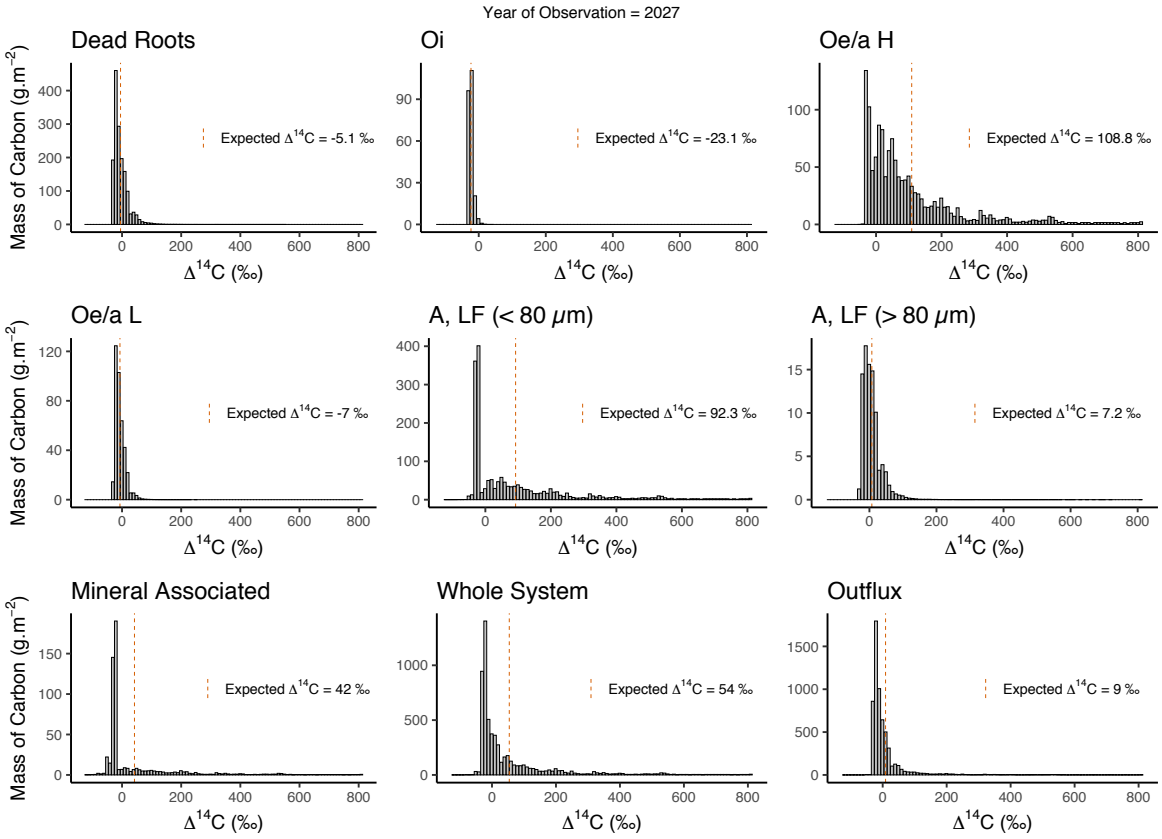

FIGURE A.4: $\Delta^{14}C$ distributions of the HFS model for each of the seven pools, outflux, and whole system . The year of observation is 2027 and the distributions are computed over 1,000 years, with discretization h = 0.1. The bin size b is equal to 10 ‰.

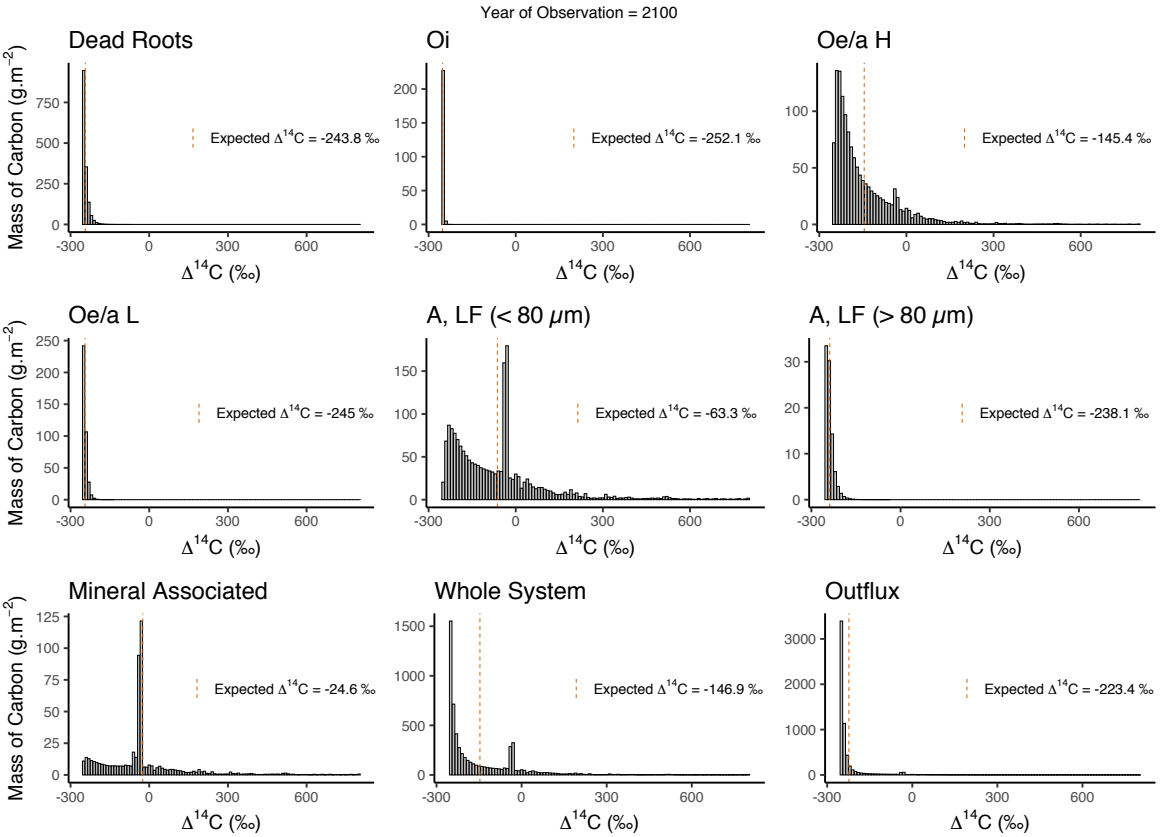

FIGURE A.5: $\Delta^{14}C$ distributions of the HFS model for each of the seven pools, outflux, and whole system . The year of observation is 2100 and the distributions are computed over 1,000 years, with discretization h = 0.1. The bin size b is equal to 10 ‰.

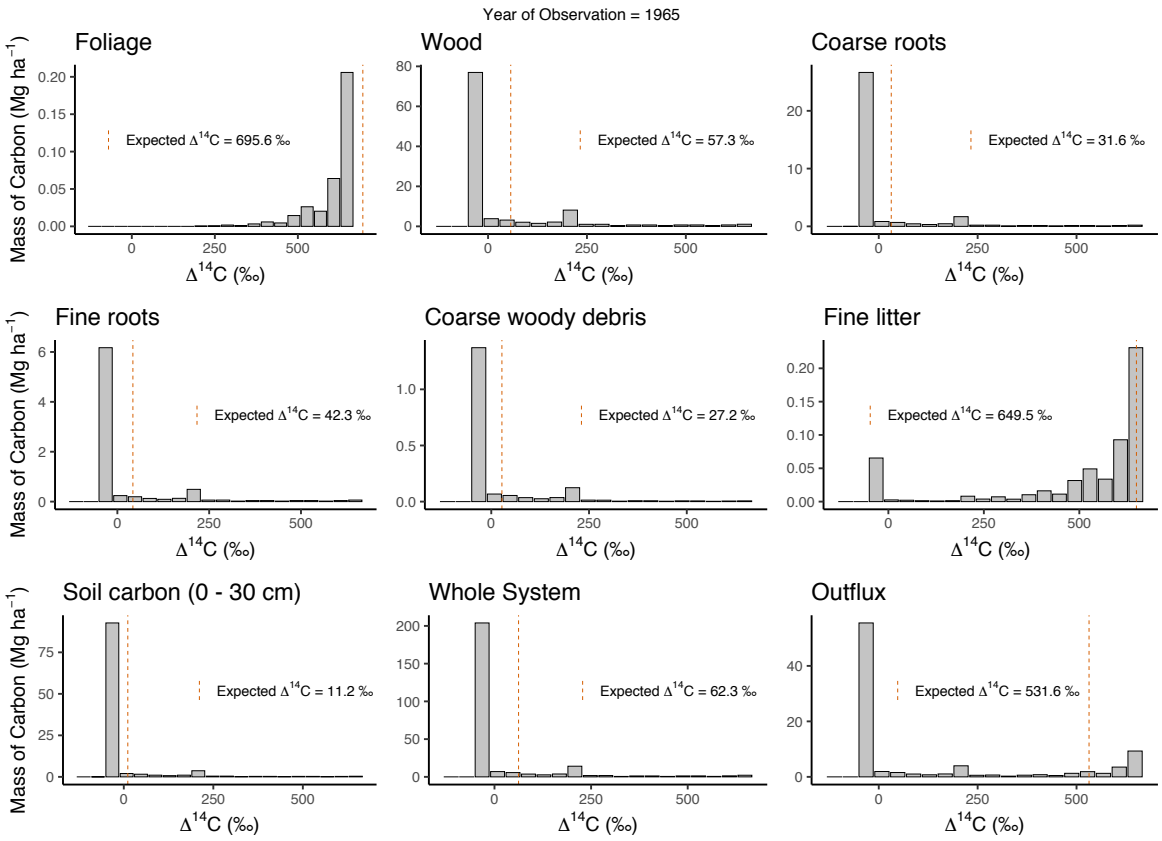

FIGURE A.6: $\Delta^{14}C$ distributions of the Porce model for each of the seven pools, outflux, and whole system . The year of observation is 1965 – just after the bomb peak in 1964 – and the distributions are computed over 1,000 years, with discretization $h = 0.1$. The bin size b is equal to 40 ‰.

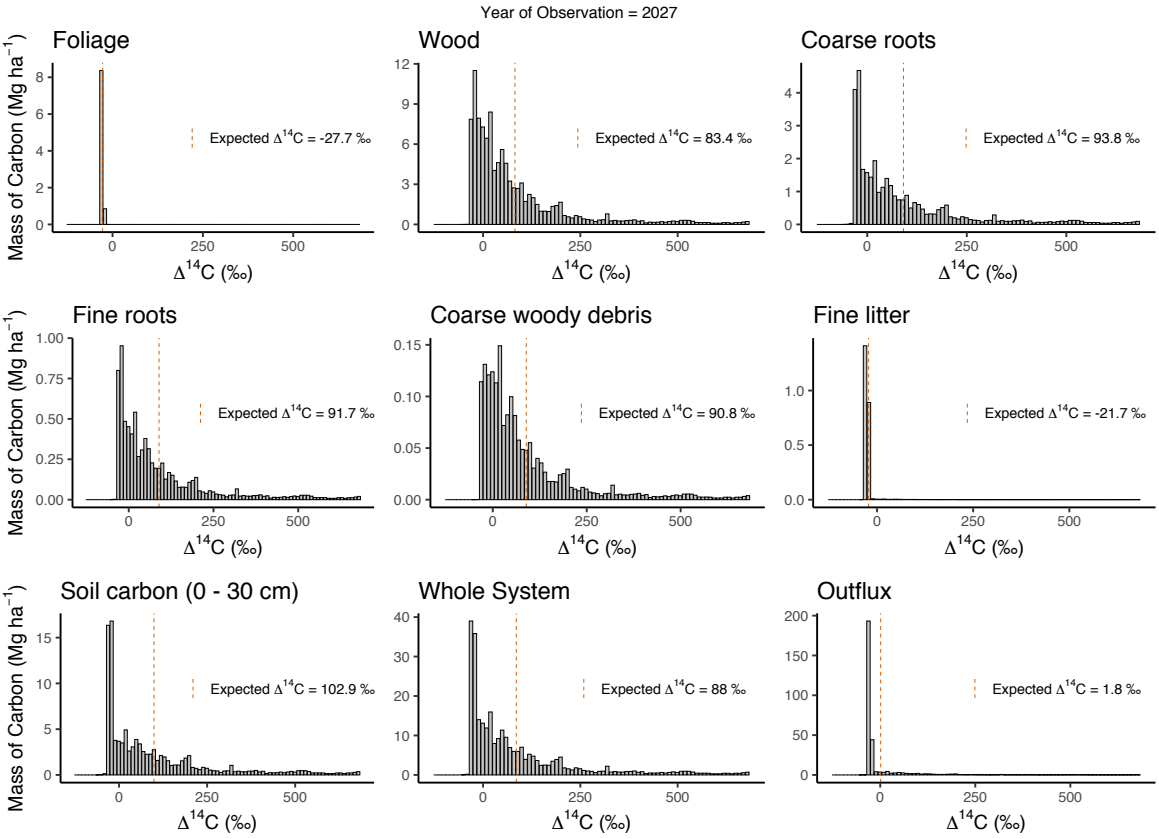

FIGURE A.7: $\Delta^{14}C$ distributions of the Porce model for each of the seven pools, outflux, and whole system . The year of observation is 2027 and the distributions are computed over 1,000 years, with discretization $h = 0.1$. The bin size b is equal to 10 ‰.

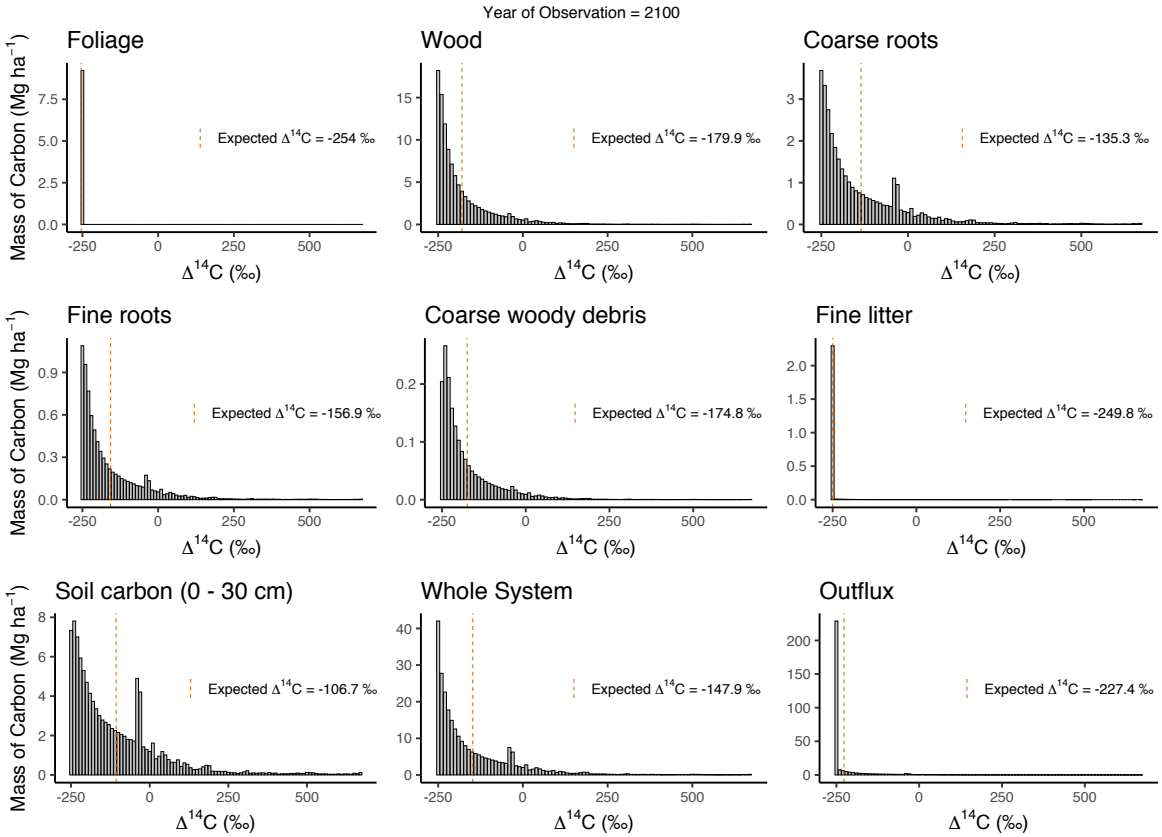

FIGURE A.8: Δ^{14}C distributions of the Porce model for each of the seven pools, outflux, and whole system . The year of observation is 2100 and the distributions are computed over 1,000 years, with discretization $h = 0.1$. The bin size b is equal to 10 ‰.

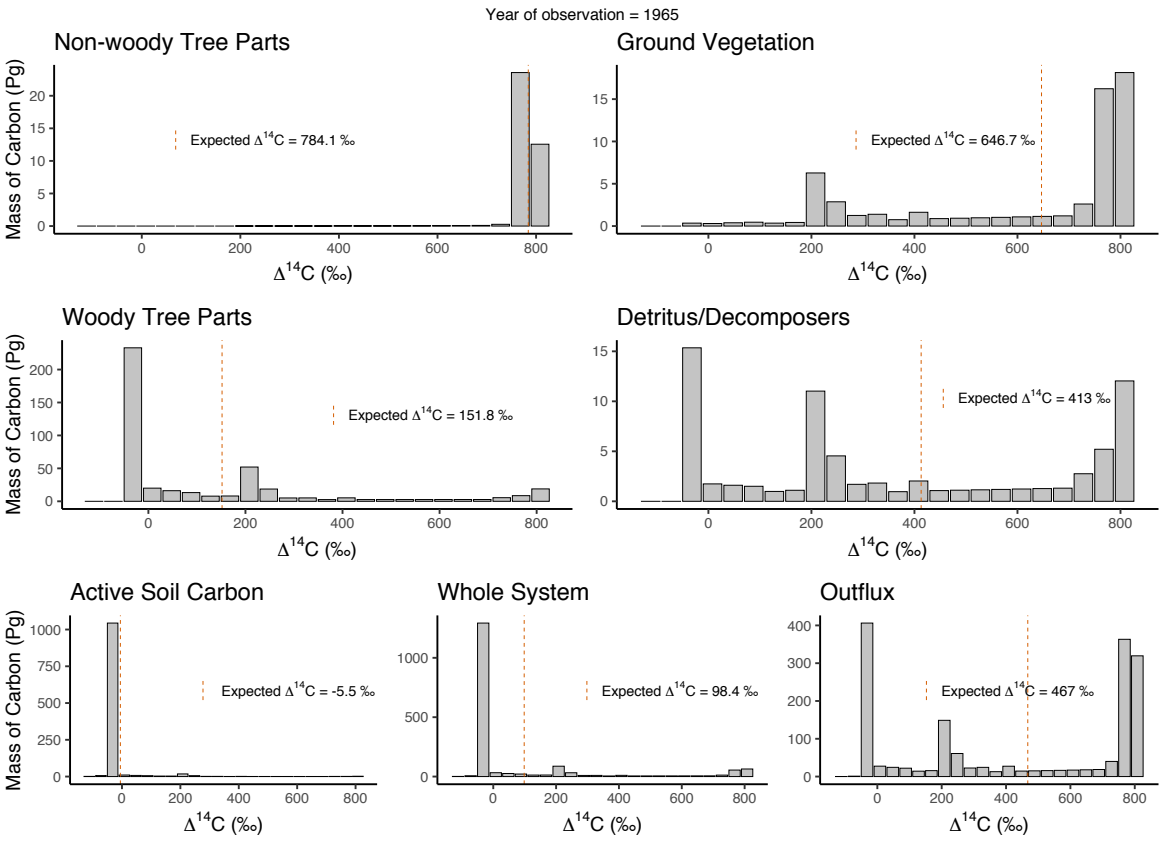

FIGURE A.9: $\Delta^{14}C$ distributions of the Emanuel model for each of the seven pools, outflux, and whole system . The year of observation is 1965 – just after the bomb peak in 1964 – and the distributions are computed over 1,000 years, with discretization $h = 0.1$. The bin size b is equal to 40 ‰.

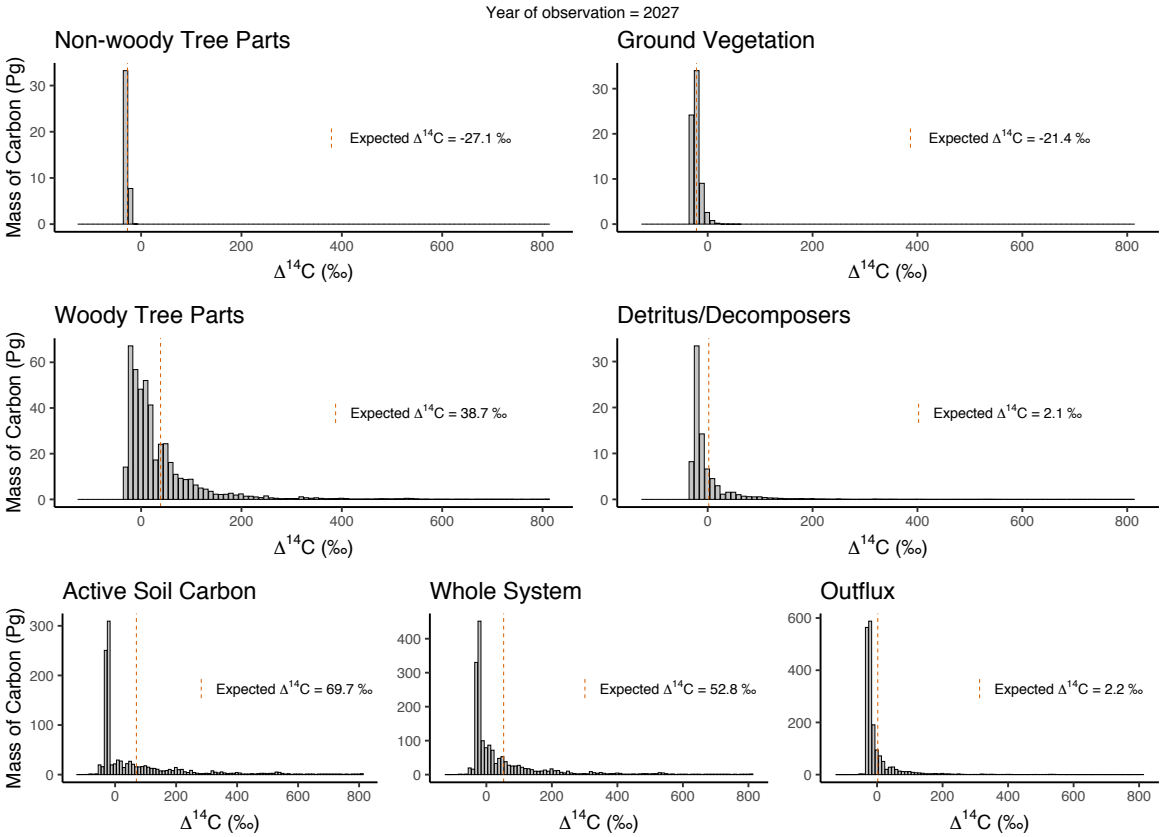

FIGURE A.10: $\Delta^{14}C$ distributions of the Emanuel model for each of the seven pools, outflux, and whole system . The year of observation is 2027 and the distributions are computed over 1,000 years, with discretization $h = 0.1$. The bin size b is equal to 10 ‰.

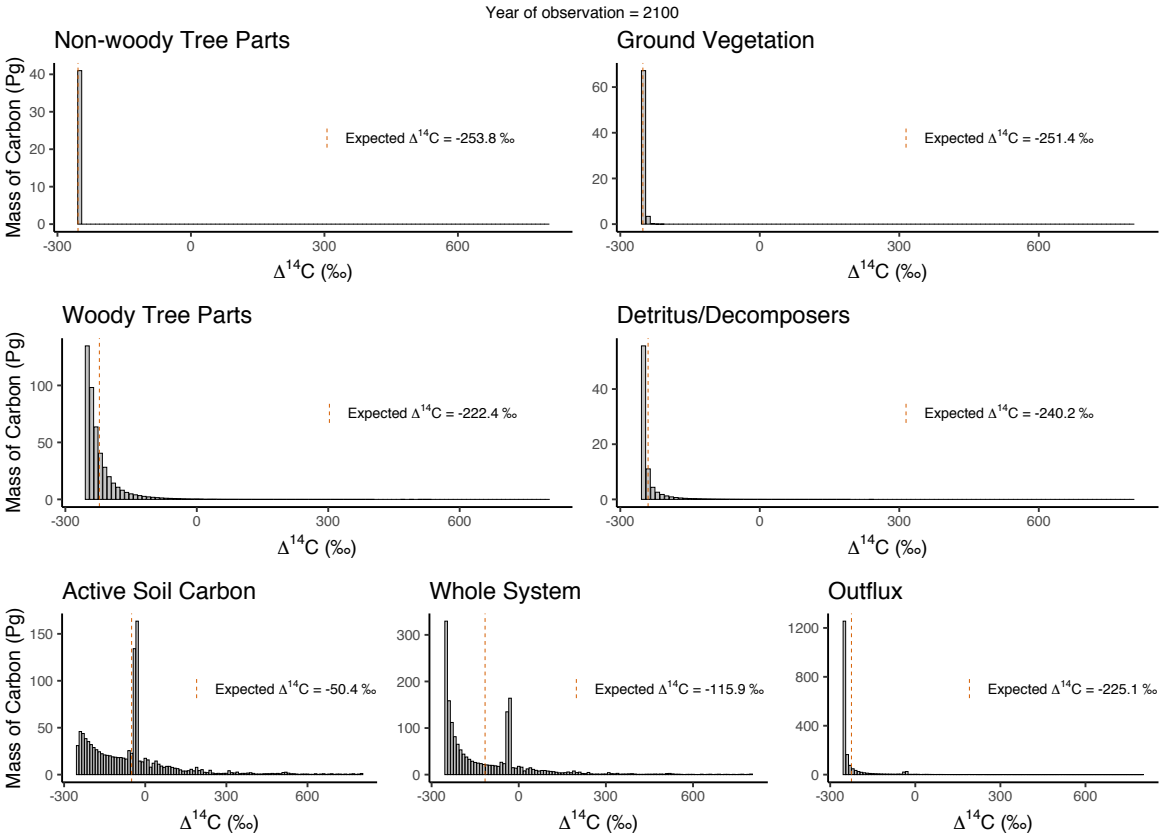

FIGURE A.11: $\Delta^{14}C$ distributions of the Emanuel model for each of the seven pools, outflux, and whole system . The year of observation is 2100 and the distributions are computed over 1,000 years, with discretization $h = 0.1$. The bin size b is equal to 10 ‰.

Bibliography

Adeney, J Marion, Christensen, Norman L, Vicentini, Alberto, and Cohn-Haft, Mario (2016). "White-sand ecosystems in Amazonia". In: *Biotropica* 48.1, pp. 7–23. DOI: 10.1111/btp.12293.

Alkass, Kanar, Buchholz, Bruce A, Ohtani, Susumu, Yamamoto, Toshiharu, Druid, Henrik, and Spalding, Kirsty L (2010). "Age estimation in forensic sciences: application of combined aspartic acid racemization and radiocarbon analysis". In: *Molecular & Cellular Proteomics* 9.5, pp. 1022–1030. DOI: 10.1074/mcp.M900525-MCP200.

Ancapichún, Santiago, De Pol-Holz, Ricardo, Christie, Duncan A, Santos, Guaciara M, Collado-Fabbri, Silvana, Garreaud, René, Lambert, Fabrice, Orfanoz-Cheuquelaf, Andrea, Rojas, Maisa, Southon, John, et al. (2021). "Radiocarbon bomb-peak signal in tree-rings from the tropical Andes register low latitude atmospheric dynamics in the Southern Hemisphere". In: *Science of the Total Environment* 774, p. 145126. DOI: 10.1016/j.scitotenv.2021.145126.

Anderson, David H (1983). *Compartmental modeling and tracer kinetics*. Vol. 50. Springer Science & Business Media. DOI: 10.1007/978-3-642-51861-4.

Andreae, M. O., Acevedo, O. C., Araùjo, A., Artaxo, P., Barbosa, C. G. G., Barbosa, H. M. J., Brito, J., Carbone, S., Chi, X., Cintra, B. B. L., and al., et (2015). "The Amazon Tall Tower Observatory (ATTO): overview of pilot measurements on ecosystem ecology, meteorology, trace gases, and aerosols". In: *Atmospheric Chemistry and Physics* 15.18, pp. 10723–10776. ISSN: 1680-7324. DOI: 10.5194/acp-15-10723-2015. URL: http://dx.doi.org/10.5194/acp-15-10723-2015.

Arnold, James R and Libby, Willard F (1949). "Age determinations by radiocarbon content: checks with samples of known age". In: *Science* 110.2869, pp. 678–680. DOI: 10.1126/science.110.2869.678.

Azizi-Rad, Mina, Chanca, Ingrid, Herrera-Ramírez, David, Metzler, Holger, and Sierra, Carlos A. (2021). "Stochastic and deterministic interpretation of pool models". In: *Global Change Biology* 27.11, pp. 2271–2272. DOI: 10.1111/gcb.15581.

Bayliss, Alex and Bronk Ramsey, Christopher (2004). "Pragmatic Bayesians: a decade of integrating radiocarbon dates into chronological models". In: *Tools for Constructing Chronologies*. Springer, pp. 25–41. DOI: 10.1007/978-1-4471-0231-1_2.

Bolin, Bert and Rodhe, Henning (1973). "A note on the concepts of age distribution and transit time in natural reservoirs". In: *Tellus* 25.1, pp. 58–62. DOI: 10.1111/j.2153-3490.1973.tb01594.x.

Boltwood, Bertram B (1907). "ART. VII. – On the Ultimate Disintegration Products of the Radio-active Elements. Part II. The Disintegration Products of Uranium". In: *American Journal of Science (1880-1910)* 23.134, p. 77. DOI: 10.2475/ajs.s4-23.134.78.

Bonneau, Adelphine, Brock, Fiona, Higham, Tom, Pearce, David G, and Pollard, A Mark (2011). "An improved pretreatment protocol for radiocarbon dating black pigments in San rock art". In: *Radiocarbon* 53.3, pp. 419–428. DOI: 10.1017/S003382220003455X.

Bragança, Daniela, Oliveira, Fabiana, Macario, Kita, Nunes, Vinicius, Muniz, Marcelo, Lamego, Fernando, Abril, Gwenaël, Nepomuceno, Aguinaldo, Solís, Corina, and Rodríguez-Ceja, María (2021). "Establishing water sample protocols for radiocarbon analysis at LAC-UFF, Brazil". In: *Radiocarbon* 63.4, pp. 1225–1232. DOI: 10.1017/RDC.2021.1.

Brando, Paulo M, Nepstad, Daniel C, Davidson, Eric A, Trumbore, Susan E, Ray, David, and Camargo, Plínio (2008). "Drought effects on litterfall, wood production and belowground carbon cycling in an Amazon forest: results of a throughfall reduction experiment". In: *Philosophical Transactions of the Royal Society of London B: Biological Sciences* 363.1498, pp. 1839–1848. DOI: 10.1098/rstb.2007.0031.

Broecker, Wallace S and Walton, Alan (1959). "Radiocarbon from Nuclear Tests: During the past 4 years man has been producing carbon-14 about 15 times faster than nature". In: *Science* 130.3371, pp. 309–314. DOI: 10.1126/science.130.3371.309.

Brown, Thomas A, Nelson, D Earle, Vogel, John S, and Southon, John R (1988). "Improved collagen extraction by modified Longin method". In: *Radiocarbon* 30.2, pp. 171–177. DOI: 10.1017/S0033822200044118.

Buchmann, Nina and Kaplan, Jed O (2001). "Carbon isotope discrimination of terrestrial ecosystems—how well do observed and modeled results match?" In: *Global biogeochemical cycles in the climate system*. Elsevier, pp. 253–266. DOI: 10.1016/B978-012631260-7/50022-4.

Campos, Peterson (2017). "Pequenas variações na fertilidade em solos oligotróficos melhor explicam a estrutura e composição florística em Campinaranas Florestadas na Amazônia Central". MA thesis. Programa de Pós Graduação em Botânica. URL: https://bdtd.inpa.gov.br/handle/tede/2581.

Cardoso, Domingos, Särkinen, Tiina, Alexander, Sara, Amorim, André M, Bittrich, Volker, Celis, Marcela, Daly, Douglas C, Fiaschi, Pedro, Funk, Vicki A, Giacomin, Leandro L, et al. (2017). "Amazon plant diversity revealed by a taxonomically verified species list". In: *Proceedings of the National Academy of Sciences* 114.40, pp. 10695–10700. DOI: 10.1073/pnas.1706756114.

Carvalhais, Nuno, Forkel, Matthias, Khomik, Myroslava, Bellarby, Jessica, Jung, Martin, Migliavacca, Mirco, Saatchi, Sassan, Santoro, Maurizio, Thurner, Martin, Weber, Ulrich, et al. (2014). "Global covariation of carbon turnover times with climate in terrestrial ecosystems". In: *Nature* 514.7521, pp. 213–217. DOI: 10.1038/nature13731.

Ceballos-Núñez, Verónika, Richardson, Andrew D, and Sierra, Carlos A (2018). "Ages and transit times as important diagnostics of model performance for predicting carbon dynamics in terrestrial vegetation models". In: *Biogeosciences* 15.5, pp. 1607–1625. DOI: 10.5194/bg-15-1607-2018.

Chambers, Jeffrey Q, Schimel, Joshua P, and Nobre, Antonio D (2001a). "Respiration from coarse wood litter in central Amazon forests". In: *Biogeochemistry* 52.2, pp. 115–131. DOI: 10.1023/A:1006473530673.

Chambers, Jeffrey Q, Santos, Joaquim dos, Ribeiro, Ralfh J, and Higuchi, Niro (2001b). "Tree damage, allometric relationships, and above-ground net primary production in central Amazon forest". In: *Forest ecology and management* 152.1-3, pp. 73–84. DOI: 10.1016/S0378-1127(00)00591-0.

Chambers, Jeffrey Q, Tribuzy, Edgard S, Toledo, Ligia C, Crispim, Bianca F, Higuchi, Niro, Santos, Joaquim dos, Araújo, Alessandro C, Kruijt, Bart, Nobre, Antonio D, and Trumbore, Susan E (2004). "Respiration from a tropical forest ecosystem: partitioning of sources and low carbon use efficiency". In: *Ecological Applications* 14.sp4, pp. 72–88. DOI: 10.1890/01-6012.

Chanca, Ingrid, Trumbore, Susan E, Macario, Kita, and Sierra, Carlos (2022). "Probability distributions of radiocarbon in open linear compartmental systems at steady-state". In: *Journal of Geophysical Research: Biogeosciences* 127.3, e2021JG006673. DOI: 10.1029/2021JG006673.

Craig, Harmon (1953). "The geochemistry of the stable carbon isotopes". In: *Geochimica et cosmochimica acta* 3.2-3, pp. 53–92. DOI: 10.1016/0016-7037(53)90001-5.

Craig, Harmon (1954). "Carbon 13 in plants and the relationships between carbon 13 and carbon 14 variations in nature". In: *The journal of geology* 62.2, pp. 115–149. DOI: 10.1086/626141.

Davis Jr, Wallace (1977). *Carbon-14 production in nuclear reactors*. Tech. rep. Oak Ridge National Lab., TN (USA). DOI: 10.2172/7114972.

De Camargo, Plínio B, Trumbore, Susan E, Martinelli, LuiZ A, Davidson, EriC A, Nepstad, Daniel C, and Victoria, Reynaldo L (1999). "Soil carbon dynamics in regrowing forest of eastern Amazonia". In: *Global Change Biology* 5.6, pp. 693–702. DOI: 10.1046/j.1365-2486.1999.00259.x.

Demarchi, Layon Oreste, Klein, Viviane Pagnussat, Aguiar, Daniel Praia Portela, Marinho, Lucas Cardoso, Ferreira, Maria Julia, Lopes, Aline, Cruz, Jefferson da, Quaresma, Adriano Costa, Schöngart, Jochen, Wittmann, Florian, et al. (2022). "The specialized white-sand flora of the Uatumã Sustainable Development Reserve, central Amazon, Brazil". In: *Check List* 18.1, pp. 187–217. DOI: 10.15560/18.1.187.

Emanuel, WR, Killough, GG, and Olson, JS (1981). "Modeling the circulation of carbon in the worlds terrestrial ecosystem, Carbon Cycle Modelling, Scope, 16 B. Bolin, 335–353". In: ed. by Bert Bolin. John Wiley, New York. URL: https://scope.dge.carnegiescience.edu/SCOPE_16/SCOPE_16_1.5.12_Emanuel_335-353.pdf.

Enoto, Teruaki, Wada, Yuuki, Furuta, Yoshihiro, Nakazawa, Kazuhiro, Yuasa, Takayuki, Okuda, Kazufumi, Makishima, Kazuo, Sato, Mitsuteru, Sato, Yousuke, Nakano, Toshio, et al. (2017). "Photonuclear reactions triggered by lightning discharge". In: *Nature* 551.7681, pp. 481–484. DOI: 10.1038/nature24630.

Fahrni, Simon M, Southon, John R, Santos, Guaciara M, Palstra, Sanne WL, Meijer, Harro AJ, and Xu, Xiaomei (2017). "Reassessment of the $^{13}C/^{12}C$ and $^{14}C/^{12}C$ isotopic fractionation ratio and its impact on high-precision radiocarbon dating". In: *Geochimica et Cosmochimica Acta* 213, pp. 330–345. DOI: 10.1016/j.gca.2017.05.038.

Fahrni, SM, Wacker, L, Synal, H-A, and Szidat, Sönke (2013). "Improving a gas ion source for ^{14}C-AMS". In: *Nuclear Instruments and Methods in Physics Research Section B: Beam Interactions with Materials and Atoms* 294, pp. 320–327. DOI: 10.1016/j.nimb.2012.03.037.

Freeman, Stewart PHT, Shanks, Richard P, Donzel, Xavier, and Gaubert, Gabriel (2015). "Radiocarbon positive-ion mass spectrometry". In: *Nuclear Instruments and Methods in Physics Research Section B: Beam Interactions with Materials and Atoms* 361, pp. 229–232. DOI: 10.1016/j.nimb.2015.04.034.

Friedlingstein, Pierre, Jones, Matthew W, O'sullivan, Michael, Andrew, Robbie M, Hauck, Judith, Peters, Glen P, Peters, Wouter, Pongratz, Julia, Sitch, Stephen, Le Quéré, Corinne, et al. (2019). "Global carbon budget 2019". In: *Earth System Science Data* 11.4, pp. 1783–1838. DOI: 10.5194/essd-11-1783-2019.

Fu, Zheng, Gerken, Tobias, Bromley, Gabriel, Araújo, Alessandro, Bonal, Damien, Burban, Benoît, Ficklin, Darren, Fuentes, Jose D, Goulden, Michael, Hirano, Takashi, et al. (2018). "The surface-atmosphere exchange of carbon dioxide in tropical rainforests: Sensitivity to environmental drivers and flux measurement methodology". In: *Agricultural and Forest Meteorology* 263, pp. 292–307. DOI: 10.1016/j.agrformet.2018.09.001.

Galli, Iacopo, Bartalini, S, Cancio, P, De Natale, P, Mazzotti, D, Giusfredi, G, Fedi, M, and Mandò, PA (2013). "Optical detection of radiocarbon dioxide: first results and AMS intercomparison". In: *Radiocarbon* 55.2–3, pp. 213–223. DOI: 10.1017/S0033822200057313.

Gaudinski, Julia B, Trumbore, Susan E, Davidson, Eric A, and Zheng, Shuhui (2000). "Soil carbon cycling in a temperate forest: radiocarbon-based estimates of residence times, sequestration rates and partitioning of fluxes". In: *Biogeochemistry* 51.1, pp. 33–69. DOI: 10.1023/A:1006301010014.

Godwin, Harry (1962). "Half-life of radiocarbon". In: *Nature* 195.4845, pp. 984–984. DOI: 10.1038/195984a0.

Goudriaan, J (1992). "Biosphere structure, carbon sequestering potential and the atmospheric ^{14}C carbon record". In: *Journal of Experimental Botany* 43.8, pp. 1111–1119. DOI: 10.1093/jxb/43.8.1111.

Graven, Heather, Allison, Colin E, Etheridge, David M, Hammer, Samuel, Keeling, Ralph F, Levin, Ingeborg, Meijer, Harro AJ, Rubino, Mauro, Tans, Pieter P, Trudinger, Cathy M, et al. (2017). "Compiled records of carbon isotopes in atmospheric CO2 for historical simulations in CMIP6". In: *Geoscientific Model Development (Online)* 10.12. DOI: 10.5194/gmd-10-4405-2017.

Graven, Heather D (2015). "Impact of fossil fuel emissions on atmospheric radiocarbon and various applications of radiocarbon over this century". In: *Proceedings*

of the National Academy of Sciences 112.31, pp. 9542–9545. DOI: 10.1073/pnas.1504467112.

Hajdas, Irka (2009). "Applications of radiocarbon dating method". In: *Radiocarbon* 51.1, pp. 79–90. DOI: 10.1017/S0033822200033713.

Hardie, SML, Garnett, MH, Fallick, AE, Ostle, NJ, and Rowland, AP (2009). "Bomb-^{14}C analysis of ecosystem respiration reveals that peatland vegetation facilitates release of old carbon". In: *Geoderma* 153.3-4, pp. 393–401. DOI: 10.1016/j.geoderma.2009.09.002.

Herrera-Ramirez, David, Muhr, Jan, Hartmann, Henrik, Römermann, Christine, Trumbore, Susan, and Sierra, Carlos A (2020). "Probability distributions of nonstructural carbon ages and transit times provide insights into carbon allocation dynamics of mature trees". In: *New Phytologist* 226.5, pp. 1299–1311. DOI: 10.1111/nph.16461.

Hogg, Alan G, Hua, Quan, Blackwell, Paul G, Niu, Mu, Buck, Caitlin E, Guilderson, Thomas P, Heaton, Timothy J, Palmer, Jonathan G, Reimer, Paula J, Reimer, Ron W, et al. (2013). "SHCal13 Southern Hemisphere calibration, 0–50,000 years cal BP". In: *Radiocarbon* 55.4, pp. 1889–1903. DOI: 10.2458/azu_js_rc.55.16783.

Hogg, Alan G, Heaton, Timothy J, Hua, Quan, Palmer, Jonathan G, Turney, Chris SM, Southon, John, Bayliss, Alex, Blackwell, Paul G, Boswijk, Gretel, Ramsey, Christopher Bronk, et al. (2020). "SHCal20 Southern Hemisphere calibration, 0–55,000 years cal BP". In: *Radiocarbon* 62.4, pp. 759–778. DOI: 10.1017/RDC.2020.59.

Hua, Quan, Barbetti, Mike, and Rakowski, Andrzej Z (2013). "Atmospheric radiocarbon for the period 1950–2010". In: *Radiocarbon* 55.4, pp. 2059–2072. DOI: 10.2458/azu_js_rc.v55i2.16177.

Hua, Quan, Turnbull, Jocelyn C, Santos, Guaciara M, Rakowski, Andrzej Z, Ancapichún, Santiago, De Pol-Holz, Ricardo, Hammer, Samuel, Lehman, Scott J, Levin, Ingeborg, Miller, John B, et al. (2021). "Atmospheric radiocarbon for the period 1950–2019". In: *Radiocarbon*, pp. 1–23. DOI: 10.1017/RDC.2021.95.

IPCC (2014a). *Climate Change 2013 – The Physical Science Basis: Working Group I Contribution to the Fifth Assessment Report of the Intergovernmental Panel on Climate Change*. Cambridge University Press. DOI: 10.1017/CBO9781107415324.

IPCC (2014b). *Climate change 2014: synthesis report. Contribution of Working Groups I, II and III to the fifth assessment report of the Intergovernmental Panel on Climate Change*.

Ed. by R.K. Pachauri Core Writing Team and L.A. Meyer (eds.) IPCC, 151 pp. URL: https://www.ipcc.ch/report/ar5/syr/.

Jacquez, John A and Simon, Carl P (1993). "Qualitative theory of compartmental systems". In: *Siam Review* 35.1, pp. 43–79. DOI: 10.1137/1035003.

Jain, Atul K, Kheshgi, Haroon S, and Wuebbles, Donald J (1997). "Is there an imbalance in the global budget of bomb-produced radiocarbon?" In: *Journal of Geophysical Research: Atmospheres* 102.D1, pp. 1327–1333. DOI: 10.1029/96JD03092.

Keeling, Charles D (1958). "The concentration and isotopic abundances of atmospheric carbon dioxide in rural areas". In: *Geochimica et cosmochimica acta* 13.4, pp. 322–334. DOI: 10.1016/0016-7037(58)90033-4.

Keeling, Charles D (1961). "The concentration and isotopic abundances of carbon dioxide in rural and marine air". In: *Geochimica et Cosmochimica Acta* 24.3-4, pp. 277–298. DOI: 10.1016/0016-7037(61)90023-0.

Keeling, Ralph F and Graven, Heather D (2021). "Insights from Time Series of Atmospheric Carbon Dioxide and Related Tracers". In: *Annual Review of Environment and Resources* 46, pp. 85–110. DOI: 10.1146/annurev-environ-012220-125406.

Köhler, Peter, Adolphi, Florian, Butzin, Martin, and Muscheler, Raimund (2022). "Toward reconciling radiocarbon production rates with carbon cycle changes of the last 55,000 years". In: *Paleoceanography and Paleoclimatology* 37.2, e2021PA004314. DOI: 10.1029/2021PA004314.

Kovaltsov, Gennady A, Mishev, Alexander, and Usoskin, Ilya G (2012). "A new model of cosmogenic production of radiocarbon ^{14}C in the atmosphere". In: *Earth and Planetary Science Letters* 337, pp. 114–120. DOI: 10.1016/j.epsl.2012.05.036.

Kutschera, Walter (2013). "Applications of accelerator mass spectrometry". In: *International Journal of Mass Spectrometry* 349, pp. 203–218. DOI: 10.1016/j.ijms.2013.05.023.

Kutschera, Walter (2022). "The versatile uses of the ^{14}C bomb peak". In: *Radiocarbon*, pp. 1–14. DOI: 10.1017/RDC.2022.13.

Lalonde, Rachelle G and Prescott, Cindy E (2007). "Partitioning heterotrophic and rhizospheric soil respiration in a mature Douglas-fir (Pseudotsuga menziesii) forest". In: *Canadian Journal of Forest Research* 37.8, pp. 1287–1297. DOI: 10.1139/X07-019.

Lawrence, Corey R, Beem-Miller, Jeffrey, Hoyt, Alison M, Monroe, Grey, Sierra, Carlos A, Heckman, K, Blankinship, JC, Crow, SE, McNicol, G, Trumbore, S, et al.

(2020). "An open source database for the synthesis of soil radiocarbon data: ISRaD version 1.0". In: *Earth System Science Data* 12.LLNL-JRNL-775042. DOI: 10.3929/ethz-b-000385703.

Levin, Ingeborg and Kromer, Bernd (1997). "Twenty years of atmospheric $^{14}CO_2$ observations at Schauinsland station, Germany". In: *Radiocarbon* 39.2, pp. 205–218. DOI: 10.1017/S0033822200052012.

Levin, Ingeborg, Münnich, KO, and Weiss, Wolfgang (1980). "The effect of anthropogenic CO_2 and ^{14}C sources on the distribution of ^{14}C in the atmosphere". In: *Radiocarbon* 22.2, pp. 379–391. DOI: 10.1017/S003382220000967X.

Levin, Ingeborg, Kromer, Bernd, Schoch-Fischer, Hildegard, Bruns, Michael, Münnich, Marianne, Berdau, Dietrich, Vogel, John C, and Münnich, Karl Otto (1985). "25 years of tropospheric ^{14}C observations in central Europe". In: *Radiocarbon* 27.1, pp. 1–19. DOI: 10.1017/S0033822200006895.

Levin, Ingeborg, Naegler, Tobias, Kromer, Bernd, Diehl, Moritz, Francey, Roger, Gomez-Pelaez, Angel, Steele, Paul, Wagenbach, Dietmar, Weller, Rolf, and Worthy, Douglas (2010). "Observations and modelling of the global distribution and long-term trend of atmospheric $^{14}CO_2$". In: *Tellus B: Chemical and Physical Meteorology* 62.1, pp. 26–46. DOI: 10.1111/j.1600-0889.2009.00446.x.

Levin, Ingeborg, Kromer, Bernd, and Hammer, Samuel (2013). "Atmospheric $\Delta^{14}CO_2$ trend in Western European background air from 2000 to 2012". In: *Tellus B: Chemical and Physical Meteorology* 65.1, p. 20092. DOI: 10.3402/tellusb.v65i0.20092.

Levin, Ingeborg, Hammer, Samuel, Kromer, Bernd, Preunkert, Susanne, Weller, Rolf, and Worthy, Douglas E (2021). "Radiocarbon in global tropospheric carbon dioxide". In: *Radiocarbon*, pp. 1–11. DOI: 10.1017/RDC.2021.102.

Libby, WF (1952). "Radiocarbon Dating, Chicago: Univ". In: *Chicago press* 124, pp. 60–61.

Libby, Willard F (1960). *Radiocarbon dating. Nobel Lecture, December 12, 1960*. URL: https://www.nobelprize.org/prizes/chemistry/1960/libby/lecture/.

Libby, Willard F, Anderson, Ernest C, and Arnold, James R (1949). "Age determination by radiocarbon content: world-wide assay of natural radiocarbon". In: *Science* 109.2827, pp. 227–228. DOI: 10.1126/science.109.2827.227.

Lu, Xingjie, Wang, Ying-Ping, Luo, Yiqi, and Jiang, Lifen (2018). "Ecosystem carbon transit versus turnover times in response to climate warming and rising atmospheric CO_2 concentration". In: *Biogeosciences* 15.21, pp. 6559–6572. DOI: 10.5194/bg-15-6559-2018.

Luizão, Flavio J (1995). "Ecological studies in contrasting forest types in central Amazonia". PhD thesis. Department of Biological and Molecular Sciences. URL: http://hdl.handle.net/1893/2160.

Luo, Yiqi, Shi, Zheng, Lu, Xingjie, Xia, Jianyang, Liang, Junyi, Jiang, Jiang, Wang, Ying, Smith, Matthew J, Jiang, Lifen, Ahlström, Anders, et al. (2017). "Transient dynamics of terrestrial carbon storage: mathematical foundation and its applications". In: *Biogeosciences* 14.1, pp. 145–161. DOI: 10.5194/bg-14-145-2017.

Lux, Johannes Thomas (2018). "A new target preparation facility for high precision AMS measurements and strategies for efficient $^{14}CO_2$ sampling". PhD thesis. Faculty of Physics and Astronomy/Institute of Environmental Physics. DOI: 10.11588/heidok.00024767. URL: http://www.ub.uni-heidelberg.de/archiv/24767.

Macario, Kita D, Gomes, PRS, Anjos, RM, Carvalho, C, Linares, R, Alves, EQ, Oliveira, FM, Castro, MD, Chanca, IS, Silveira, MFM, et al. (2013). "The Brazilian AMS Radiocarbon Laboratory (LAC-UFF) and the intercomparison of results with CENA and UGAMS". In: *Radiocarbon* 55.2, pp. 325–330. DOI: 10.1017/S003382220005743X.

Macario, Kita D, Oliveira, Fabiana M, Carvalho, Carla, Santos, Guaciara M, Xu, Xiaomei, Chanca, Ingrid S, Alves, Eduardo Q, Jou, Renata M, Oliveira, Maria Isabela, Pereira, Bruna B, et al. (2015). "Advances in the graphitization protocol at the Radiocarbon Laboratory of the Universidade Federal Fluminense (LAC-UFF) in Brazil". In: *Nuclear Instruments and Methods in Physics Research Section B: Beam Interactions with Materials and Atoms* 361, pp. 402–405. DOI: 10.1016/j.nimb.2015.03.081.

Macario, Kita D, Alves, Eduardo Q, Oliveira, Fabiana M, Moreira, Vinicius N, Chanca, Ingrid S, Carvalho, Carla, Jou, Renata M, Oliveira, Maria Isabela, Pereira, Bruna B, Hammerschlag, Izabela, et al. (2016). "Graphitization reaction via zinc reduction: How low can you go?" In: *International Journal of Mass Spectrometry* 410, pp. 47–51. DOI: 10.1016/j.ijms.2016.10.020.

Macario, Kita D, Oliveira, Fabiana M, Moreira, Vinicius N, Alves, Eduardo Q, Carvalho, Carla, Jou, Renata M, Oliveira, Maria Isabela, Pereira, Bruna B, Hammerschlag, Izabela, Netto, Bruna, et al. (2017). "Optimization of the amount of zinc in the graphitization reaction for radiocarbon AMS measurements at LAC-UFF". In: *Radiocarbon* 59.3, pp. 885–891. DOI: 10.1017/RDC.2016.42.

Malhi, Yadvinder, Baldocchi, DD, and Jarvis, PG (1999). "The carbon balance of tropical, temperate and boreal forests". In: *Plant, Cell & Environment* 22.6, pp. 715–740. DOI: 10.1046/j.1365-3040.1999.00453.x.

Malhi, Yadvinder, Saatchi, Sassan, Girardin, Cecile, and Aragão, Luiz EOC (2009). "The production, storage, and flow of carbon in Amazonian forests". In: *Amazonia and global change*, pp. 355–372. DOI: 10.1029/2008GM000733.

Mäntynen, P, Äikää, O, Kankainen, T, and Kaihola, L (1987). "Application of pulse-shape discrimination to improve the precision of the carbon-14 gas-proportional-counting method". In: *International Journal of Radiation Applications and Instrumentation. Part A. Applied Radiation and Isotopes* 38.10, pp. 869–873. DOI: 10.1016/0883-2889(87)90186-9.

Masuda, Kimiaki, Nagaya, Kentaro, Miyahara, Hiroko, Muraki, Yasushi, and Nakamura, Toshio (2009). "Cosmogenic radiocarbon and the solar activity". In: *Journal of the Physical Society of Japan* 78.Suppl. A, pp. 1–6. DOI: 10.1143/JPSJS.78SA.1.

Metzler, Holger and Sierra, Carlos A (2018). "Linear autonomous compartmental models as continuous-time Markov chains: Transit-time and age distributions". In: *Mathematical Geosciences* 50.1, pp. 1–34. DOI: 10.1007/s11004-017-9690-1.

Metzler, Holger, Müller, Markus, and Sierra, Carlos A (2018). "Transit-time and age distributions for nonlinear time-dependent compartmental systems". In: *Proceedings of the National Academy of Sciences*, p. 201705296. DOI: 10.1073/pnas.1705296115.

Millard, Andrew R (2014). "Conventions for reporting radiocarbon determinations". In: *Radiocarbon* 56.2, pp. 555–559. DOI: 10.2458/56.17455.

Miller, John B and Tans, Pieter P (2003). "Calculating isotopic fractionation from atmospheric measurements at various scales". In: *Tellus B: Chemical and Physical Meteorology* 55.2, pp. 207–214. DOI: 10.3402/tellusb.v55i2.16697.

Miyake, Fusa, Nagaya, Kentaro, Masuda, Kimiaki, and Nakamura, Toshio (2012). "A signature of cosmic-ray increase in AD 774–775 from tree rings in Japan". In: *Nature* 486.7402, pp. 240–242. DOI: 10.1038/nature11123.

Miyake, Fusa, Masuda, Kimiaki, and Nakamura, Toshio (2013). "Another rapid event in the carbon-14 content of tree rings". In: *Nature communications* 4.1, pp. 1–6. DOI: 10.1038/ncomms2783.

Miyake, Fusa, Masuda, Kimiaki, Hakozaki, Masataka, Nakamura, Toshio, Tokanai, Fuyuki, Kato, Kazuhiro, Kimura, Katsuhiko, and Mitsutani, Takumi (2014). "Verification of the cosmic-ray event in AD 993–994 by using a Japanese Hinoki tree". In: *Radiocarbon* 56.3, pp. 1189–1194. DOI: 10.2458/56.17769.

Miyake, Fusa, Masuda, Kimiaki, Nakamura, Toshio, Kimura, Katsuhiko, Hakozaki, Masataka, Jull, AJ Timothy, Lange, Todd E, Cruz, Richard, Panyushkina, Irina P, Baisan, Chris, et al. (2017). "Search for annual ^{14}C excursions in the past". In: *Radiocarbon* 59.2, pp. 315–320. DOI: 10.1017/RDC.2016.54.

Muhr, Jan, Trumbore, Susan, Higuchi, Niro, and Kunert, Norbert (2018). "Living on borrowed time–Amazonian trees use decade-old storage carbon to survive for months after complete stem girdling". In: *New Phytologist* 220.1, pp. 111–120. DOI: 10.1111/nph.15302.

Münnich, Karl Otto and Vogel, JC (1958). "Durch Atomexplosionen erzeugter Radiokohlenstoff in der Atmosphäre". In: *Naturwissenschaften* 45.14, pp. 327–329. DOI: 10.1007/BF00640209.

Naegler, Tobias, Ciais, Philippe, Rodgers, Keith, and Levin, Ingeborg (2006). "Excess radiocarbon constraints on air-sea gas exchange and the uptake of CO_2 by the oceans". In: *Geophysical Research Letters* 33.11. DOI: 10.1029/2005GL025408.

Němec, Mojmír, Wacker, Lukas, and Gäggeler, Heinz (2010). "Optimization of the graphitization process at AGE-1". In: *Radiocarbon* 52.3, pp. 1380–1393. DOI: 10.1017/S0033822200046464.

Nydal, Reidar (1968). "Further investigation on the transfer of radiocarbon in nature". In: *Journal of Geophysical Research* 73.12, pp. 3617–3635. DOI: 10.1029/JB073i012p03617.

Oliveira, Fabiana, Macario, Kita, Carvalho, Carla, Moreira, Vinicius, Alves, Eduardo Q, Chanca, Ingrid, Diaz, Maikel, Jou, Renata, Hammerschlag, Izabela, Netto, Bruna M, et al. (2021). "LAC-UFF status report: current protocols and recent developments". In: *Radiocarbon* 63.4, pp. 1233–1245. DOI: 10.1017/RDC.2020.138.

Pataki, DE, Ehleringer, JR, Flanagan, LB, Yakir, Dan, Bowling, DR, Still, CJ, Buchmann, N, Kaplan, Jed O, and Berry, JA (2003). "The application and interpretation of Keeling plots in terrestrial carbon cycle research". In: *Global biogeochemical cycles* 17.1. DOI: 10.1029/2001GB001850.

Phillips, Claire L, McFarlane, Karis J, LaFranchi, Brian, Desai, Ankur R, Miller, John B, and Lehman, Scott J (2015). "Observations of $^{14}CO_2$ in ecosystem respiration

from a temperate deciduous forest in Northern Wisconsin". In: *Journal of Geophysical Research: Biogeosciences* 120.4, pp. 600–616. DOI: 10.1002/2014JG002808.

Ramsey, Christopher Bronk (2009). "Bayesian analysis of radiocarbon dates". In: *Radiocarbon* 51.1, pp. 337–360. DOI: 10.1017/S0033822200033865.

Randerson, JT, Enting, IG, Schuur, EAG, Caldeira, K, and Fung, IY (2002). "Seasonal and latitudinal variability of troposphere $\Delta^{14}CO_2$: Post bomb contributions from fossil fuels, oceans, the stratosphere, and the terrestrial biosphere". In: *Global Biogeochemical Cycles* 16.4. DOI: 10.1029/2002GB001876.

Rasmussen, Martin, Hastings, Alan, Smith, Matthew J, Agusto, Folashade B, Chen-Charpentier, Benito M, Hoffman, Forrest M, Jiang, Jiang, Todd-Brown, Katherine EO, Wang, Ying, Wang, Ying-Ping, et al. (2016). "Transit times and mean ages for nonautonomous and autonomous compartmental systems". In: *Journal of mathematical biology* 73.6-7, pp. 1379–1398. DOI: 10.1007/s00285-016-0990-8.

Reimer, Paula J, Bard, Edouard, Bayliss, Alex, Beck, J Warren, Blackwell, Paul G, Ramsey, Christopher Bronk, Buck, Caitlin E, Cheng, Hai, Edwards, R Lawrence, Friedrich, Michael, et al. (2013). "IntCal13 and Marine13 radiocarbon age calibration curves 0–50,000 years cal BP". In: *Radiocarbon* 55.4, pp. 1869–1887. DOI: 10.2458/azu_js_rc.55.16947.

Reimer, Paula J, Austin, William EN, Bard, Edouard, Bayliss, Alex, Blackwell, Paul G, Ramsey, Christopher Bronk, Butzin, Martin, Cheng, Hai, Edwards, R Lawrence, Friedrich, Michael, et al. (2020). "The IntCal20 northern hemisphere radiocarbon age calibration curve (0–55 cal kBP)". In: *Radiocarbon* 62.4, pp. 725–757. DOI: 10.1017/RDC.2020.41.

Rinyu, László, Molnár, Mihály, Major, István, Nagy, Tamás, Veres, Mihály, Kimák, Ádám, Wacker, Lukas, and Synal, Hans-Arno (2013). "Optimization of sealed tube graphitization method for environmental C-14 studies using MICADAS". In: *Nuclear Instruments and Methods in Physics Research Section B: Beam Interactions with Materials and Atoms* 294, pp. 270–275. DOI: 10.1016/j.nimb.2012.08.042.

Rosman, KJR and Taylor, PDP (1998). *Isotopic compositions of the elements 1997 (Technical Report)*. Tech. rep. 1. International Union of Pure and Applied Chemistry, pp. 217–235. DOI: 10.1351/pac199870010217.

Santos, Guaciara M, Oliveira, Fabiana M, Park, Junghun, Sena, Ana CT, Chiquetto, Júlio B, Macario, Kita D, and Grainger, Cassandra SG (2019). "Assessment of the regional fossil fuel CO_2 distribution through $\Delta^{14}C$ patterns in ipê leaves: The case

of Rio de Janeiro state, Brazil". In: *City and Environment Interactions* 1, p. 100001. DOI: 10.1016/j.cacint.2019.06.001.

Sapronov, DV and Kuzyakov, Ya V (2007). "Separation of root and microbial respiration: comparison of three methods". In: *Eurasian Soil Science* 40.7, pp. 775–784. DOI: 10.1134/S1064229307070101.

Saugier, Bernard, Roy, Jacques, and Mooney, Harold A. (2001). "23 - Estimations of Global Terrestrial Productivity: Converging toward a Single Number?" In: *Terrestrial Global Productivity*. Ed. by Jacques Roy, Bernard Saugier, and Harold A. Mooney. Physiological Ecology. San Diego: Academic Press, pp. 543–557. ISBN: 978-0-12-505290-0. DOI: 10.1016/B978-012505290-0/50024-7.

Schuur, Edward AG, McGuire, A David, Schädel, Christina, Grosse, Guido, Harden, Jennifer W, Hayes, Daniel J, Hugelius, Gustaf, Koven, Charles D, Kuhry, Peter, Lawrence, David M, et al. (2015). "Climate change and the permafrost carbon feedback". In: *Nature* 520.7546, pp. 171–179. DOI: 10.1038/nature14338.

Schuur, Edward AG, Druffel, Ellen RM, and Trumbore, Susan E, eds. (2016). *Radiocarbon and climate change*. Springer International Publishing Switzerland, pp. VII, 315. DOI: 10.1007/978-3-319-25643-6.

Sierra, CA, Müller, M, Trumbore, SE, et al. (2012a). "Models of soil organic matter decomposition: the SoilR package, version 1.0". In: *Geoscientific Model Development* 5, pp. 1045–1060. DOI: 10.5194/gmd-5-1045-2012.

Sierra, Carlos, Müller, Markus, and Trumbore, Susan E (2014). "Modeling radiocarbon dynamics in soils: SoilR version 1.1". In: *Geoscientific Model Development* 7.5, pp. 1919–1931. DOI: 10.5194/gmd-7-1919-2014.

Sierra, Carlos A (2018). "Forecasting Atmospheric Radiocarbon Decline to Pre-Bomb Values". In: *Radiocarbon* 60.4, pp. 1055–1066. DOI: 10.1017/RDC.2018.33.

Sierra, Carlos A, Trumbore, SE, Davidson, EA, Frey, SD, Savage, KE, and Hopkins, FM (2012b). "Predicting decadal trends and transient responses of radiocarbon storage and fluxes in a temperate forest soil". In: *Biogeosciences* 9.8, pp. 3013–3028. DOI: 10.5194/bg-9-3013-2012.

Sierra, Carlos A, Jiménez, Eliana Maria, Reu, Björn, Peñuela, María Cristina, Thuille, Angelika, and Quesada, Carlos Alberto (2013). "Low vertical transfer rates of carbon inferred from radiocarbon analysis in an Amazon Podzol". In: *Biogeosciences* 10.6, pp. 3455–3464. DOI: 10.5194/bg-10-3455-2013.

Sierra, Carlos A, Müller, Markus, Metzler, Holger, Manzoni, Stefano, and Trumbore, Susan E (2017). "The muddle of ages, turnover, transit, and residence times in the

carbon cycle". In: *Global change biology* 23.5, pp. 1763–1773. DOI: 10.1111/gcb.13556.

Sierra, Carlos A, Ceballos-Núñez, Verónika, Metzler, Holger, and Müller, Markus (2018). "Representing and understanding the carbon cycle using the theory of compartmental dynamical systems". In: *Journal of Advances in Modeling Earth Systems* 10.8, pp. 1729–1734. DOI: 10.1029/2018MS001360.

Sierra, Carlos A, Estupinan-Suarez, Lina M, and Chanca, Ingrid (2021). "The fate and transit time of carbon in a tropical forest". In: *Journal of Ecology*. DOI: 10.1111/1365-2745.13723.

Soepadmo, Engkik (1993). "Tropical rain forests as carbon sinks". In: *Chemosphere* 27.6, pp. 1025–1039. DOI: 10.1016/0045-6535(93)90066-E.

Soter, Steven (2011). "Radiocarbon anomalies from old CO_2 in the soil and canopy air". In: *Radiocarbon* 53.1, pp. 55–69. DOI: 10.1017/S0033822200034354.

Steffen, Will, Grinevald, Jacques, Crutzen, Paul, and McNeill, John (2011). "The Anthropocene: conceptual and historical perspectives". In: *Philosophical Transactions of the Royal Society A: Mathematical, Physical and Engineering Sciences* 369.1938, pp. 842–867. DOI: 10.1098/rsta.2010.0327.

Stephens, Britton B, Gurney, Kevin R, Tans, Pieter P, Sweeney, Colm, Peters, Wouter, Bruhwiler, Lori, Ciais, Philippe, Ramonet, Michel, Bousquet, Philippe, Nakazawa, Takakiyo, et al. (2007). "Weak northern and strong tropical land carbon uptake from vertical profiles of atmospheric CO_2". In: *Science* 316.5832, pp. 1732–1735. DOI: 10.1126/science.1137004.

Stuiver, Minze and Polach, Henry A (1977). "Discussion reporting of ^{14}C data". In: *Radiocarbon* 19.3, pp. 355–363. DOI: 10.1017/S0033822200003672.

Suess, Hans E (1955). "Radiocarbon concentration in modern wood". In: *Science* 122.3166, pp. 415–417. DOI: 10.1126/science.122.3166.415.b.

Synal, Hans-Arno, Stocker, Martin, and Suter, Martin (2007). "MICADAS: a new compact radiocarbon AMS system". In: *Nuclear Instruments and Methods in Physics Research Section B: Beam Interactions with Materials and Atoms* 259.1, pp. 7–13. DOI: 10.1016/j.nimb.2007.01.138.

Talamo, Sahra, Fewlass, Helen, Maria, Raquel, and Jaouen, Klervia (2021). ""Here we go again": the inspection of collagen extraction protocols for ^{14}C dating and palaeodietary analysis". In: *STAR: Science & Technology of Archaeological Research* 7.1, pp. 62–77. DOI: 10.1080/20548923.2021.1944479.

Tans, Pieter P (1980). "On calculating the transfer of carbon-13 in reservoir models of the carbon cycle". In: *Tellus* 32.5, pp. 464–469. DOI: 10.1111/j.2153-3490.1980.tb00973.x.

Telles, Everaldo de Carvalho Conceição, Camargo, Plínio Barbosa de, Martinelli, Luiz A, Trumbore, Susan E, Costa, Enir Salazar da, Santos, Joaquim, Higuchi, Niro, and Oliveira Jr, Raimundo Cosme (2003). "Influence of soil texture on carbon dynamics and storage potential in tropical forest soils of Amazonia". In: *Global Biogeochemical Cycles* 17.2. DOI: 10.1029/2002GB001953.

Ter Steege, Hans, Vaessen, Rens W, Cárdenas-López, Dairon, Sabatier, Daniel, Antonelli, Alexandre, De Oliveira, Sylvia Mota, Pitman, Nigel CA, Jørgensen, Peter Møller, and Salomão, Rafael P (2016). "The discovery of the Amazonian tree flora with an updated checklist of all known tree taxa". In: *Scientific Reports* 6, p. 29549. DOI: 10.1038/srep29549.

Thompson, Matthew V and Randerson, James T (1999). "Impulse response functions of terrestrial carbon cycle models: method and application". In: *Global Change Biology* 5.4, pp. 371–394. DOI: 10.1046/j.1365-2486.1999.00235.x.

Trumbore, Susan (2000). "Age of soil organic matter and soil respiration: radiocarbon constraints on belowground C dynamics". In: *Ecological applications* 10.2, pp. 399–411. DOI: 10.1890/1051-0761(2000)010[0399:AOSOMA]2.0.CO;2.

Trumbore, Susan (2006). "Carbon respired by terrestrial ecosystems – recent progress and challenges". In: *Global Change Biology* 12.2, pp. 141–153. DOI: 10.1111/j.1365-2486.2006.01067.x.

Trumbore, Susan and De Camargo, Plínio B (2009). "Soil carbon dynamics". In: *Amazonia and global change* 186, pp. 451–462. DOI: 10.1029/2008GM000741.

Trumbore, Susan, Chambers, Jeffrey Q, Camargo, Plinio, Martinelli, Luiz, and Santos, Joaquim (2005). *Carbon Dynamics in Vegetation and Soils*. Tech. rep. Instituto Nacional de Pesquisas da Amazônia.

Trumbore, Susan, Da Costa, Enir Salazar, Nepstad, Daniel C, Barbosa De Camargo, Plinio, Martinelli, Luiz A, Ray, David, Restom, Teresa, and Silver, Whendee (2006). "Dynamics of fine root carbon in Amazonian tropical ecosystems and the contribution of roots to soil respiration". In: *Global Change Biology* 12.2, pp. 217–229. DOI: 10.1111/j.1365-2486.2005.001063.x.

Trumbore, Susan E, Davidson, Eric A, Camargo, Plinio Barbosa de, Nepstad, Daniel C, and Martinelli, Luiz Antonio (1995). "Belowground cycling of carbon in forests

and pastures of Eastern Amazonia". In: *Global Biogeochemical Cycles* 9.4, pp. 515–528. DOI: 10.1029/95GB02148.

Trumbore, Susan E, Sierra, Carlos A, and Hicks Pries, Caitlin E (2016). "Radiocarbon nomenclature, theory, models, and interpretation: Measuring age, determining cycling rates, and tracing source pools". In: Radiocarbon and climate change, Springer. Chap. 3, pp. 45–82. DOI: 10.1007/978-3-319-25643-6.

Turnbull, Jocelyn C, Lehman, Scott J, Miller, John B, Sparks, Rodger J, Southon, John R, and Tans, Pieter P (2007). "A new high precision $^{14}CO_2$ time series for North American continental air". In: *Journal of Geophysical Research: Atmospheres* 112.D11. DOI: 10.1029/2006JD008184.

Van Der Merwe, Nikolaas J and Medina, Ernesto (1991). "The canopy effect, carbon isotope ratios and foodwebs in Amazonia". In: *Journal of archaeological science* 18.3, pp. 249–259. DOI: 10.1016/0305-4403(91)90064-V.

Verkouteren, R Michael and Klouda, George A (1992). "Factorial design techniques applied to optimization of AMS graphite target preparation". In: *Radiocarbon* 34.3, pp. 335–343. DOI: 10.1017/S0033822200063517.

Vieira, Simone, Trumbore, Susan, Camargo, Plinio B, Selhorst, Diogo, Chambers, Jeffrey Q, Higuchi, Niro, and Martinelli, Luiz Antonio (2005). "Slow growth rates of Amazonian trees: consequences for carbon cycling". In: *Proceedings of the National Academy of Sciences* 102.51, pp. 18502–18507. DOI: 10.1073/pnas.0505966102.

Villa Zegarra, Boris Eduardo et al. (2017). "Biomassa florestal e equações alométricas para estimar carbono em uma floresta de campinarana na Reserva de Desenvolvimento Sustentável Uatumã, Amazônia Central". PhD thesis. Clima e Ambiente (CLIAMB). URL: https://bdtd.inpa.gov.br/handle/tede/2545.

Vogel, Johann C (1980). "Fractionation of the carbon isotopes during photosynthesis". In: *Fractionation of the Carbon Isotopes During Photosynthesis*. Springer, Berlin, Heidelberg, pp. 5–29. DOI: 10.1007/978-3-642-46428-7_1.

Vries, Hessel de (1958). "Atomic bomb effect: variation of radiocarbon in plants, shells, and snails in the past 4 years". In: *Science* 128.3318, pp. 250–251. DOI: 10.1126/science.128.3318.250.

Wacker, Luckas, Němec, Mojmír, and Bourquin, Joël (2010). "A revolutionary graphitisation system: fully automated, compact and simple". In: *Nuclear Instruments and Methods in Physics Research Section B: Beam Interactions with Materials and Atoms* 268.7-8, pp. 931–934. DOI: 10.1016/j.nimb.2009.10.067.

Waring, RH, Landsberg, JJ, and Williams, M (1998). "Net primary production of forests: a constant fraction of gross primary production?" In: *Tree physiology* 18.2, pp. 129–134. DOI: 10.1093/treephys/18.2.129.

Wild, Eva M, Kutschera, Walter, Meran, Annemarie, and Steier, Peter (2019). "^{14}C bomb peak analysis of African elephant tusks and its relation to cites". In: *Radiocarbon* 61.5, pp. 1619–1624. DOI: 10.1017/RDC.2019.82.

Xu, Xiaomei, Trumbore, Susan E, Zheng, Shuhui, Southon, John R, McDuffee, Kelsey E, Luttgen, Madelyn, and Liu, Julia C (2007). "Modifying a sealed tube zinc reduction method for preparation of AMS graphite targets: reducing background and attaining high precision". In: *Nuclear Instruments and Methods in Physics Research Section B: Beam Interactions with Materials and Atoms* 259.1, pp. 320–329. DOI: 10.1016/j.nimb.2007.01.175.